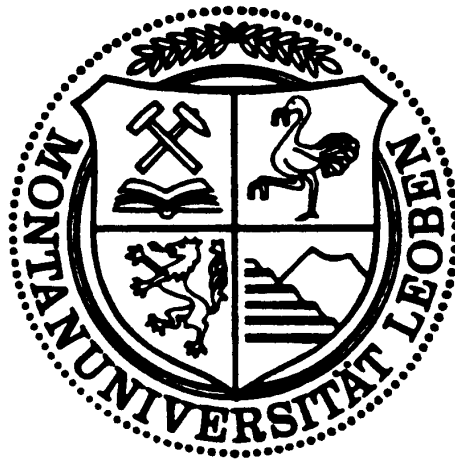**Montanuniversität Leoben**

Dissertation

Crevice Corrosion with Additional Heating and Cooling Cycles in Automotive Exhaust Systems

A Doctoral Thesis Submitted to

The University of Leoben Examination Board

In Partial Fulfillment

of the requirements for the degree

Doctor in Science

Muhammad Yasir

Declaration

The work has been done in the frame of Christian Doppler Laboratory of Localised Corrosion. The partner organisation of this project was Faurecia Emissions Control in Augsburg.

I declare that this research dissertation is my own work. It is being submitted for the degree of Doctor of science at the University of Leoben, Austria. It has not been submitted before any degree or examination at any other university.

Augsburg, August 2011   Muhammad Yasir

Acknowledgements

Dedication

To my loving parents

who take care of me and teach me

in their simple ways

Table of Contents

1. Introduction

Exhaust system of an automobile is a complex assembly and often ignored part comprising of various components, performing important tasks in aggressive conditions. The exhaust system can be divided into two parts, namely the hot (or front) end and cold (or rear) end [1]. There are varieties of material properties which are required in an exhaust system [2-5]. At the hot end, high temperature oxidation occurs, while at the cold end, corrosion due to external salts and internal condensate is a key factor.

Presently, a large number of high alloyed ferritic and austenitic stainless steels are commonly used worldwide by automotive exhaust manufactures [6-8]. In past, most commonly used materials were mild steels and aluminized steels. The reason behind this shift is to achieve a maximum life time in such components. They offer good corrosion prevention but it's very difficult to predict the long term behaviour of the material when submitted to real conditions [9].

Furthermore, presently there are a lot of activities within the automotive industry to find appropriate ferritic stainless steels in order to substitute austenitic alloys. This trend is compelled due to the high price of nickel. Generally, material selection in the automotive exhaust industry is done on the basis of pitting resistance equivalent number PREN. The pitting resistance equivalent number (PREN or PRE) was introduced as an attempt to compare the pitting resistance of corrosion resistant stainless steels. The concept of the pitting resistance equivalent has been used extensively over the years [10-13]. It is generally agreed that higher the PREN value the better the pitting corrosion resistance [14-19].

The life time of a muffler is shorter as compared to any other part of an exhaust system. Of all automotive exhaust failures, about 80% are caused by corrosion and oxidation while the majority of the remainder is caused by fatigue [20]. In figure 1 some examples from field are given. It can be seen that the parts showed corrosion attack even after a short period of time. This unique phenomenon of crevice corrosion was frequently observed during field investigation. This problem is more common in double sheet mufflers. Even after a very short mileage, lot of systems suffered from this type of corrosion between the sheets without showing any signs of corrosion on outside.

The mechanism of crevice corrosion in stainless steels is well known from the literature. Crevice corrosion, on passive alloys, is a result of the degradation of a thin tenacious oxide layer, the passive film or layer, which is present on the surface of the alloy. Several interacting phenomena are involved in this process including: anodic dissolution and one or more cathodic reactions; mass transport to and from all metal-solution interfaces and in the electrolytic medium and chemical and electrochemical reactions in the crevice and bull solutions. The combination of these phenomena can produce a crevice a solution that has higher acidity and chloride ion content than the bulk solutions. If this solution has sufficiently low pH and high chloride ion content, the passive film may be destroyed, resulting in active corrosion. When this occurs, a critical crevice solution has developed and the alloy corrodes rapidly. Principally, this mechanism can also be observed in automotive exhaust systems but some additional periodic wet - dry cycles and sensitization of the material make it different from the classical mechanism.

Outer view after 24145 Km   Inner view after 24145 Km

Outer view after 989 Km   Inner view after 989 Km
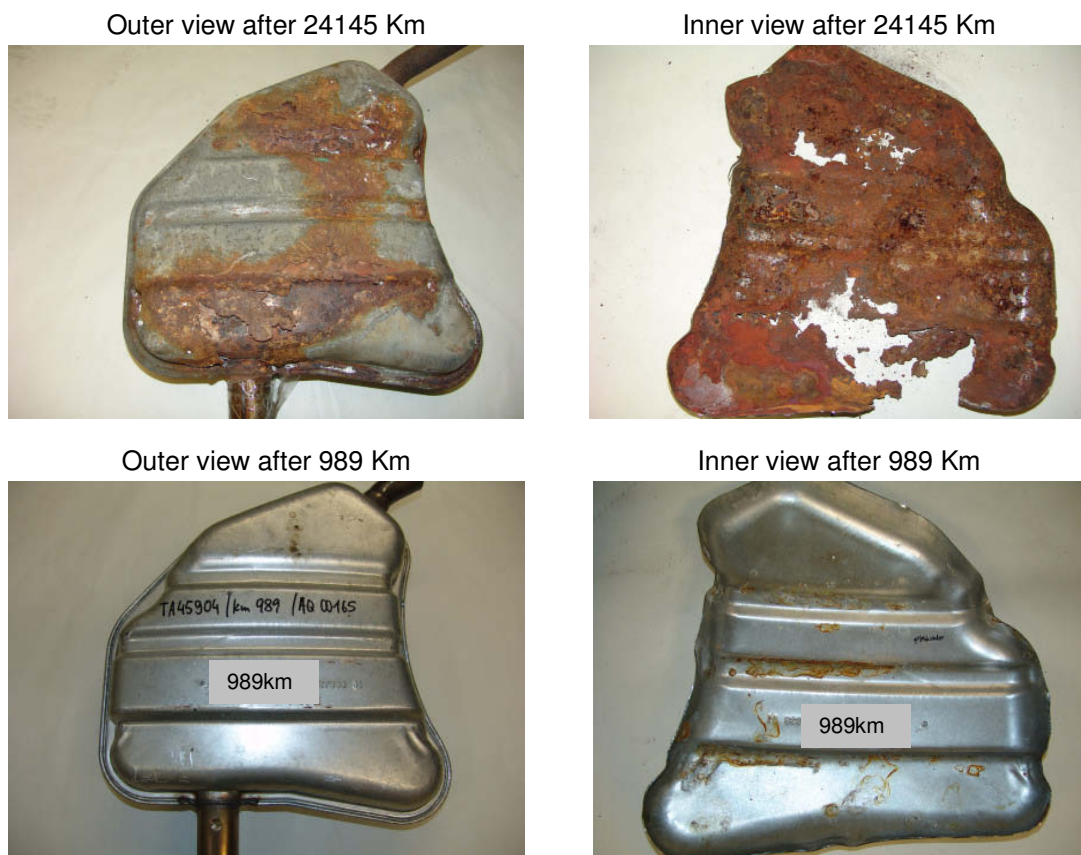
Figure 1.1: Field mufflers from material 1.4509 after different mileages

When specifying materials for use in exhaust systems, it is imperative that they exhibit sufficient corrosion resistance for the specific conditions to which exhaust components are exposed. It is therefore necessary to establish the corrosion behaviour of the materials in conditions and environments to which exhausts would typically come into contact with. Most car exhaust manufacturers and material suppliers have specific corrosion testing methods which they use to determine the corrosion resistance of candidate materials, but unfortunately there appears to be no standard procedure for these studies. In a summary, correct testing methods are required for different scenarios in the exhaust system.

The effect of material sensitization on corrosion resistance of stainless steels is well understood from the literature. Besides, sensitization, materials in exhaust systems have to withstand different cyclic heating and cooling phases. There are no existing test methods and information available in automotive exhaust section.

Besides the properties of the materials, the design of the muffler itself has a big influence on its corrosion resistance. This was also observed from the results of the field studies. To predict the life time of a complete system under real conditions is always a difficult task and sometimes also uncertain. There is no test available in which simulation of material and design can be performed simultaneously.

In light of the questions that still remain concerning, this thesis looks separately at the influencing factors which accelerates the rate of corrosion and tries to assess possible impacts to increase the life expectancy of the mufflers by selecting proper material and design combination. Furthermore, this study seeks to contribute to the understanding of the crevice corrosion with additional heating and cooling cycles. In order to achieve this, the thesis addresses the following questions:

- How far the existing corrosion testing methods are relevant to the actual problem in practice? Are they correlated to the real issue?
- What is the influence of different crevice gaps on the rate of corrosion?
- To conduct experimental investigations on how temperature and the presence of chlorides affect crevice corrosion behaviour.
- To determine the applicable electrochemical measurement techniques to study this phenomenon.
- How does phenomenon of sensitization in stainless steels affect the rate of corrosion in crevices?

- To understand the interaction of sensitization and cyclic heating impacts.
- To design and set up an experimental testing setup which could be used for life time estimation of real parts having different material and design combinations.
- To determine the chemical composition and morphology of corrosion products generated on the field parts and parts after artificial tests.

2. Literature Survey

2.1 State of the Art

There is no fixed standard criterion for material selection for various components of exhaust components. In some cases, materials are selected on the basis of PREN value and in other some existing corrosion testing methods are used for the relative ranking among different grades. These test procedures vary from one exhaust manufacturer and material supplier to the other where everyone has their own standard. Similarly, correlation of these testing methods with field often leads to a disagreement. The reason that these methods do not accurately reproduce corrosion performance for automotive exhaust parts because they cannot simulate the conditions in which automotive parts must exist. As it's mentioned in section 1 that crevice corrosion is one of the biggest problems due to which exhaust components have a very limited lifetime despite of high grade stainless steels.

The mechanism of crevice corrosion is well known from the literature. In 1922, R.J. McKay was the first researcher to demonstrate that crevice corrosion is a serious corrosion hazard [21]. Later, in 1925 he defined electrolytic concentration cells, in which the cell was powered by potential difference, a result of two electrodes of the same material in different electrolytes [22]. In the following years, an increasing number of researchers studied the mechanism of crevice corrosion due to its potential serious influence on various materials. Various researchers have made attempts to examine the problems of crevice corrosion as well as propose mechanisms for its progression [23-28]. Majority of the literature findings also show the results based on electrochemical tests and some other monitoring methods in artificial crevices. The reproducibility of the results, namely, the corrosion initiation and propagation rate, has always been a problem in crevice corrosion studies.

Single crevices have been fabricated by various researchers such as Alavi and Cottis [29] Klassen et al. [30], Wolfe et al. [31], Young et al. [32-33] and Bocher et al. [34]. The results obtained show significant variances in the crevice solution composition possibly arising from differences in the crevice geometry and experimental procedures.

2.1.1 The Artificial Crevice of Alavi and Cottis (1987)

Alavi and Cottis studied the potential, pH and chloride concentration variations in an engineered crevice of AISI 304 stainless steel and AA 7475 aluminum alloy, in 0.6 M bulk NaCl solutions. The crevice used in their experiment was built from a 304 SS plate with dimensions 80 mm long and 25 mm wide and encased in epoxy resin with a Perspex electrode holder as shown in figure 2.1.

(a)

(b)
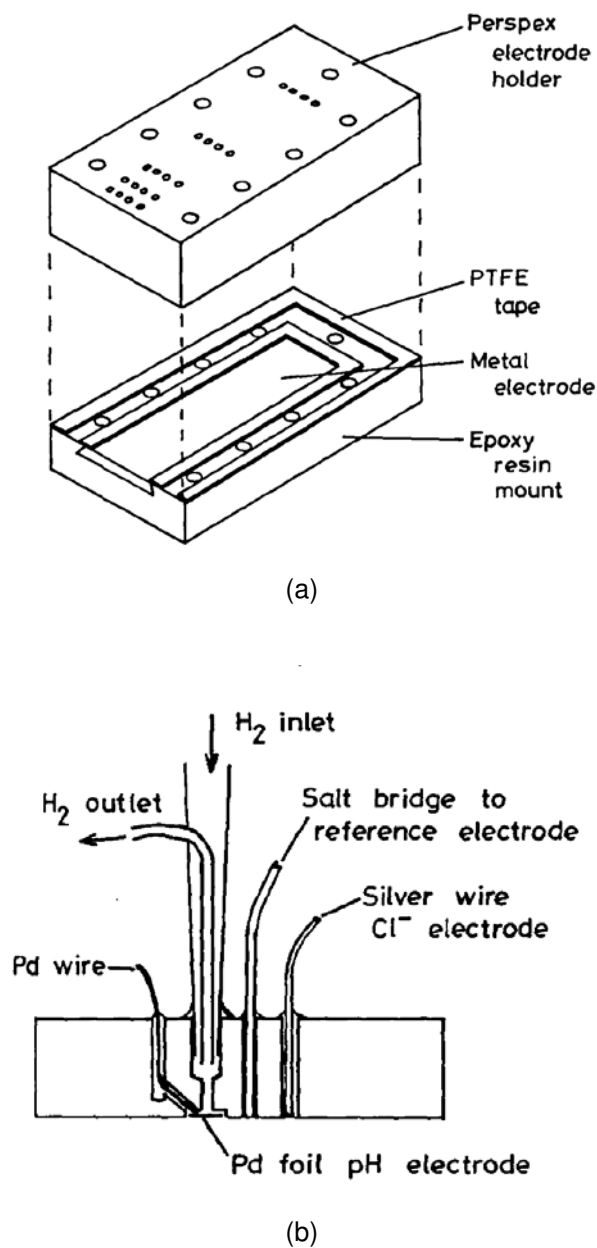
Figure 2.1: Schematic of artificial crevice in Alavi and Cottis's experiment [29]

The crevice gap was approximately 90 μm and the temperature of the electrolyte was set at 23 ± 1℃. pH values of 1-2 near the crevice mouth were measured for the 304 SS alloy and pH levels of 3-4 near the crevice mouth was measured for the AA 7475 aluminum alloy as well. Furthermore, a pH of near 8 was measured around the crevice tip for both stainless steel and aluminum alloys. Results from the experiments show that the external potential dropped slowly to positive (noble) values as time and distance from the crevice mouth increased for both metals. This indicates that both crevices were subject to anodic dissolution, due to reduction in the oxygen concentration of the crevice electrolyte compared with the oxygen concentration in the bulk solution. The potential drops between the external solution and the various parts of the crevice are plotted in figure 2.2 as a function of external potential.
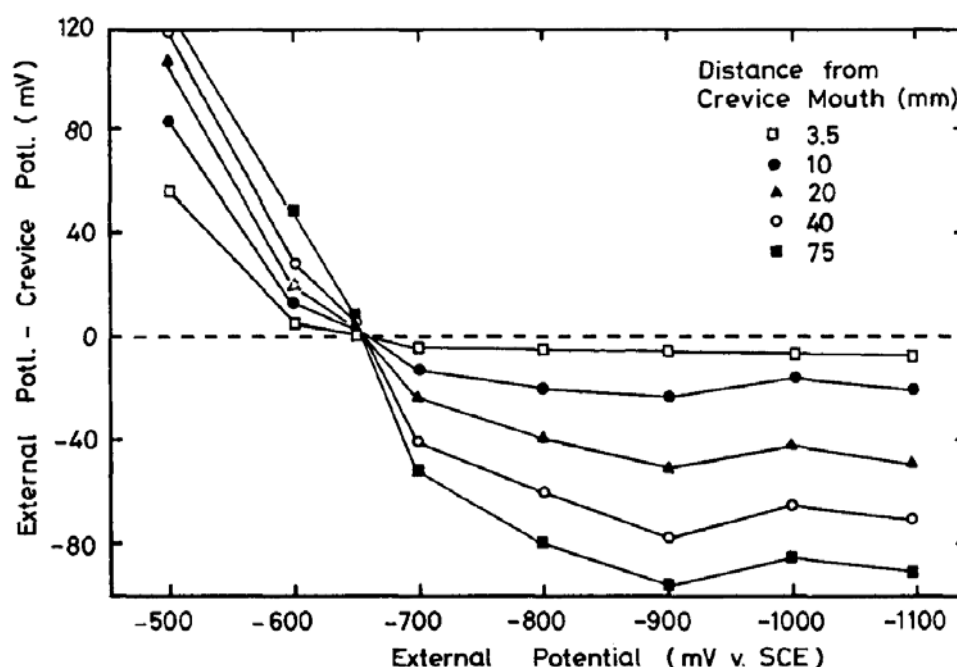
Figure 2.2: Potential Drop in Crevice v. External Potential [29]

2.1.2 The Artificial Crevice of Klassen et al. (2001)

Klassen et al. designed a test apparatus that allowed direct measurement of the corrosion current between the test specimen and the counter electrode, and the corrosion potential versus a reference electrode. The crevice design was a modification to the gap crevice design found in the literatures [29, 35]. The gap crevice design has the crevice width parallel to the specimen surface, whereas, the

crevice assembly designed for their study was such that the crevice was oriented perpendicular to the specimen surface by placing a crevice cover with a hole over the specimen. The test specimens were made of nickel-aluminum-bronze material embedded in a cylindrical epoxy mount as one part of the crevice, and the other part of the crevice plate made from Perspex® material. A conducting wire was attached to the metal epoxy block connected the potentiostat to the metal sample. The electrolyte used for their experiment was 3.5 wt% NaCl solution. A crevice hole of 0.18 mm diameter was drilled into the crevice plates as shown in figure 2.3.
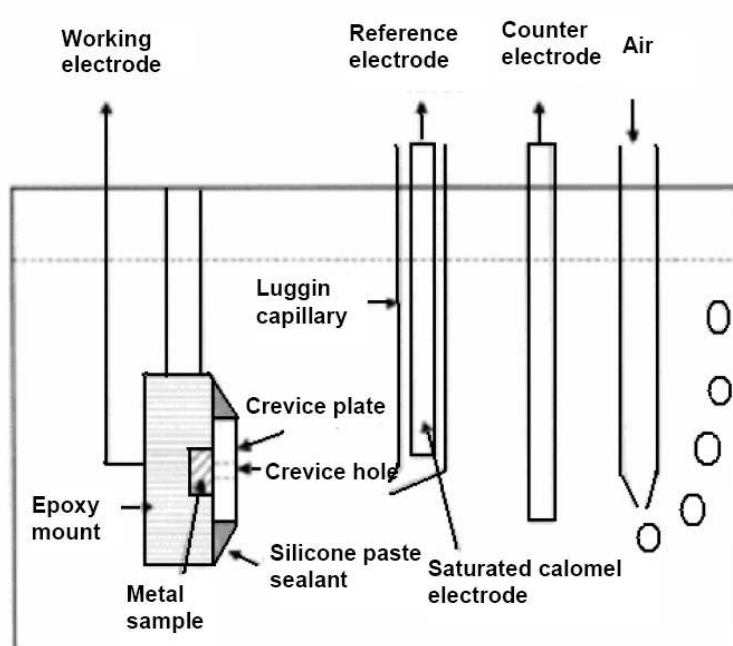
Figure 2.3: Schematic of the experimental crevice corrosion setup by Klassen et al. [30]

A positive shift in the specimen's potential that is consistent with the increase in equilibrium potential of the controlling anodic reaction was observed for this crevice gap. A similar observation was reported by Alavi and Cottis. Klassen et al.'s apparatus is relatively simple and easy to produce, and it is convenient to observe the solution in the crevice due to the transparency of Perspex®. However, it is doubtful that using a hole to simulate a crevice could really mimic the real crevice corrosion processes.

2.1.3 The Closed Crevice of Wolfe et al. (2006)

Wolfe et al. investigated the interaction of IR voltage, changes in pH, active peak formation and corrosion product accumulation during the induction period in delayed crevice corrosion of iron in 0.2 M Na_2SO_4 + 0.025 M $K_2Cr_2O_4$ with a pH of 9.1. A rectangular channel machined into a Plexiglas plate was placed against iron to form a crevice with an opening dimension of 0.06 cm, width of 0.5 cm, and depth of 11 mm as shown in figure 2.4. A pH/electrode microprobe was positioned in the crevice to measure in situ pH and the local electrode potential along a distance, x, on the crevice wall.
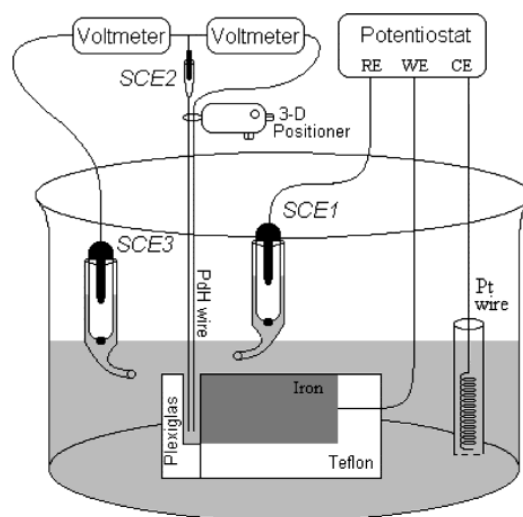
Figure 2.4: Schematic of crevice corrosion cell [31]

A platinum wire counter electrode and a standard calomel reference electrode were used. The crevice opening faced upwards and the bottom of the crevice was closed to prevent it from undergoing convective movement in and out of the crevice from the bulk solution. It was observed that as the pH decreased in the crevice solution, an active peak was observed in the polarization curve for iron.
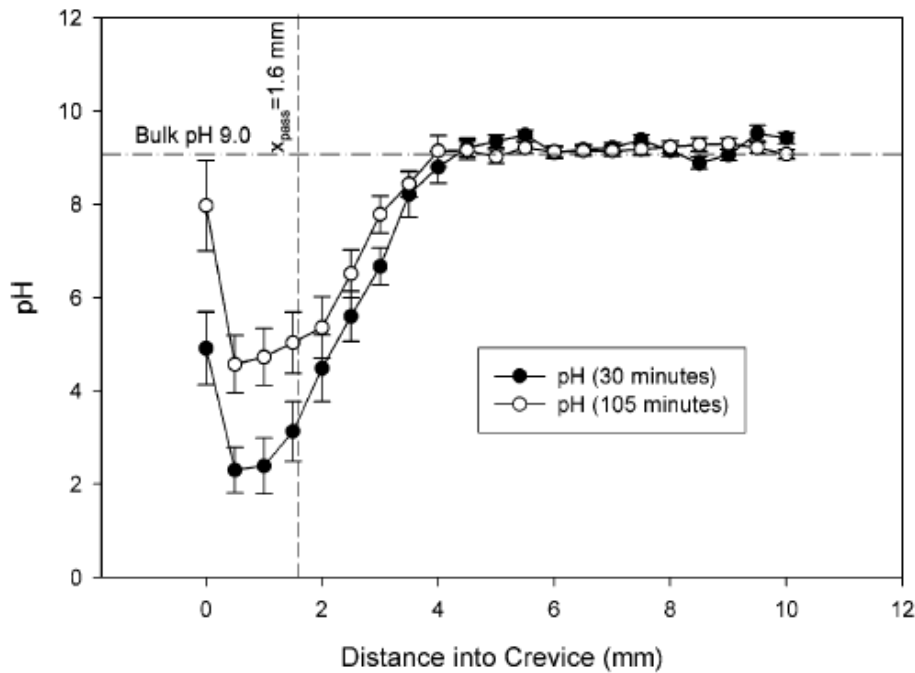
Figure 2.5: Profiles of pH for iron in 0.5 M Na_2SO_4 (a) 0.7 mm). A large decrease in pH is observed near the active region of the crevice wall [31]

2.1.4 Crevice with Microcapillary Tubing Method of Young et al. (2006)

In this experiment the potential drop inside the crevice was measured by inserting a microcapillary tube into it in order to examine the mechanism of crevice corrosion related to the IR drop. The 3×16 mm artificial crevice was formed in the same position on each sample and three different crevice widths were used, viz. 0.1, 0.2 and 0.5 mm and the crevices were formed using Plexiglas. The experimental sample containing the artificial crevice and the microcapillary tube placed in the crevice are shown in figure 2.6. The electrode potential on the crevice wall could be measured by positioning the microcapillary tube at the vertical boundary on the crevice wall.
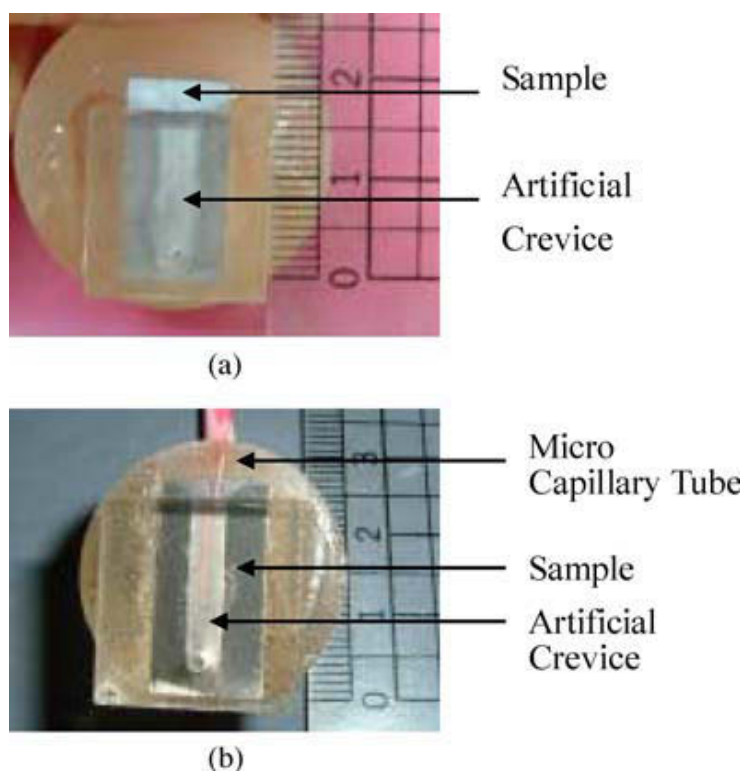
Figure 2.6: Experimental sample used for crevice corrosion test; (a) crevice corrosion sample, and (b) assembly of microcapillary tube & sample [32]

The crevice corrosion initiation time shortened and the current density values increased as the width of the crevice decreased, but no crevice corrosion was observed when the width of the crevice was 0.5 mm. The relations between the current density and time for the crevice corrosion of various widths are shown in figure 2.7. It was confirmed that the critical crevice size for initiating crevice corrosion is between 0.2 and 0.5 mm.
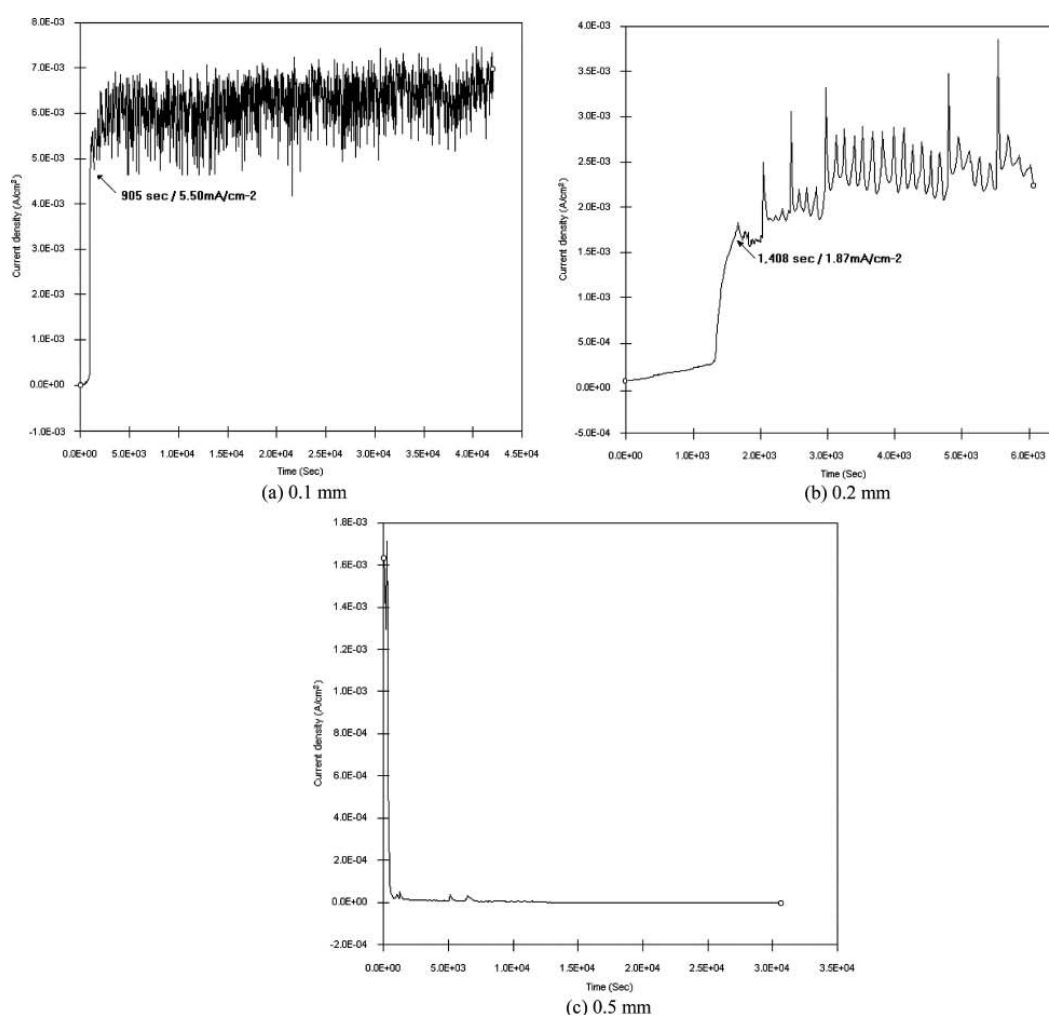
Figure 2.7: The relation between the current density and time for the crevice corrosion of 430 stainless steel in 1 N H_2SO_4 + 0.1 N NaCl at 20°C with a crevice size of 3×16 mm and various widths; (a) 0.1 mm, (b) 0.2 mm, and (c) 0.5 mm [32]

2.1.5 The Multiple Crevice Assembly of Bocher et al. (2008)

Bocher et al. monitored the anodic current evolution as a function of position during crevice corrosion initiation and propagation of AISI 316 and Alloy 625 stainless steel in an aerated 0.6 M NaCl solution at 50°C. The crevice assembly consisted of 100 wires of alloy 625 and 316 stainless steel respectively, each wire with diameter of 250 μm, inserted into a groove in a 2.54 cm AISI 316 stainless steel rod and polyformaldehyde (Delrin) in the case of alloy 625. Figure 2.8 displays the array of wires encased in an AISI 316 stainless steel rod.
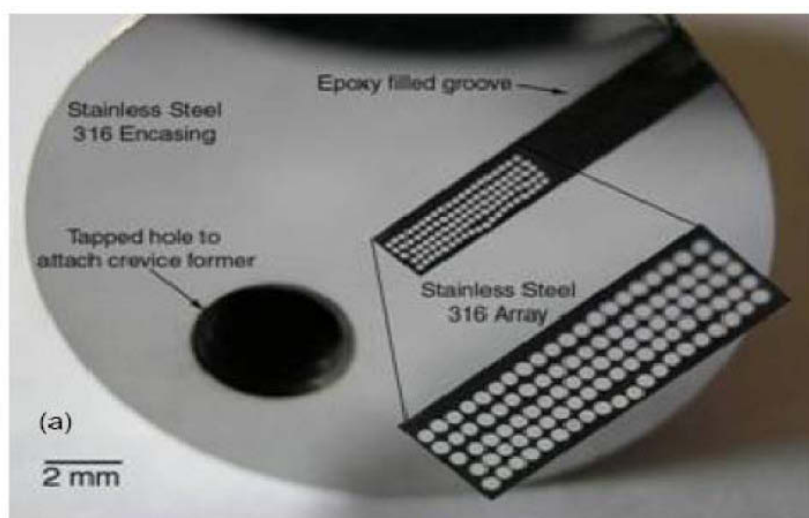
Figure 2.8: Close packed array of one hundred 250 μm diameter wires of AISI 316 stainless
steel mounted in a 5x20 arrangement in AISI 316 stainless steel rod [33]

The arrays of wires were coated with a poly-imide film to ensure electrical insulation. The crevice was designed to cover 12 columns of 5 wires leaving remaining 8 columns open to bulk solution. The crevice array was immersed in the heated solution for 2 days at the open circuit potential to allow passive film stabilization and solution wicking into the whole crevice. Crevice corrosion was found to be readily initiated close to crevice mouth at $X_{crit} = 0$ for 316 stainless steel. X_{crit} is the distance from the crevice mouth to the location where the potential reaches a critical passive potential value, E_{flade}, on the crevice wall. E_{flade} is defined as the lowest potential in the passive region below which marks a steep fall from the passive region to the active region.

However, crevice corrosion was observed to initiate further inside the crevice for Alloy 625, at the distance where the potential reached a critical passive potential value, E_{flade}, on the crevice wall. This was in agreement with the prediction that if the flade potential, E_{flade}, is greater than the applied potential E_{app}, then crevice corrosion occurs at the mouth, but if the E_{flade} is less than E_{app} with a significant IR drop in the system, then crevice corrosion will initiate at a fixed distance from the crevice mouth [36].

In spite of various studies, there is little understanding on the process that occurs during the onset of stainless steel crevice corrosion. All literature findings also show

the results based on electrochemical tests and some other monitoring methods in artificial crevices. Furthermore, studies involving the electrochemical evaluation of crevice corrosion are limited by the small size of the crevices. In addition, despite the increasing consumption of stainless steels in exhaust components, no research has been done on crevice corrosion. The other reason which makes the current research problem totally unique from the others is an additional effect of sensitization and periodic heating cycles on stainless steels.

2.2 Automobile Exhaust Systems

Exhaust system of an automobile is a complex assembly and often ignored part of various components, performing important tasks in harsh conditions. It performs four distinct jobs: controlling noise, directing fumes away from the people travelling in the car, improving the performance of the car's engine, and last but not least is improving fuel consumption. The exhaust system can be divided into two parts, namely the hot (or front) end and cold (or rear end) [1]. The hot end includes the manifold, downpipe and catalytic converter. The cold end includes the resonator, intermediate pipe, muffler and tail pipe. Figure 2.1 shows this configuration and the associated temperature scale for each component.
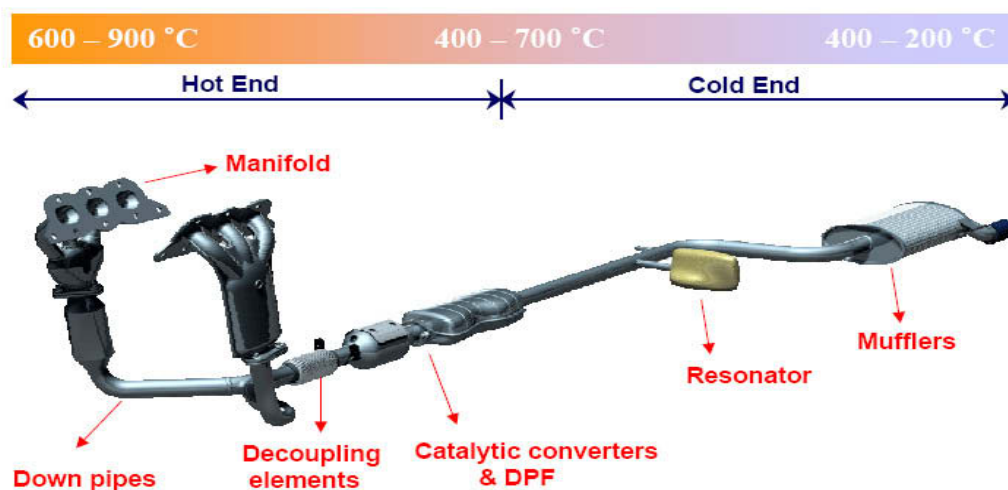
Figure 2.9: Schematic of a complete exhaust system

All major components including their functions and operating conditions are discussed in detail:

2.2.1 Hot End Components

In the hot end near the engine, high-temperature strength, good thermal fatigue properties, oxidation resistance, low coefficient of thermal expansion and good impact properties in cold start conditions at high temperatures are the required features [5, 37]. The important hot end components are:

2.2.1.1 Exhaust Manifold

In creating the power to drive most piston engine vehicles, the engine produces extremely hot exhaust gases from each cylinder. The exhaust manifold is directly mounted to the engine and collects the exhaust gas from each of the engine cylinders and delivers it to the down pipes. The manifold has been traditionally made of cast iron [5, 38]. However, due to some essential required properties (e.g. good oxidation resistance) and vehicle requirements (e.g. light weight); presently stainless steels are used worldwide. Some important properties required in an exhaust manifold are oxidation resistance, thermal fatigue strength, good workability and weldability for manufacturing [37].

2.2.1.2 Down Pipe

The down pipe is attached to the exhaust manifold for the purpose of minimizing heat radiation and thus preventing the cooling down of exhaust gas, to ensure that the activity of the catalytic converter does not decrease. Furthermore, the noise level should be lowered. Due to these reasons, materials used for this part of an exhaust system need to cope with higher exhaust gas temperatures and hence should have good high temperature resistance.

2.2.1.3 Decoupling Element

The decoupling element, which is also known as flexible pipe, is the continuation of the down pipe. Its function is to control the vibration from the engine to the following parts of the exhaust system. It consists of a bellow-shaped double pipe and is cladded with a stainless steel wire mesh. The decoupling element may also be subject to a severe external environment especially in areas where de-icing salts are

used on roads to prevent freezing in winter times. This high temperature salt corrosion with high temperature fatigue could deteriorate this part.

2.2.1.4 Catalytic converter

The presence of catalytic converter is mandatory because of global emission regulations. It is located below the exhaust manifold and its function is to diminish the air pollution induced by automobile exhaust gas. The effect of the catalytic converter is based on the conversion of hydrocarbons and carbon monoxide into carbon dioxide and water, and nitrogen oxides (NO_x) into nitrogen and oxygen. Due to its position in the exhaust system, the employed stainless steel has to resist severe service conditions of high temperature, salt damages and vibrations.

2.2.2 Cold End Components

The required properties for cold end materials are good weldability, corrosion resistance to external salt solution and internal condensate, good formability, attractive cosmetic appearance, fatigue strength and noise reduction. The primary cold end components are:

2.2.2.1 Muffler/Silencer

The muffler or silencer is the main source in an exhaust system whose function is silencing the exhaust gas noises, by absorbing and dissipating noise pulses while moving the exhaust gases and vapour smoothly through and ultimately out of the tail pipe. It consists of tuning chambers, formed by partitions and ventilated or solid tubes. Rock (mineral), wool, fiber-mat, or fiber glass roving placed in the muffler cavities serves to further absorb and eliminate unwanted exhaust sounds. Most mufflers are located towards the rear of the vehicle, but the location of a muffler inside an exhaust system varies considerably depending on the vehicle models. Mufflers can be of many shapes from round to oval, to custom stamped, but internal muffler design is determined by frequency of the noises that needs to be controlled.

2.2.2.2 Tail end pipe

The tail pipe is located behind the rear muffler and it's the final outlet of an exhaust gas. It ensures that exhaust gas is emitted past the end of the body of a vehicle. The materials used in manufacturing the tail pipe and the corrosion suffered by the tail pipe are similar to that of the muffler, since they are both subjected to similar

conditions. The cosmetic appearance of stainless steel especially in the tail pipe is vital since most of the time it's the only visible part of the exhaust system. Therefore, besides the requirement for a good resistance against wet corrosion, a good optical appearance is also required.

2.3 Stainless Steels in Exhaust Systems

There are varieties of material properties which are required in an exhaust system [2-4]. At the hot end components high temperature oxidation occurs, while at the cold end corrosion due to external salts and internal condensate is of prime importance. Table 2.1 gives an example for a typical material selection with regard to the different components and temperature ranges.

Table 2.1: Overview of components and materials

Components	Exhaust Manifold	Manifold Pipe	Catalytic Converter	Intermediate Pipe	Front Muffler	Rear Muffler	Tail Pipe
	Hot End			Cold End			
Gas-Temp. [℃]	1050-800	800-600		600-500	500-200		
Ferritic	1.4509 1.4513	1.4509 1.4513	1.4509 1.4513	1.4512 1.4509	1.4113 1.4509	1.4512 1.4509	1.4509 1.4513
Austenitic	1.4301 1.4828	1.4301 1.4828	1.4301 1.4541	1.4301	1.4301 1.4541	1.4301 1.4541	1.4301 1.4541

Stainless steels were invented almost a century ago by Monnartz [39]. Today, their use is increasing at an average rate of about 5% per annum. The ASM handbook [40], the Steel handbook [41] and the books by Peckner and Bernstein [42], Marshall [43] and by Lula [44] cover different types of stainless steels. Stainless steels are iron-based alloys with a minimum chromium content of approximately 11%, to prevent the formation of rust in the atmosphere. Chromium plays an essential role in the passive layer stabilization. It is more oxidable than iron and forms together with oxygen an invisible and adherent chromium rich oxide surface film. This layer has a low ionic permeability, decreases the metal dissolution to a very negligible value and heals itself in the presence of oxygen or other oxidizing species in certain media. Stainless steels also have additional elements including nickel, molybdenum, nitrogen and others to improve particular characteristics. Stainless steels are

primarily classified in five main categories according to their crystal structure and strengthening precipitates: Austenitic, Ferritic, Martensitic, Precipitation hardened and Duplex stainless steels. Each family exhibits its own general characteristics in terms of mechanical properties and corrosion resistance. Within each family, there is a range of grades that vary in composition, corrosion resistance, properties and costs [45]. Exhaust systems today are manufactured from both ferritic and austenitic steels. In following sections, differences between these two types of stainless steels and the influence of different alloying elements on their different properties are discussed.

2.3.1 Ferritic Stainless Steels

Ferritc stainless steels are the simplest type of stainless steels. Due to their adequate corrosion resistance and lower cost, sometimes ferritic stainless steels are preferred over high cost austenitic stainless steels. Ferritic stainless steels have a body-centred cubic (bcc) crystal structure and contain between 11 to 30% Cr, with few amounts of austenite forming elements, like carbon, nitrogen and nickel. They are magnetic and cannot be hardened by heat treatment [46]. In general, ferritic stainless steels do not have particularly high strength. Their poor toughness and susceptibility to sensitization limit their ability for fabrication, but they have a good resistance against chloride stress-corrosion cracking, atmospheric corrosion and oxidation and are available at relatively low cost.

2.3.2 Austenitic Stainless Steels

Austenitic stainless steels are famous for their high corrosion resistance, ability to strain and account for 60% of stainless steel usage all over the world. They are non-magnetic and like the ferritic alloys, cannot be hardened by heat treatments, but by cold working and have a face-centred cubic (fcc) crystal structure. They possess excellent ductility, formability and toughness, even at cryogenic temperatures [47]. Austenitic stainless steels have high nickel contents to stabilize the austenite at room temperature. To stabilize the austenite, nickel is the main element, but also carbon and nitrogen are used for this purpose, because of their solubility in the fcc structure. Austenitic stainless steels contain 17-18% Cr, 8-15% nickel and may contain additional Mo to increase their corrosion resistance. These steels provide a good stability against low and high temperatures but their major drawbacks are their low mechanical strength and their high susceptibility to cost variations.

2.4 Influence of Alloying Elements

Different stainless steel grades exhibit different mechanical properties and corrosion resistances. Both of these properties are partially influenced by the chemical composition of the different grades, due to the differences in the contents of alloying elements. The effect of the most important elements is described in this section.

Chromium (Cr) is a ferrite former, meaning that the addition of chromium stabilizes the body-centred cubic structure of iron. To form an austenitic structure at higher chromium contents, more nickel is necessary. Austenitic stainless steels usually contain chromium content of 17% or higher to maintain good corrosion resistance properties. The chromium reacts with the oxygen, forming a 1-10 nm thick protective passive film of chromium oxide. Chromium increases oxidation resistance at elevated temperatures [48-49].

Nickel (Ni) is an austenite stabilizer, its addition to iron-based alloys leads to a change of the crystal structure of stainless steels from body-centred cubic (ferritic) to face-centred cubic (austenitic). Their face-centred cubic structure is the reason for the excellent toughness. Nickel increases yield strength, toughness and the resistance in reducing environments by promoting repassivation. The 300-series austenitic stainless steels contain at least 8% nickel. Increasing nickel content beyond 8-9% further improves both corrosion resistance and workability.

Molybdenum (Mo) stabilizes ferrite and when added to improve corrosion resistance to steel formulated to be fully austenitic, its effect must be compensated by reducing the chromium content and increasing the nickel content. Molybdenum also replaces some of the chromium in the complex carbides, $Cr_{23}C_6$ and Cr_7C_3. Unfortunately, high molybdenum contents promotes sigma-phase formation in austenitic as well as in ferritic steels and therefore molybdenum contents in stainless steels are normally restricted to <3.5% [47].

Nitrogen (N) enhances austenite stability and is the most effective solid solution strengthening element. It increases the resistance to localized corrosion like pitting or intergranular corrosion. The latter is due to the formation of Cr_2N instead of $Cr_{23}C_6$. It

can be used to replace the expensive nickel in the austenitic stainless steels. The nitrogen enhanced austenitic stainless steels also have increased toughness, because of their higher strength.

<u>Manganese (Mn)</u> is an austenite former and it's a strong oxide and sulphide former (MnO and MnS). It is usually added to improve deoxidation and to prevent formation of sulphide inclusions, which might cause hot cracking.

<u>Silicon (Si)</u> improves the corrosion resistance and prevents carburizing at high temperatures. It is a ferrite stabilizer.

<u>Carbon (C)</u> is a strong austenitizer and increases the strength by solid solution strengthening. It is kept at low levels in austenitic steels to retain desired properties, as it might form chromium carbides depleting the material from chromium and thus reduce the corrosion resistance.

<u>Titanium (Ti)</u> and other strong carbide formers (Nb, V) are used to stabilize the steel and to avoid $Cr_{23}C_6$ precipitation [50]. It's a ferrite stabilizer.

<u>Niobium (Ni)</u> increases strength [51-53], develops good textures [54], improves surface quality [55] and increases formability [56]. The main benefit of the niobium is its ability to suppress recovery, recrystallization and grain growth in steels. This occurs from both niobium in solid solutions and niobium in precipitates [57, 58]. It's a ferrite stabilizer.

2.5 Passivation

All metals and alloys (it is commonly held that gold is an exception), have a thin protective corrosion product film present on their surface resulting from reaction with the environment. If such a film did not exist on metallic materials exposed to the environment, they would revert back to the thermodynamically stable condition of their origin, the ores used to produce them. These protective "passive" films are responsible for the phenomenon of passivity [59, 60].

The reason for a good corrosion resistance of stainless steels is that they form a very thin, invisible surface film in oxidizing environments. This film is an oxide that protects the steel from attack in an aggressive environment. All stainless steels have a thin (1-10nm) protective film present on their surface resulting from reactions with the environment [61-63]. As chromium is added to steel, a rapid reduction in corrosion rate is observed because of the formation of this protective layer or passive film. An example is shown in figure 2.10. In order to obtain a compact and continuous passive film, a chromium content of at least 11% is required. Passivity increases fairly rapidly with increasing chromium content up to about 17% chromium. This is the reason why many stainless steels contain 17-18% chromium. Some schematic passive oxide films are shown in figure 2.11 for some metals and alloys.
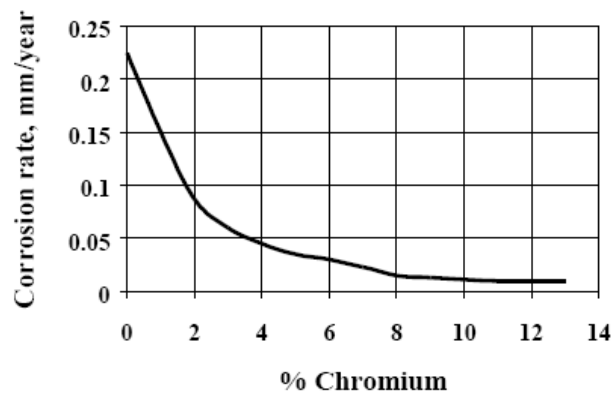
Figure 2.10: The Effect of Chromium Content on Passivity [64]
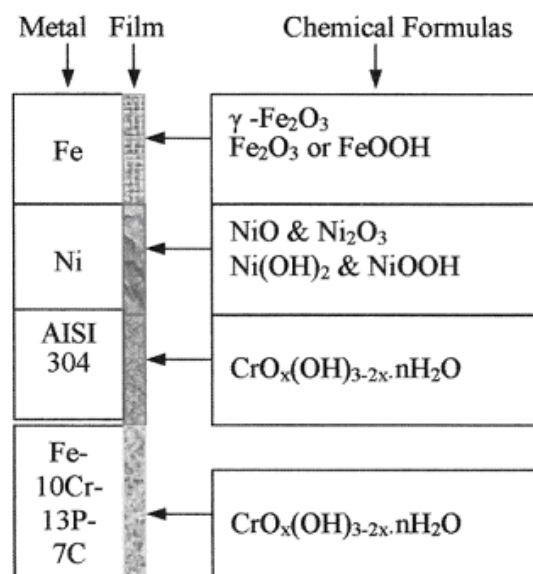

Figure 2.11: Schematic Oxide Passive Films [65]

During passive film formation, an oxide, oxyhydroxide or hydroxide film is produced by the precipitation of dissolved metal ions. Cr is enriched at the outer surface of the steel and OH⁻ anions of the medium absorb onto the surface, what results in a formation of chromium hydroxide:

$$Cr \rightarrow Cr^{3+} + 3e^{-} \hspace{3cm} \text{(Equation 2.1)}$$

$$Cr^{3+} + 3H_2O \rightarrow Cr(OH)_3 + 3H^{+} \hspace{2cm} \text{(Equation 2.2)}$$

Then the $Cr(OH)_3$ dehydrates at the inner part and forms chromium oxide, which is more protective. For a given aggressive media, oxidation kinetics of steel compounds is different. In particular, oxidation kinetics of iron is higher than of chromium so that chromium enrichment happens at the material surface after preferential dissolution of iron. The passive layer should be continuous, non-porous, insoluble and self-healing if it's damaged. If passivity is destroyed under conditions that do not permit the restoration of the passive film, then stainless steels will corrode more like a carbon or low-alloy steel [66].

Passivity of iron has been long recognised [67-68]; the modern theories concerning the passivating oxide film are primarily due to Evans [69]. Passivity of a metal lies in contrast to its activity, in which the metal corrodes freely under an anodic driving force. The passive state is well illustrated by reference to a classical polarisation curve prepared potentiostatically or potentiodynamically as shown in figure 2.12.
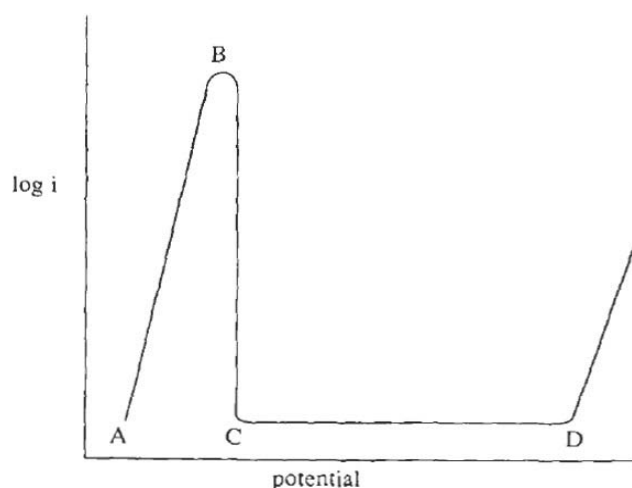
Figure 2.12: Schematic anodic polarisation curve for a metal. Region AB describes active dissolution of the metal. BC is the active/passive transition, with passivation commencing at B. Passivation is complete only at potentials higher than C. The metal is passive over the range CD [70]

As the potential is raised (in the anodic or positive sense) above the equilibrium potential between the metal and its dissolved ions, so the driving force towards oxidation increases and the rate of dissolution increases, in the classical case representing an exponential rise of current with potential [70]. When the potential is high enough, a dramatic reduction in the dissolution rate occurs, and the rate of dissolution remains low with further increase in potential. This latter state is the state of passivity, and the minimum potential at which the low oxidation rate exists is the passivation potential. The state of passivity is never perfect, and a passive metal always corrodes at a finite rate, albeit that this rate may be very low. The surface film forms a barrier between the metal and its environment, which retards further oxidation. Raising the potential in the passive state, while increasing the driving force towards oxidation, serves to thicken the surface oxide film, thereby increasing the barrier towards further oxidation. It is this increase in the barrier film thickness with increase in potential which generates the potential-independence of the oxidation rate as long as the metal remains passive.

2.6 Corrosion of Exhaust Systems

The corrosion protection of automotive exhaust systems is a problem of great economic importance. Costs due to the corrosion of different components are very high. Exhaust systems degrade both by structural and cosmetic corrosion. Structural corrosion involves deterioration of exhaust components, while cosmetic corrosion involves rust staining and minor corrosion of the exhaust components [71]. The exhaust systems of vehicles are exposed to two different environments: externally to the atmosphere and internally to exhaust gases with their products of combustion [72]. It has also been found that in exhaust systems corrosion occurs in four out of five cases of failures while fatigue accounts for the remainder [73]. All the major degradation problems like high temperature oxidation, internal corrosion, external corrosion, material sensitization and oxidation are discussed in the following sections:

2.6.1 High Temperature Oxidation

Stainless steels can react at elevated temperatures with hot gases, like exhaust gas, without presence of aqueous electrolytes. This form of corrosion is called high temperature oxidation or scaling and generally occurs in hot end components. The

materials with oxygen form a chromium oxide (Cr_2O_3, chromia) film. This oxide film may be protective and persist for a finite time after which scale breakaway occurs and thereafter a scaling rate develops. Consequently, oxides formed at higher temperatures loose their adherence to the substrate alloy when cooled to lower temperatures and become non-protective when reheated [74-76]. Oxides have coefficients of thermal expansion that differ from those of the metals from which they have formed. Therefore, stresses develop when the temperature changes, particularly during running and stopping of the vehicle [77-79]. The oxide film converts into a nonprotective scale with various defects including cavities, microcracks and porosity as shown in figure 2.13.
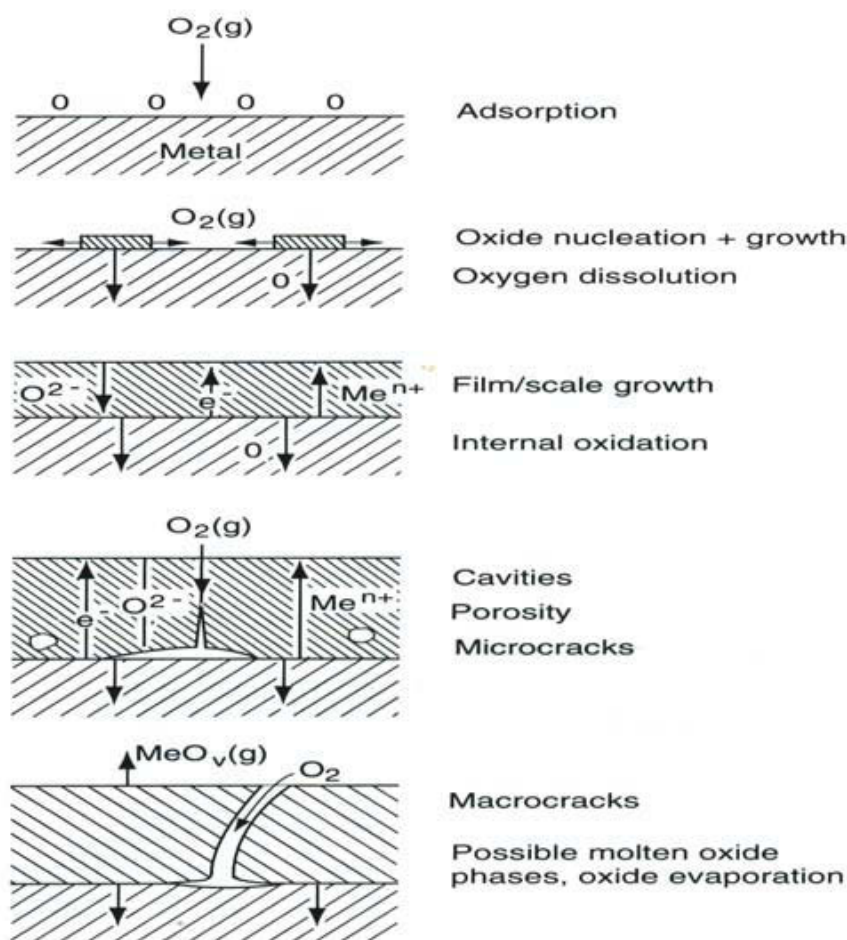
Figure 2.13: Film and scale formation during high-temperature metal oxidation [75]

Hence, the resistance to high temperature corrosion of materials depends on the development of a protective layer and its chemical, thermal and mechanical

properties. In general, damages caused by high temperature corrosion have less relevance compared to damages caused by wet corrosion. The reason for this is that deep knowledge about stability limits of materials at high temperature is available. A stainless steel grade is resistant to high temperature corrosion if it has an adequate oxidation resistance, appropriate mechanical properties, like high temperature strength, creep strength, ductility and formability. The established layers should not crack or lift off under cycling temperatures.

2.6.2 Internal Corrosion

Inside the cold end components, a relatively low exhaust gas temperatures lead to aggressive condensate formation. Condensate corrosion is the major cause for degradation of stainless steels particularly on the internal surfaces of the cold end components. The condensate usually consists of NH_4^+, CO_3^{2-}, SO_4^{2-}, Cl^-, organic acids and many other substances originating in components of the exhaust gas [80, 81]. Condensate may also contain salts like NaCl, coming as fine dust from the road through the combustion chamber. Investigations have shown that the variation of the pH value is extraordinary high, ranging from mildly alkaline to appreciably acidic. The concentration of these ions is less in the beginning of condensation and increase with the time [82]. This is because the condensate volume changes as water evaporates during the stoppage or the combustion during running of the engine [83-86].

Table 2.2 shows that composition of the condensate in the diesel and petrol engine differs. These compositions were obtained by analysing condensates from the silencer. It can be also seen in table 2.2 that the exhaust gas condensate of petrol engines with a catalytic converter is neutral, while those in petrol engines without a catalytic converter and in diesel engines are highly acidic. If the vehicle is continually driven over short distances or in 'stop and go' conditions, the rate of corrosion will accelerate, as the exhaust system is unable to reach condensation evaporation temperature. This is a key factor in premature corrosion-induced failure of exhaust systems.

Table 2.2: Physical characteristics and chemical composition of representative exhaust gas condensates [87]

Type of Engine	PH value	SO_4^{2-}	Cl^-	NH_4^+	NO_3^-	NO_2^-	PO_4^{3-}
		(ppm)					
Petrol Engine with catalytic converter (unleaded)	6.5	15	2.2	60	10	110	<0.1
Petrol Engine without catalytic converter (unleaded)	3.2	320	4.2	1.1	<2	0.16	<0.5
Petrol Engine with catalytic converter (leaded)	3.6	-	23.5	-	-	-	-
Diesel Engine with catalytic converter	2.9	41	2.9	<0.1	18	<0.01	0.19
Diesel Engine without catalytic converter	2.4	175	52	<0.1	35	<0.01	1.3

Internal corrosion is a major problem in cold end components because their temperature is much lower than the hot end, which leads to exhaust gas condensation in the cold end creating aggressive conditions. Internal corrosion is evaluated by performing tests like condensate tests often called dip and dry tests. During vehicle operation, as condensate forms in the cold end, one of three scenarios can occur: 1) once the condensate comes in contact with the surface of the components, it evaporates immediately without reducing the temperature of the components; 2) the condensate evaporates but reduces the temperature of the components: 3) when the condensate forms, it does not evaporate [37]. The dip and dry test is widely used in the automotive industry for accelerated cyclic corrosion tests in changing wet, humid and dry environment [1, 88, 89].

2.6.3 External Corrosion

In colder countries, during severe winter conditions, de-icing reagents are used to maintain efficient road usage. These de-icers have been found to be a major contributor in corrosion of exhaust systems [90, 91].This type of corrosion is experienced by both the hot and cold end components. Road de-icing salts locally destroy the protective chromium oxide layer and result in localized attack if kept in contact with the components for a longer period of time.

De-icing is a process by which a de-icer (like rock salt) is used to penetrate through the accumulation of snow and ice to break its bond with the pavement. Once this bond is broken, the road can be plowed [92]. If ice bonds with pavement, it cannot be removed by plowing without damaging the road surface or plowing equipment. The Salt Institute provides a simple description of how salt works [93]: The whole mechanism is also explained in figure 2.14.

1. Salt is applied to roads, which lowers the freezing point of water.
2. Salt melts through snow and ice, and forms liquid brine below the surface of snow/ice which prevents bonding with pavement.
3. Due to the action of the brine, the bond between the ice/snow and the road surface begins to weaken as the ice melts. Eventually the bond is broken and the remaining ice/snow floats on the brine layer rather than on the road surface
4. Traffic breaks through surface of snow/ice, reducing it to a plowable slush which is gradually moved to the roadsides.
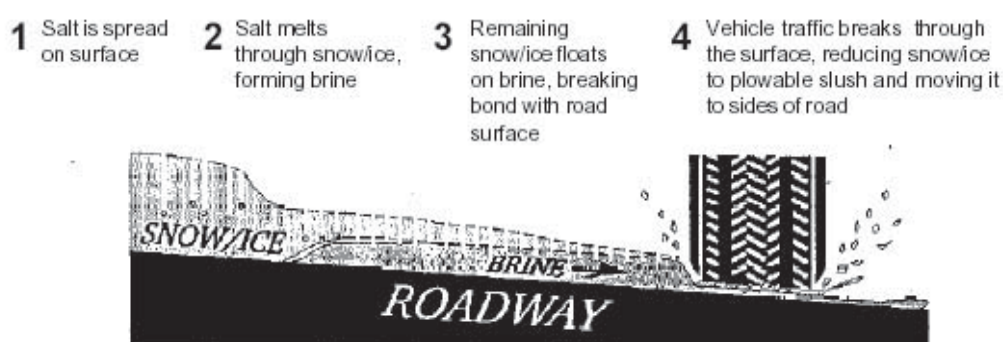
Figure 2.14: The Role of Salt in Ice Removal [93]

Sodium chloride is not the only salt used for de-icing. Sodium chloride dissolves into two types of particles: one sodium ion and one chloride ion per sodium chloride 'molecule'. A compound that yields more ions into water would lower the freezing

point of water more than rock salt. For example, calcium chloride ($CaCl_2$) dissolves into three ions (one of calcium and two of chloride) and lowers the freezing point of water more than sodium chloride. Table 2.3 shows an example of some de-icing alternatives which are used in various combinations and concentrations in common practice. Combinations of those salts are more aggressive than pure NaCl due to the acidic character of $MgCl_2$ and $CaCl_2$. In Germany, 5 weight% of a 12:1 mixture of NaCl and $CaCl_2$ is commonly used [89].

Table 2.3: List of some de-icing reagents [94]

Substance	Formula
Sodium Chloride (rock salt)	NaCl
Magnesium Chloride	$MgCl_2$
Calcium Chloride	$CaCl_2$
Potassium Chloride	KCl
Urea	NH_2CONH_2
Calcium Magnesium Acetate (CMA)	$CaCO_3$, $MgCO_3$ and CH_3COOH
Ammonium Sulfate	$(NH_4)_2SO_4$
Potassium Acetate	CH_3COOK

2.6.4 Types of Localized Corrosion

Stainless steel and its alloys are widely used in industrial systems due to their excellent corrosion resistance properties. However, they are more susceptible to localized corrosion than uniform corrosion in aggressive environments [95]. The corrosion of stainless steels in automotive exhaust components is also mainly in the form of localized attack like pitting, crevice and intergranular corrosion. Stainless steels are generally protected by their passive films, but under certain conditions, the passive layer is susceptible to localized breakdown, resulting in accelerated dissolution of the underlying metal. Localized corrosion has a higher perforation rate than that in uniform corrosion. Each of the above mentioned types is discussed in detail in following sections.

2.6.4.1 Pitting Corrosion

Pitting corrosion is one of the most prevalent forms of localised corrosion which is quantitatively difficult to predict. The attack is highly localised and pits can penetrate inward extremely rapidly and the deepest of them can damage the structure by perforating the material [96, 97]. Stainless steels are the most prominent examples of this type of corrosion [98].

Pitting corrosion is caused by halides and especially Cl⁻ ions, which are relatively small anions with a high diffusivity, tending to form deep pits on stainless steels. Inside the cold end of an exhaust system the condensation of combustion gases generates a very corrosive environment, containing sulphurous and sulphuric acid, low levels of hydrochloric acid and chloride ions [99]. Pits almost always initiate at some chemical or physical heterogeneity at the surface, such as inclusions, second-phase particles, solute-segregated grain boundaries, flaws, mechanical damages or dislocations. Pits in stainless steels are often associated with manganese sulphide inclusions, which can be found in many commercial steels [48]. When localized areas of the surface passive layer are damaged, they are no longer able to protect the underlying metal against corrosion attack [100, 101].

It is stated that pits begin by the breakdown of passivity at favoured nuclei on the metal surface [102]. The breakdown is followed by the formation of an electrolytic cell. The anode of this cell is a minute area of active metal, and the cathode is a considerable area of passive metal. The large potential difference characteristic of this passive-active cell accounts for considerable flow of current with rapid corrosion at the small anode. The corrosion-resistant passive metal surrounding the anode and the activating property of the corrosion products within the pit account for the tendency of corrosion to penetrate the metal rather than spread along the surface. Once pits are initiated, they may continue to grow by a self-sustaining, or autocatalytic, process; that is, the corrosion processes within a pit produce conditions that are both stimulating and necessary for the continuing activity of the pit. This process is illustrated schematically in figure 2.15.
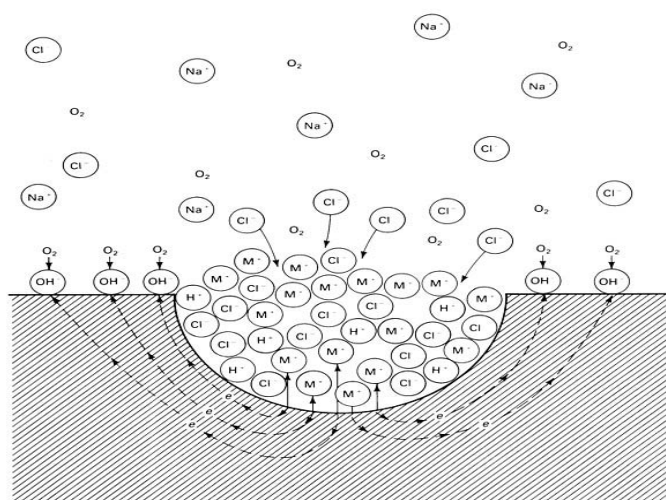
Figure 2.15: Autocatalytic processes occurring in corrosion pit. The metal, M, is being pitted by an aerated NaCl solution. Rapid dissolution occurs within the pit, while oxygen reduction takes place on the adjacent surfaces [102]

The propagation of pits is thought to involve the dissolution of metal and the maintenance of a high degree of acidity at the bottom of the pit by the hydrolysis of the dissolved metal ions. The anodic metal dissolution reaction at the bottom of the pit ($M \rightarrow M^{n+} + ne$) is balanced by the cathodic reaction on the adjacent surface ($O_2 + 2H_2O + 4e \rightarrow 4OH^-$). The increased concentration of M^{n+} within the pit results in the migration of chloride ions (Cl^-) to maintain neutrality. The metal chloride formed, M^+Cl^-, is hydrolyzed by water to the hydroxide and free acid ($M^+Cl^- + H_2O \rightarrow MOH + H^+Cl^-$). The generation of this acid lowers the pH values at the bottom of the pit (pH approximately 1.5 to 1.0), while the pH of the bulk solution remains neutral [102].

Theoretical models that describe the initiation process leading to passive film breakdown may be grouped into three classes: (1) adsorption and adsorption-induced mechanisms, where the adsorption of aggressive ions like Cl^- is of major importance, (2) ion migration and penetration models, and (3) mechanical film breakdown theories, as shown in figure 2.16 [103,104].

In the case of the cluster adsorption model, originally proposed by Heusler and Fischer [105], localized adsorption of chlorides leads to enhanced oxide dissolution at these sites with subsequent thinning of the oxide film until finally a complete removal is achieved and active dissolution starts [103, 104, 105].

(a) Penetration mechanism

(b) Adsorption mechanism

(c) Film rupture mechanism
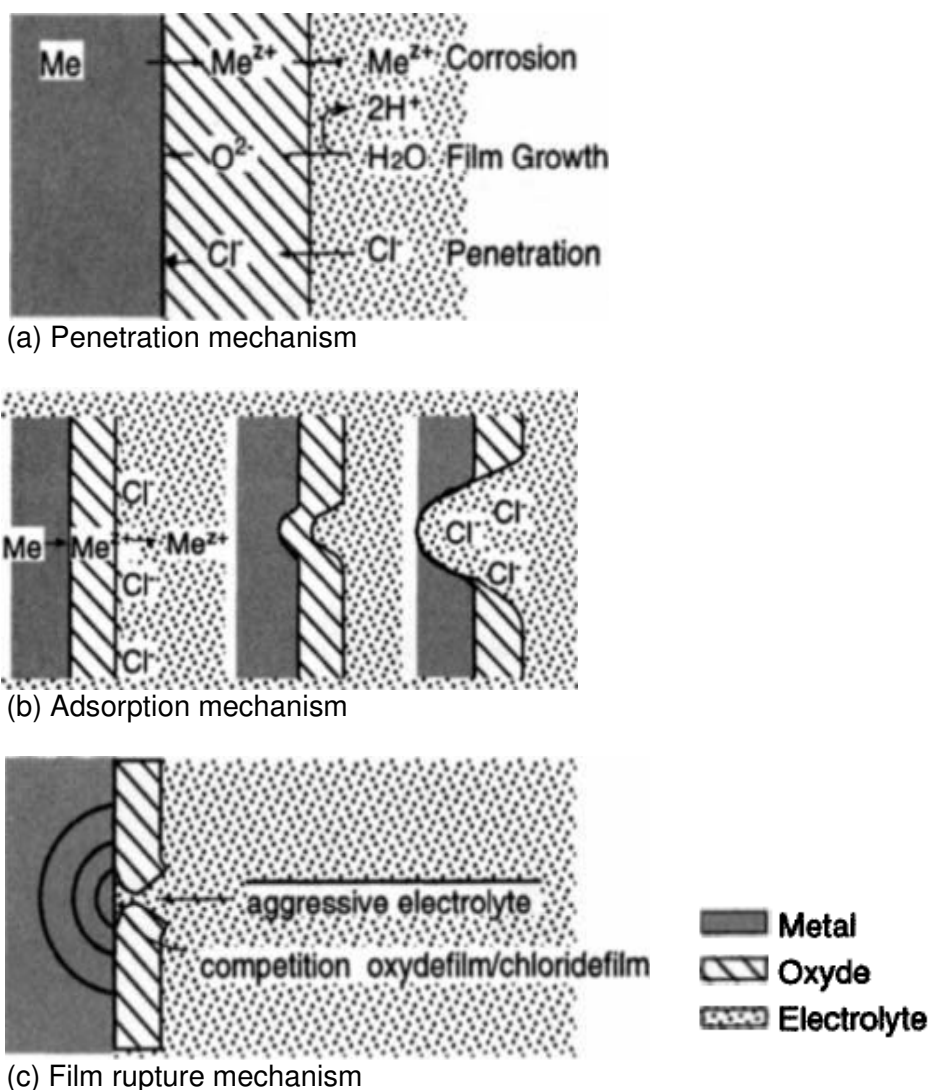
Figure 2.16: Three types of pit initiation processes: (a) Penetration of Cl⁻ through the film, (b) Island adsorption of chloride ions on the film, (c) Mechanical failure due to internal stresses in the film. Models for pit initiation leading to passive film breakdown [103, 104]

Pitting corrosion, may assume different shapes, as illustrated in figure 2.17. Pitting corrosion can produce pits with their mouth open (uncovered) or covered with a semi-permeable membrane of corrosion products. Pits can be either hemispherical or cup-shaped. In some cases they are flat-walled, revealing the crystal structure of the metal, or they may have a completely irregular shape [103, 106,107].
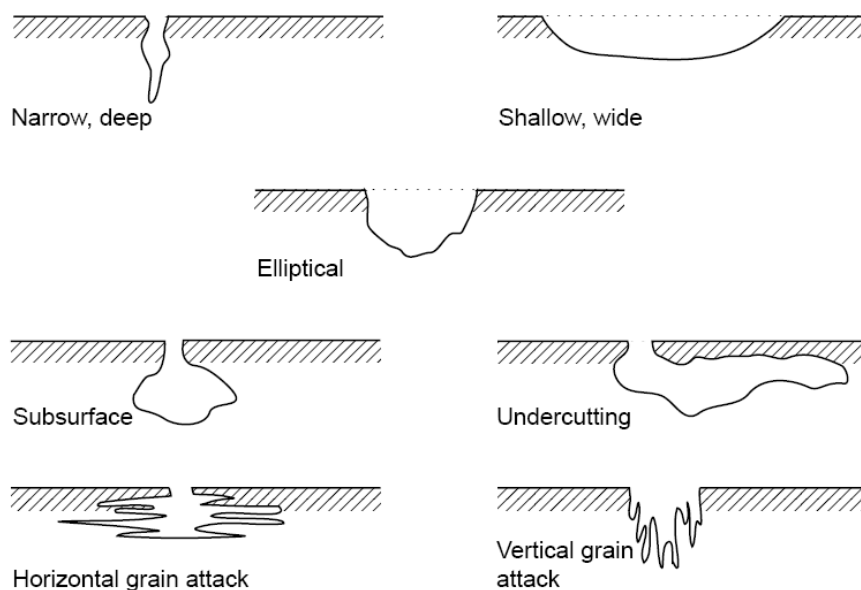
Figure 2.17: Typical variations in the cross-sectional shape of pits [106, 107]

Stainless steels have a pitting resistance equivalent number (PREN) which is used to measure the relative susceptibility of a stainless steel to pitting corrosion. It was introduced as an attempt to compare the pitting resistance of corrosion resistant stainless steels. This idea of relating corrosion resistance to composition was first introduced by Lorenz and Medawar in 1969 [108]. They found that both pitting potentials and the extent of crevice corrosion in artificial seawater correlated well to a "Wirksumme" given by %Cr + 3.3%Mo. A number of subsequent works have elaborated upon this approach and extended the analysis to other alloying elements, most notably nitrogen. The most generally accepted correlation is of the form [109,110]:

$$PREN = \%Cr + 3.3\ (\%Mo) + 16\ (\%N) \qquad \text{(Equation 2.3)}$$

However, some controversy has developed about the exact equivalence factor for nitrogen. Some have proposed higher multipliers like:

$$PREN = \%Cr + 3.3\ (\%Mo) + 30\ (\%N) \qquad \text{(Equation 2.4)}$$

In either case, it is generally agreed that, all else being equal, alloys with higher PREN should exhibit greater resistance to pitting corrosion [14-19]. The studies have revealed the often ignored fact that the PREN concept is only a rough estimator and should not be used uncritically [111, 112].

2.6.4.2 Crevice Corrosion

Crevice Corrosion is a form of localized attack that occurs frequently on metals exposed to stagnant solutions within shielded areas such as holes, gaskets, lap joints and crevice under bolts. Well known examples of susceptible metals are stainless steels, nickel, titanium and aluminium [113]. Crevice corrosion is a complex phenomenon in which several simultaneous and interacting processes occur. Based on the work of different scientists, a unified crevice corrosion mechanism is employed for this purpose [45, 49-51, 114,115]. The mechanism is composed of four steps and starts with the alloy are initially passive and the crevice and bulk solutions oxygenated. When the alloy first comes into contact with the solution, the anodic dissolution in the crevice, due to the passive current, is balanced by the reduction of oxygen. The pH of the solution remains at or close to the bulk value. For crevices with severely restricted geometry, an oxygen deficit may occur in the crevice due to the fact that the rate of supply, from the bulk solution, is outpaced by the cathodic reaction rate. The site at which crevice is formed becomes the anode and the side outside the crevice becomes the cathode. The following reactions take place:

Anode (in the crevice): $M \rightarrow M^+ + e^-$ (Equation 2.5)

Cathode (outside the crevice): $O_2 + 2\,H_2O + 4\,e^- \rightarrow 4\,OH^-$ (Equation 2.6)
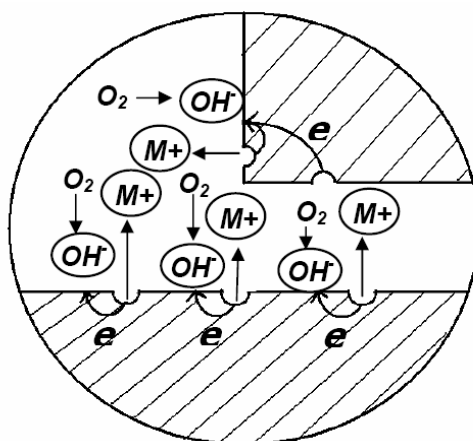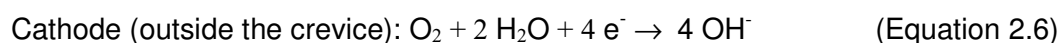
Figure 2.18: Crevice corrosion-initial stage [24, 114]

At this point, those areas of the crevice that have depleted levels of oxygen, an imbalance occurs and hydrolysis of the cations, which are produced by the dissolution process, causes acidification of the solution. In effect, the deoxygenated

areas of the crevice attain anodic potentials with respect to the oxygenated areas, and a differential aeration cell is produced. Once deoxygenation has occurred, a significant amount of chloride ions migrate into the crevice from the bulk solution as shown in figure 2.19. The following reaction takes place:

$$M^+ + Cl^- + HOH \rightarrow MOH \downarrow + HCl \qquad \text{(Equation 2.7)}$$
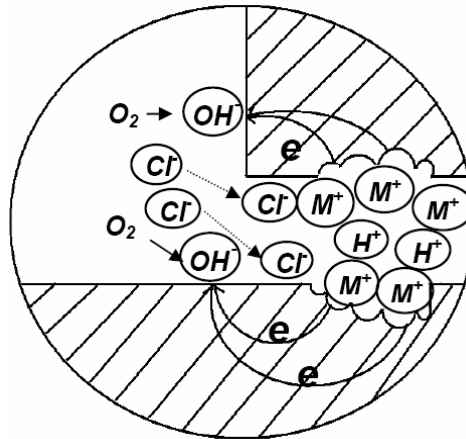
Figure 2.19: Crevice corrosion-later stage [24, 114]

If the pH and chloride ion concentration reach critical levels (often denoted as critical crevice solution), the passive film of the alloy is destroyed and the crevice corrodes actively. However, the external area of the alloy, where cathodic reactions occur, still remains passive during this process [116,117]. Table 2.4 illustrates the process.

Table 2.4: Crevice Corrosion Mechanistic Model [24]

Stage	Process
1	**Deoxygenation of the crevice**. The cathodic reduction rate of oxygen is faster the rate of diffusion of oxygen into the crevice.
2	**Acidification of the crevice.** Once depleted of oxygen, the crevice becomes anodic and the corresponding hydrolysis of the dissolution products produces a reduction in pH.
3	**Development of critical crevice solution** (low pH, high Cl⁻)
4	**Active corrosion.** If a critical crevice solution is developed the passive film is destroyed and rapid corrosion ensues. A passive steady-state situation may also be attained.

2.6.4.3 Intergranular Corrosion

When stainless steels are heated to approximately the temperature range 450 to 850°C, they become sensitized or susceptible to IG corrosion [114, 115]. Sensitization is associated with the precipitation of chromium rich carbides such as $M_{23}C_6$ or M_7C_3 along grain boundaries during the detrimental heat treatments [118, 119]. The M represents metal atoms, mainly chromium. During carbide precipitation, interstitial carbon can diffuse rapidly to the grain boundaries. Unlike carbon, chromium diffuses much more slowly, resulting in the chromium- depleted zone near the grain boundaries. A schematic diagram showing the chromium carbides and the resulting chromium depleted zone is shown in figure 2.20. Corrosion then proceeds along the grain boundary network at a much higher rate than in the matrix.

a

b
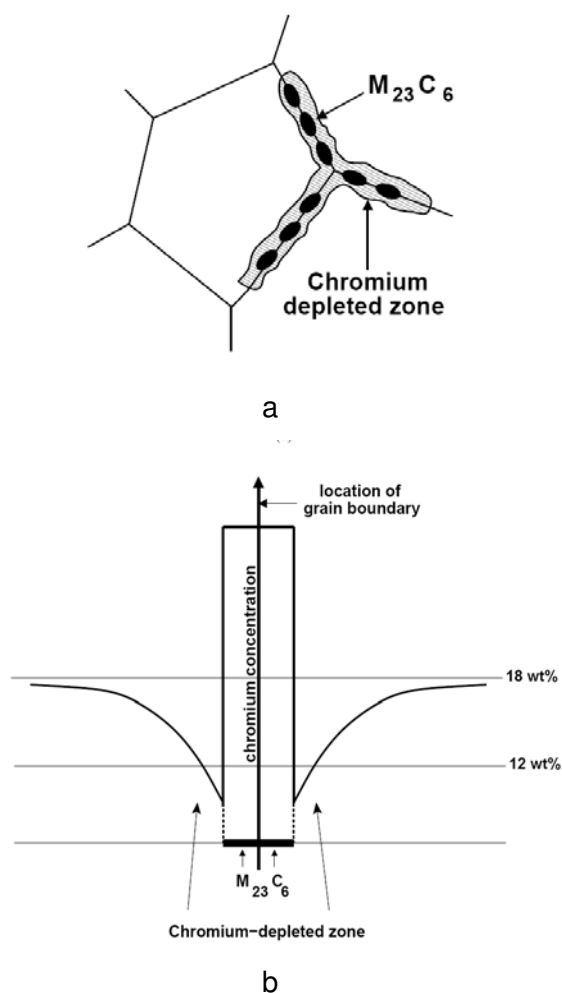
Figure 2.20: Schematic diagrams (a, b) showing chromium depleted zone at a grain boundary [126]

When the intergranular corrosion propagates along grain boundaries from the surface into the material, grain dropping may occur, leading to material loss [120-125]. Typical weight losses versus time curves for an alloy undergoing intergranular corrosion are shown in figure 2.21. The simplified mechanism of intergranular corrosion is also summarized in table 2.10.
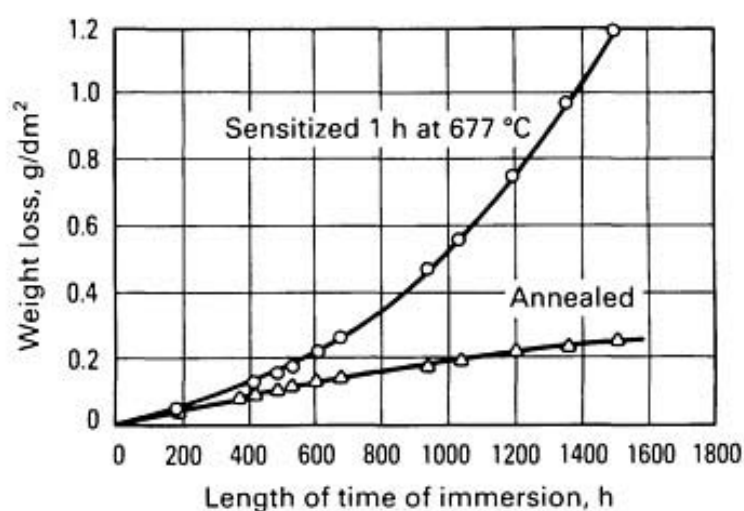
Figure 2.21: Corrosion of type 304 steel in inhibited boiling 10% H_2SO_4 [127]

Table 2.5: Intergranular Corrosion Mechanistic Model

Step	Process
1	Sensitization of stainless steel in the temperature range 450-850 °C.
2	Diffusion of carbon to a grain boundary and formation of chromium-carbide. This leads to depletion of chromium content along the grain boundary.
3	Weakening of the grain boundary and disintegration of the grains.

This phenomenon usually occurs in some sections of the system, where the temperature is quiet high, like manifold, down pipes and catalytic converters. However, sometimes it can also be observed in mufflers especially in hot spot zones where the hot exhaust gases directly strike the metal surface. To describe the effects of varying elevated temperatures and holding times on subsequent intergranular corrosion behaviour, some data for different stainless steel grades are available in

terms of Time-Temperature-Sensitization (TTS) diagram. These types of diagrams are established by determining the attack after heating a given material with different carbon content to various temperatures and holding them at those temperatures for various times. Example of a TTS diagram of 1.4301 steel is shown in figure 2.22. This diagram shows curves which separate the area to the left, where sensitization is negligible, from that to the right of the curve, where sensitization is present. It can be seen that the critical cooling to avoid sensitization depends strongly on the carbon content.
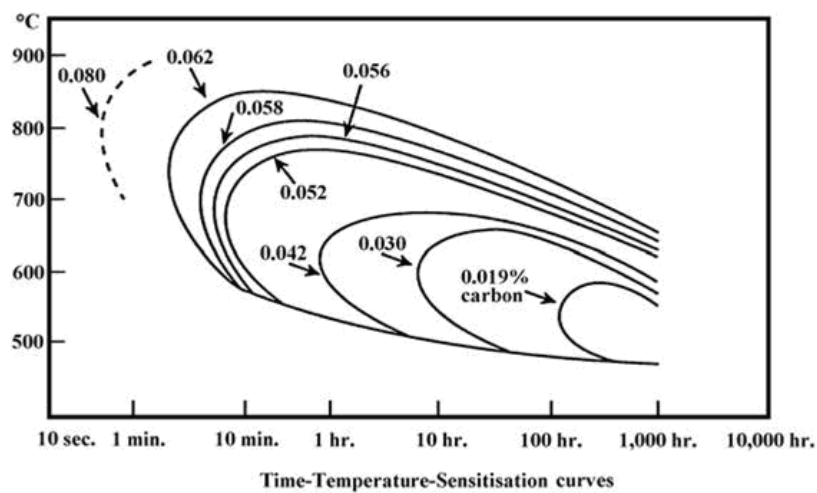
Figure 2.22: Time-Temperature-Sensitization curves for type 1.4301 stainless steel [128]

3. Experimental

3.1 Studied Materials

Two grades which are frequently used in automotive exhaust applications were selected for this study. The grade 1.4509 is a ferritic stainless steel while 1.4301 is an austenitic stainless steel. Type 1.4509 is a stabilized grade with the addition of niobium and titanium for improved weldability, high temperature strength and oxidation resistance [129]. Titanium and niobium have low free energies of formation when reacting with carbon and prevent the formation of chromium carbides [75]. The addition of titanium plus niobium has also been found to increase the corrosion resistance [130] and increase the formability [131, 132]. Furthermore, the type 1.4509 is a cost reducing alternative to the austenitic grade 1.4301. The surface finish and sheet thickness of investigated materials are given in table 3.1. These materials were supplied in a form of sheets and the chemical composition is given in table 3.2.

Table 3.1: As-received surface finishes of the investigated materials

Stainless steel type Material No.	AISI Type	DIN 17006	Standard finish	Thickness (mm)
1.4509	441	X2CrTiNb18	Standard cold rolled	1.0 & 1.5
1.4301	304	X5CrNi18-10	Standard cold rolled	1.0 & 1.5

Table 3.2: Chemical composition of investigated stainless steels (weight %)

Material	C	Si	Mn	P	S	Cr	Mo	Ni	Nb	Ti	PREN
1.4509	0.02	0.70	0.38	0.01	<0.005	17.8	0.05	0.21	0.364	0.148	17,9
1.4301	0.07	0.46	1.14	0.01	<0.005	17.5	0.02	9.11	0.0052	<0.0020	17.6

PREN = % Cr + 3.3 * % Mo + 16 * % N

The results of the light microscopy examination are summarized in figure 3.1. The microstructure of both grades has been showed in two different magnifications. The microstructure of 1.4509 has an average grain size of about 45 µm. The microstructure of 1.4301 consists of polyhedral austenitic grains with twinning typical of an fcc microstructure. The average austenitic grain size in this state is about 40 µm. Metallographic observation did not show any forms of precipitation and only homogeneous microstructure with fine grains was observed, as shown in figure 3.1. Mechanical properties of these grades are shown in table 3.3.
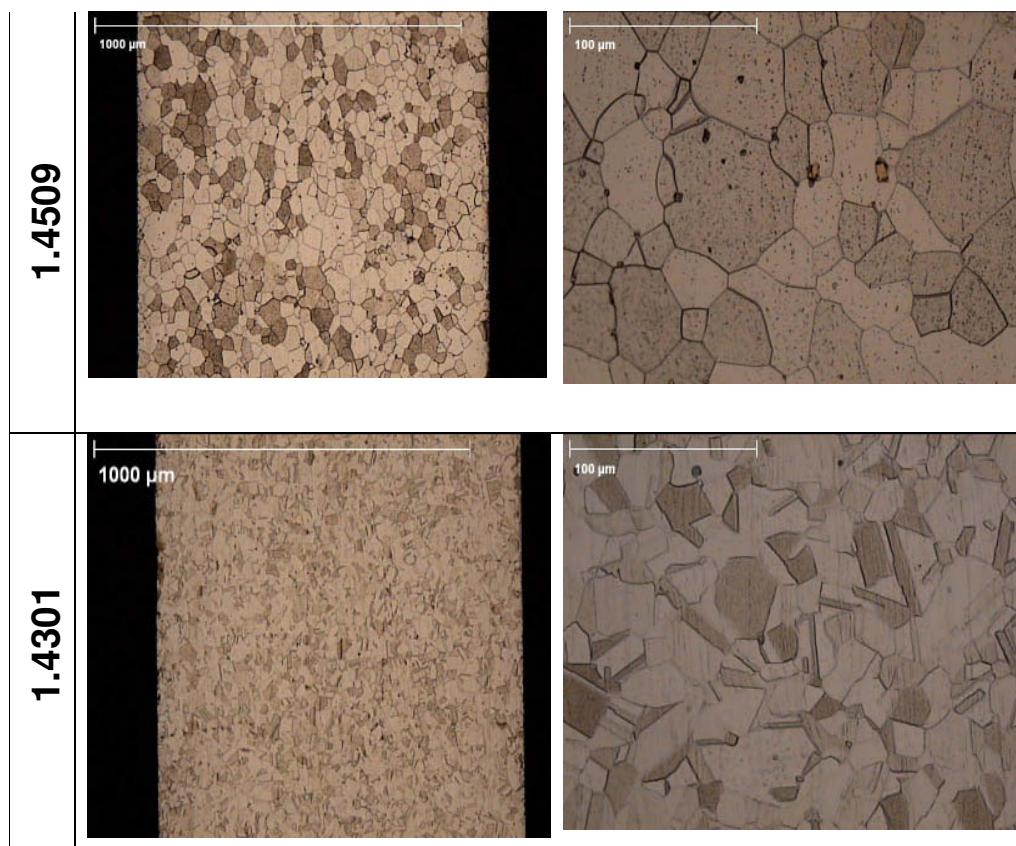
Figure 3.1: Microstructure as received condition 1.4509 and 1.4301

Table 3.3: Mechanical properties of investigated materials at room temperature

Stainless steel type	0.2% Proof strength $R_{p0.2}$ [N/mm^2] min.	Tensile strength R_m [N/mm^2]	Elongation at fracture A80% min.
1.4509	250	430-630	18
1.4301	230	540-750	45

3.2 Sensitization of Materials

This part of work consists of cyclic oxidation test and micro-structural examination after holding the materials at different temperature and time. The test coupons were 1.0 mm thick, 100 mm wide and also 100 mm long. The samples were placed in a furnace at different temperatures after being degreased ultrasonically in acetone for 10 minutes and rinsed with distilled water. The difference in weight was reported to make a comparison between two grades. The weight gain due to oxidation after the heat treatment for 10 and 100 hours at temperatures of 500°C, 600°C, 700°C, 750°C and 800°C was measured. A complete testing procedure is given in table 3.4. To study the sensitization behaviour, metallographic sections were prepared and the change in the microstructure was examined with the help of optical, scanning and transmission electron microscopy. Some previous studies have shown that the combination of different types of microscope help to locate, identify and quantify the precipitates [133].

Table 3.4: Overview of a scheme of oxidation test

Alloy	Temperature [°C]					Sample size [mm]^2	Thickness [mm]	Oxidation time [h]	
1.4509	500	600	700	750	800	100X100	1.0	10	100
1.4301	500	600	700	750	800	100X100	1.0	10	100

3.3 Cyclic Oxidation Test

These types of aging heat treatments were performed in order to study the role of different heating cycles on degradation rate. Samples were heated for 10 hours in two different ways to simulate long and short driving cycles without any corrosive medium. In 1st approach, heating was done in a furnace at a temperature of 500℃ for 10 hours. In 2nd approach, heating was also done for 10 hours but with additional cooling cycles. After every 1 hour, samples were taken out from the furnace for cooling i.e. holding the material for 30 minutes at the room temperature. A complete test procedure is given in table 3.5. Figure 3.2 explains the difference between two heating treatments. Surface characterization was done with the help of scanning electron microscope.

Table 3.5: Aging heat treatments under different conditions

Stainless steel type	Heating temp. [℃]	One step heating [h]	Heating with additional cooling intervals [h]
1.4509	500	10	10
1.4301	500	10	10
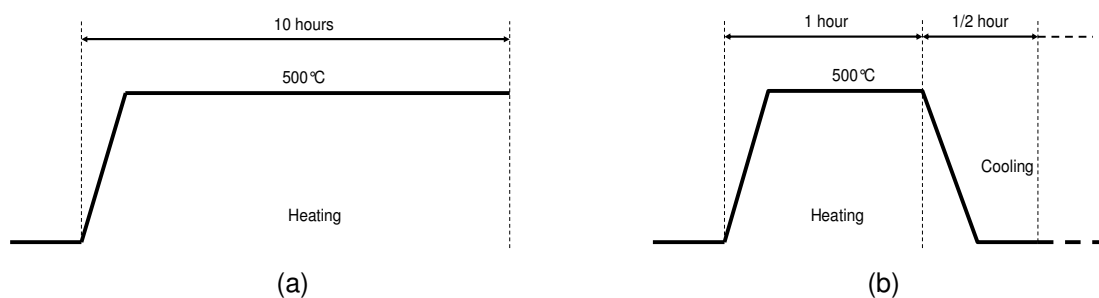
Figure 3.2: Graphical representation of two different heat treatments (a) Continuous heating, (b) Heating with additional cooling intervals

3.4 Corrosion Testing Methods

The following corrosion tests were carried out to study the onset of crevice corrosion with additional heating effects.

1. Modified VDA Salt Spray Tests
2. Ferric Chloride Immersion Tests
3. Potential Measurements in Crevice
4. Dip and Dry Tests
5. Component Tests
6. Tests to Determine Degree of Sensitization
7. Potentiodynamic Polarization Measurements

3.4.1 Modified VDA Salt Spray Tests

After a thorough assessment of all existing testing methods which were used to evaluate materials for exhaust applications, the tests mentioned in this section were developed by identifying commonalities and differences, integrating them where possible, and as far as possible simulating actual environments and operating conditions. For the development, two main criterions were considered: aggressiveness of the tests to obtain rapid results, reproducibility of the results from the tests. Therefore, in the following developed tests, the standard exposure cycles have been modified and additional heating cycles were introduced to meet the objectives of this research work.

Salt spray testing is the oldest and most widely used corrosion testing method [134]. This test is used extensively in different ways for specification purposes and determining the relative corrosion resistance among different materials [135]. For automotive exhaust applications a standard test named VDA 621-415 is common in practice. This test has additional humid and dry cycles instead of continuous salt spraying. But again, it does not accurately reproduce corrosion performance for the automotive exhaust parts. The high temperature phase which occurs in an actual practice is not present in any standard test. Therefore, different testing cycles with additional heating effects were performed during this study. Some modifications have been made in standard VDA 621-415 including different heating temperatures and times for different phases. In all these methods a solution with 5wt% NaCl was used. These different cycles are explained in detail and the schematic illustrations of the

applied four different test procedures are shown in figure 3.3-3.6. These tests were evaluated and integrated to develop standard test protocols for cold end components of the exhaust component.

Method A VDA 621-415

This method is frequently used in automotive exhaust industry to validate the materials. Surprisingly, there is no heating cycle involved in this test to simulate the impact of different temperatures on materials which actually is a common practice. A correlation of this testing method with field often leads to a disagreement. The reason that this method does not accurately reproduce corrosion performance for automotive exhaust parts is that it does not accurately reproduce the conditions under which automotive parts are exposed. The standard test cycles for this test are shown in figure 3.3.
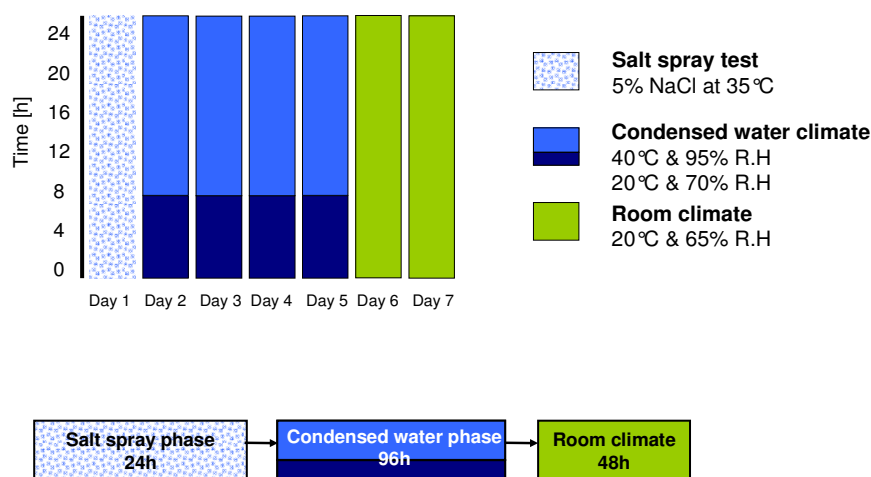
Figure 3.3: Layout of a standard VDA 621-415 Test

Method B:

This method involves a change of one cycle in the VDA test. A heating cycle where samples were heated at 500°C for 24 hours was introduced. The maximum possible material temperature in a muffler is 500°C which was the reason to choose that temperature. The 48 hour room climate in the end was reduced to only 24 hours. A schematic layout of this cycle is shown in figure 3.4.
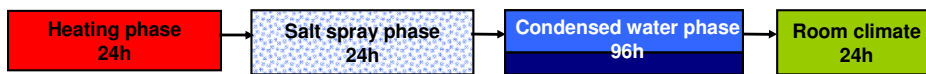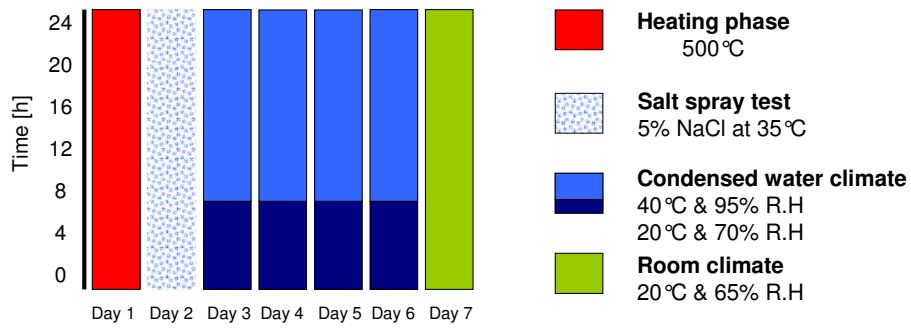
Figure 3.4: Modified VDA test with weekly heating

Method C:

Here testing with daily heating of samples with same temperature was performed. The reason was to accelerate corrosion and to create a testing cycle more relevant for a short distance driving cycle e.g. a typical urban driving behaviour. The testing cycles are given in figure 3.5.
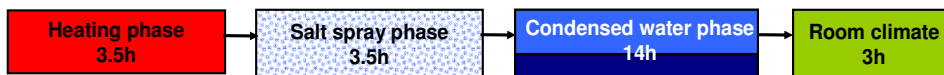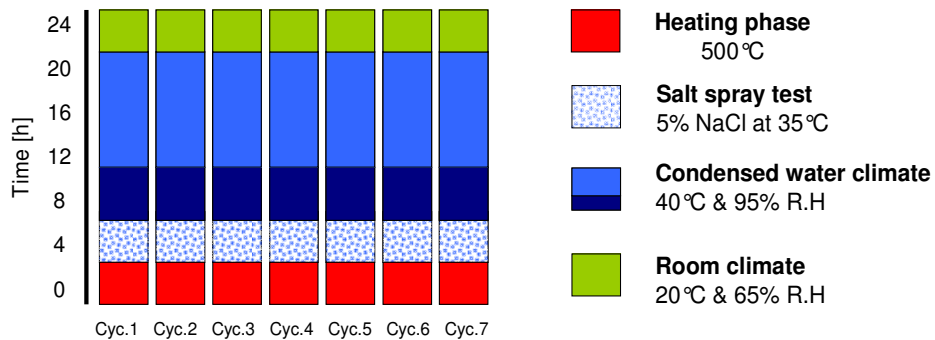
Figure 3.5: Modified VDA Test with daily heating

Method D:

A method D was different from the method C only in terms of shortened condensed water climate and long room climate duration. In both these methods, the effect of condensed water climate duration on corrosion behaviour was studied. A complete detail of testing cycles is given in figure 3.6.
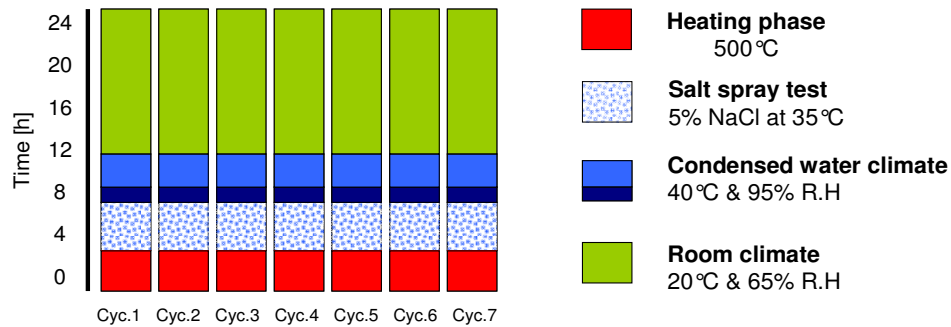
Figure 3.6: Modified VDA test with daily heating and less condensed water climate

Specimens from both grades 1.4509 and 1.4301 were cut out in the dimensions of 100x100mm^2 from the flat panels. Flat samples without any crevice assembly were investigated in a first phase with all four testing cycles. The crevice corrosion studies were done with a method D. Two steel plates from each grade were welded together, while placing crevice distance pieces between them having defined width. Crevice width was varied from 0.1, 0.3, 0.5 and 1.0 mm were assembled, as shown in figure 3.7 and table 3.6. The specimen with 0.0 mm crevice was built with a single specimen, without any welding. All specimens were cleaned with acetone to degrease and clean the surface. After cleaning, the samples were placed vertically in a sample holder, having a 15° inclination. An automated corrosion chamber was used to control the temperature and humidity containing 5wt.% sodium chloride (NaCl). The progress of corrosion on test samples was evaluated after the salt spray test.

Figure 3.7: Specimen assembly with well defined crevice

Table 3.6: Test plan for samples with different crevice gaps

Grade	Crevice gaps [mm]	Sensitization Temperature [°C]	Method D Sample removal [No. of cycles]
1.4509	0.1/ 0.3 / 0.5 / 1.0	500 °C	3,6,9,12
1.4301	0.1/ 0.3 / 0.5 / 1.0	500 °C	3,6,9,12

3.4.2 Ferric Chloride Immersion Test

This test method demonstrates a standard with the purpose of determining the resistance of stainless steels to pitting and crevice corrosion when exposed to oxidizing chloride environments. In this study, modification in standard test method was performed with the aim to evaluate how different crevice width and setups affect 1.4509 ferritic stainless steels resistance to crevice corrosion. The test solution 6% $FeCl_3$ was used. This electrolyte represents more aggressive environment as compared to the real conditions in the rear muffler. It was adequate to achieve crevice corrosion during a one week test period and to permit comparison of crevice size and setup as function of investigated parameters.

The 1.4509 specimen plates of dimensions 75mm x 25mm x 1.5mm were used. Their sides and edges had been grinded with 220 grit SiC paper and afterwards rinsed with acetone, to remove dirt, fingerprints and residues from grinding from the surface. Two different crevice setups were used, which are presented in figures 3.8 and 3.9.

The first assembly consisted of two 1.4509 plates separated with a ceramic shim with a defined width, the second assembly with one 1.4509 plate and a Plexiglas counter piece also separated by a ceramic shim of defined width.
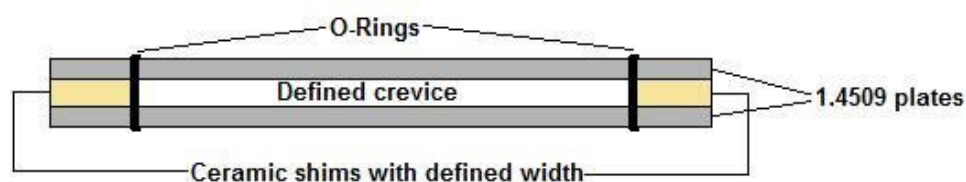
Figure 3.8: Sample assembly with two 1.4509 sheets
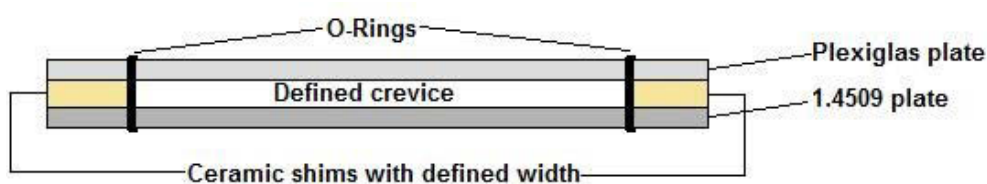
Figure 3.9: Sample assembly with 1.4509 and Plexiglas counter piece

The specimens were placed in separated plastic flasks, according to their setup type, as shown in table 3.7.

Table 3.7: Specimen setup for ferric chloride test

Setup type	Specimen number	Crevice width [mm]	Applied stainless steel grade	Counter piece
	1	≈ 0	1.4509	Plexiglas
	2	0.1	1.4509	Plexiglas
Stainless steel / Plexiglas	3	0.3	1.4509	Plexiglas
	4	0.5	1.4509	Plexiglas
	5	1.0	1.4509	Plexiglas
	7 / 8	≈ 0	1.4509	1.4509
	9 / 10	0.1	1.4509	1.4509
Stainless steel / Stainless steel	11 / 12	0.3	1.4509	1.4509
	13 / 14	0.5	1.4509	1.4509
	15 / 16	1.0	1.4509	1.4509

The flasks were filled with the 6% $FeCl_3$ solution until specimen surface was completely covered by the solution and all of them were stored for one week in the laboratory, maintaining a constant temperature of 22°C. After one week, all samples were removed from the flasks, separated from each other and cleaned in ultrasonic bath with acetone. The surfaces were investigated by visual and optical methods. Furthermore, pit depths and distribution were measured for each single specimen.

3.4.3 Polarization Measurements in Crevice

Crevice potential measurements were performed with a specific crevice setup. Three platinum wires with a 0.5 mm diameter were embedded into a resin, with the same length and width like the specimens. The lower side of the embedded compound afterwards was polished until the surfaces of the platinum wires were uncovered with embedding mass. The position of these three platinum wires is shown in figure 3.10.
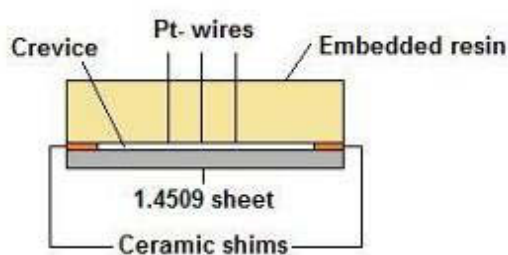
Figure 3.10: Alignment of Pt- wires in crevice

This compound was put together with the specimen, separated from each other with small ceramic shims. The ceramic shims were plates of different thicknesses i.e. 0.1 mm, 0.5 mm and 1.0 mm, with the function to constitute different crevice widths. This setup out of the embedding compound, ceramic shims and specimen had been fixed with two O-rings and put into the electrolyte. The specimen was connected as working electrode, while the three platinum wires were connected as three separate reference electrodes to the potentiostat. The usefulness of the platinum as an electrochemical reference electrode was already studied in detail by some authors [136]. An outer platinum electrode was also placed on the backside of the specimen to have no affect on the three crevice platinum electrodes. The reason for using outer platinum electrode (outside the crevice) was to measure the difference in potential between inside and outside the crevice in the solution. Experimental setup is shown in figure 3.11.
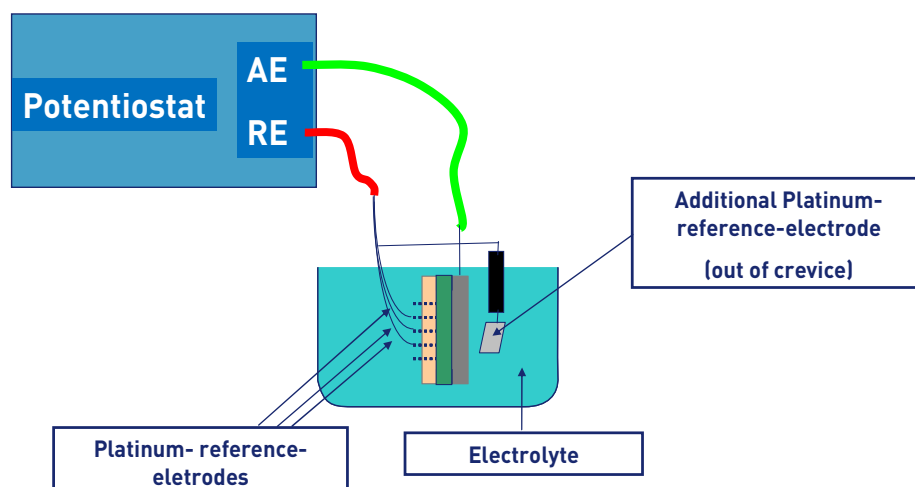
Figure 3.11: Setup for electrochemical crevice potential measurements

3.4.3.1 Measurement in 6% FeCl₃ solution

In the first step, an aggressive medium was selected for these measurements. The same 6% $FeCl_3$ solution which was also used in immersion tests was used. For this electrochemical measurement, test duration of 100h and crevice sizes of 0.1 mm and 0.5 mm was selected.

3.4.3.2 Measurement in 10 ppm Cl⁻ solution

In a second step, a medium with very low concentration of chloride was selected. For this electrochemical measurement, test duration of 100 h and crevice sizes of 0.1 mm and 0.5 mm was selected.

Table 3.8: Summary of performed potential measurement tests

Electrolyte	Crevice size [mm]		Tests per crevice	Aeration	Duration [h]	Outer electrode
	0.1	0.5				
6% $FeCl_3$	X	X	2	X	100	X
10 ppm Cl⁻	X	X	2	X	100	X

3.4.4 Dip and Dry Test

This test simulates the internal corrosion in exhaust components. A dip and dry test apparatus was specially constructed during this research work. A fully automated system was build up and used for controlling the periodic dip and dry test cycles as immersion into the condensate, followed by air drying and humid atmosphere exposure. An overview and schematic layout of dip and dry testing setup is shown in figures 3.12 and 3.13.

Figure 3.12: Overview of a constructed dip and dry testing equipment
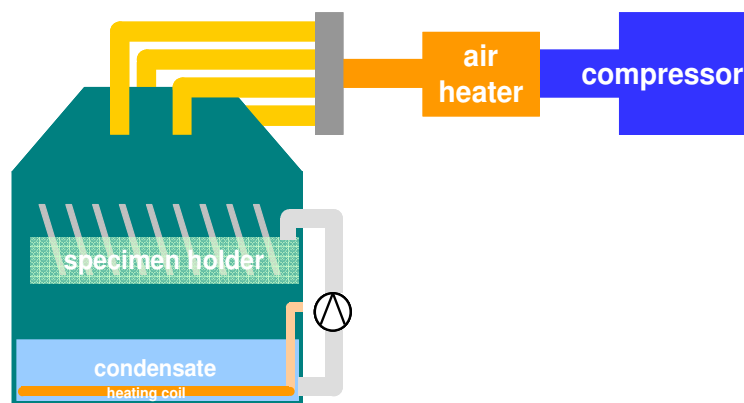
Figure 3.13: Schematic sketch of dip and dry tester

The test which was used in this study is shown in figure 3.14. It involves the following cyclic procedure:

- Heating phase: Heating cycles were applied at 500°C for 5 hours to simulate the heat impact during a driving cycle.
- Wet phase in artificial condensate: Samples were immersed partially in a hot condensate.
- Drying phase: Samples were dried with hot air with a help of a heater in this phase.
- Humidity phase: Samples were placed under humidity in a same chamber.
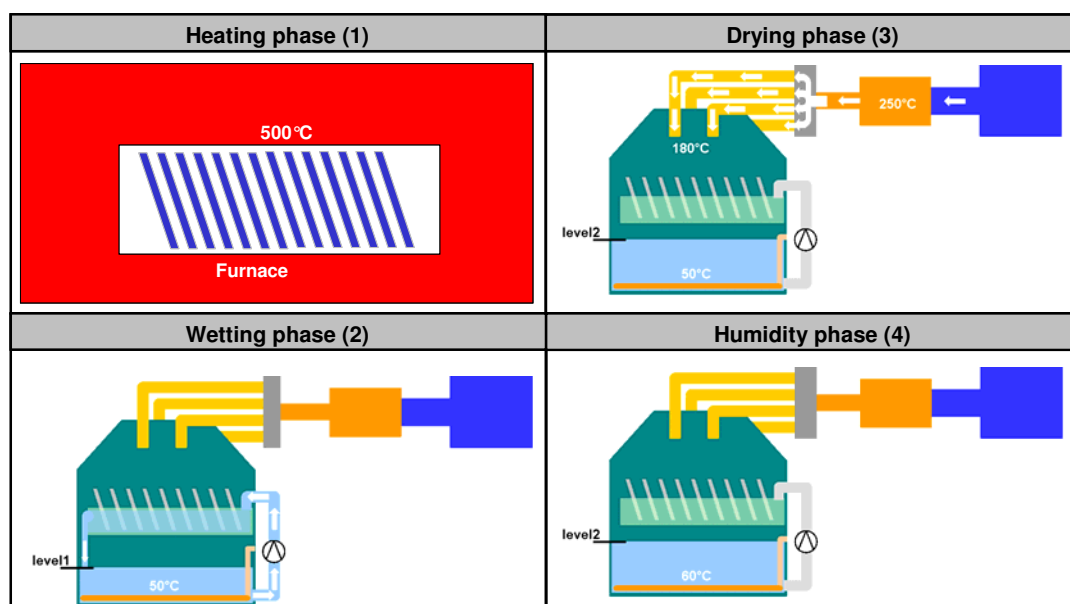
Figure 3.14: Schematic view of testing phases: (1) Heating phase, (2) Wet phase (3) Dry phase and (4) Humid phase

Samples were cut in sizes of 100x100mm and degreased ultrasonically in acetone for 5 minutes and rinsed with distilled water before investigation. After cleaning, samples had been placed on metal sample holders at an angle of 15° to the vertical. The condensate was changed regularly to maintain the same pH during the whole experiment. The composition of the dip and dry condensate with a pH value of 3.4 is described in table 3.9.

Table 3.9: Chemical composition of dip and dry test condensate

Chemical substance	$C_6H_8O_7$	NaOH	NaCl	Distilled water
Amount	768g	120g	328g	40l

The dip and dry test procedure is illustrated schematically in figure 3.15. The condensate was circulated from lower section to the upper one with the help of a pump. Approximately, 2/3 of the surface area of each sample was exposed to acidic condensate for 2 hours. The condensate temperature was 50°C and the condensate level at the upper section of the chamber was controlled by circulation. Wet phase was followed by the 1 hour hot phase where hot air at 250°C was send by a heater to the chamber. In the 3 hours humid phase, condensate temperature was introduced to the bottom of the chamber at 60°C to provide humid effect in the chamber. Hot air supply or condensate contact with samples did not take place in this phase. This procedure was done fully automatically. Heating was done in a separate furnace.
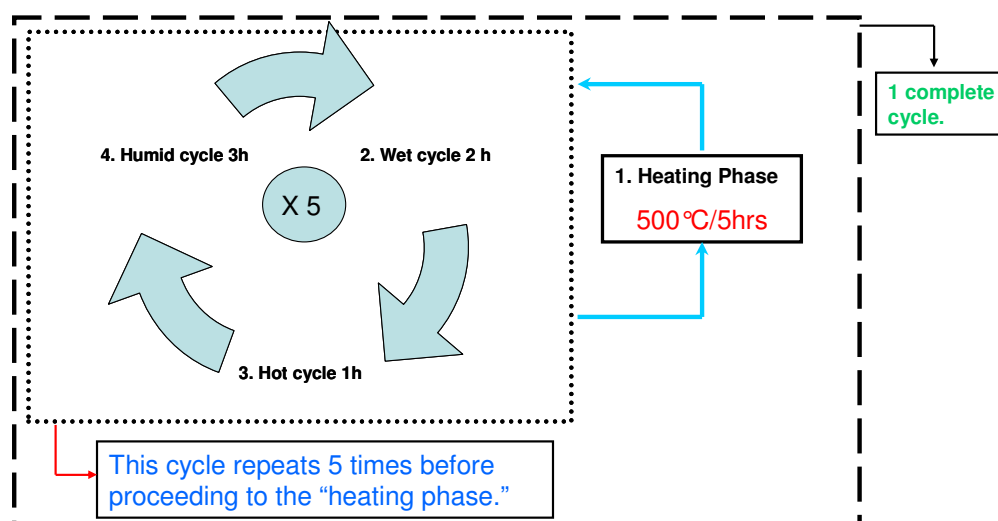
Figure 3.15: Layout of dip and dry cycle

The whole test was applied until 5 cycles. After 2, 3, 4 and 5 cycles one sample from each grade and crevice size was taken out for characterization as shown in table 3.10. The quantification of corrosion attack on samples was done by measuring the pit depths with the help of X-ray radiography.

Table 3.10: Overview of test plan for dip and dry tests

Grade	Crevice gaps [mm]	Heating treatment (Daily, °C)	Sample removal [No. of cycles]
1.4509	0.1/ 0.3 / 0.5 /1.0	500	2,3,4,5
1.4301	0.1/ 0.3 / 0.5 /1.0	500	2,3,4,5

3.4.5 Component Testing

The concept of testing a complete muffler system under near practical conditions was designed. The idea behind this proposal was to develop a testing method in which the real problems from the field can be simulated. This corrosion rig has been developed to validate the corrosion resistance of components in a short period of time. A schematic layout of corrosion rig is shown in figures 3.16, 3.17 and 3.18 respectively. To investigate both external and internal corrosion with additional heating in one test was the task. A testing chamber with heaters, blowers and pumps was constructed where the following different conditions can be programmed individually:

- Hot gas flow with various flow rates with maximum temperature 650°C depending on the service temperature for the investigated part.
- Injection of an artificial condensate.
- Salt spray conditions with the help of different nozzles.
- Water or salt water sprinkling including a thermal shock effect.
- High humidity condition and controlled chamber temperature.

Figure 3.16: Overview of a constructed corrosion rig
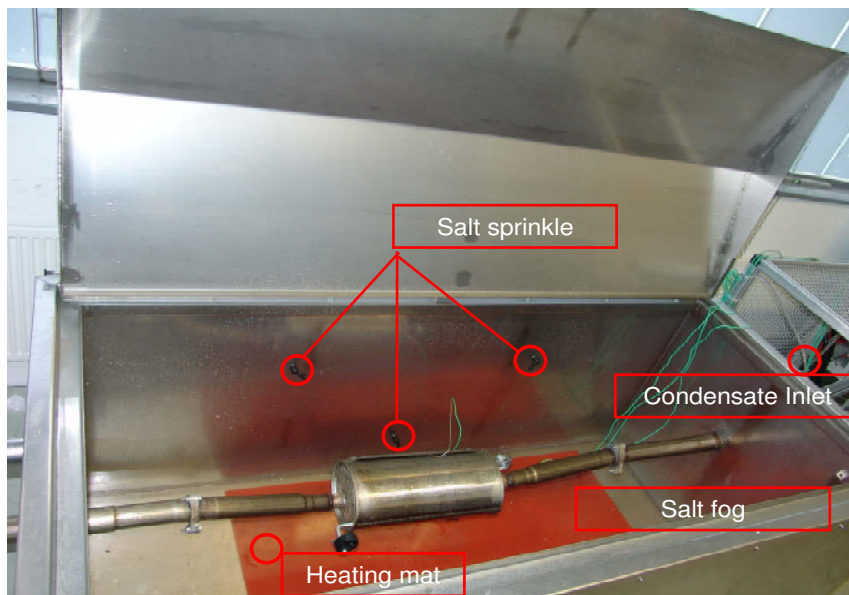
Figure 3.17: Inner view of corrosion rig with muffler inside
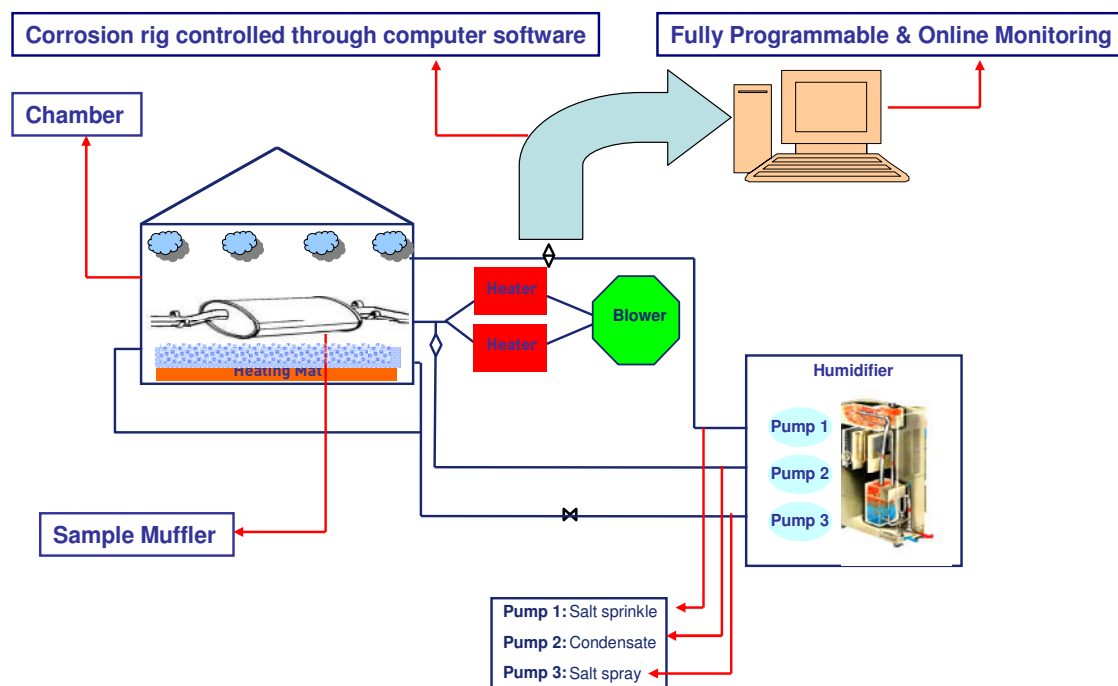
Figure 3.18: Schematic layout of test setup for components

A life time determination of a component with different material and design combinations was planned. The testing setup has following features:

- An exact simulation of real conditions which are not possible with the standard lab tests could be done with this test.
- Simulation of long driving (highway type) and short driving (urban type) cycles is also possible.
- All influencing factors like the role of welding, deformations etc. can be studied in one single test.
- Study of different designs & material combinations.
- A thermal shock effect can also be simulated.
- Results in a very short period of time.
- Low cost, especially when compared to a vehicle test.
- Life time estimation of a component is possible.
- Enhanced reproducibility compared to other tests.

A large field study was done on 15 parts in order to compare the behaviour of field parts and parts from the corrosion rig. Cooperation with one garage was made to obtain some corroded mufflers with some basic information for the investigation. Initially, a questionnaire sheet was provided with some important questions including type of car, mileage, number of years in field, mode of driving (long distance or short distance travelling) etc. Then, photo documentation was done before and after cutting the systems to highlight the interesting factors like: corrosion status both from outside and inside, strong and weak aspects of design etc. Corrosion attack was quantified by measuring pit depths from some defined positions. Also, the same types of systems were tested in a corrosion rig to make a comparison study. With regard to outer appearance the corrosion rig provides a "worst case" scenario where testing parameters were adjusted in order to simulate the desired testing conditions.

3.4.6 Tests to Determine Degree of Sensitization

3.4.6.1 Streicher Test

This test is widely used to detect susceptibility to intergranular corrosion associated primarily with chromium carbide precipitation. The Streicher test was performed at a temperature of boiling sulphuric acid for a time of 120 hours. This test procedure was according to ASTMG28B [137]. Streicher test solution was composed of 236 ml sulphuric acid (H_2SO_4), 25 g iron (III) sulfate hydrate ($Fe_2(SO_4)_3.XH_2O$) and 400 ml distilled water. The testing equipment consists of 1-liter Erlenmeyer flask with an Allihn condenser. The samples were placed in a flask in a glass cradle whereupon the solution is added. A complete testing scheme is given in table 3.11. During Streicher test, the amount of corrosive attack is determined by quantity of dissolved volume of chromium depleted zones as well as by the amount of dropped grains. The higher the sensitization of the specimen, the higher is the amount of dropped grains Therefore, the extent of dissolved volume increases drastically.

Table 3.11: Overview of test plan for Streicher tests

Streicher Test	1.4509	1.4301
As Received	X	X
500 °C 1X10h	X	X
500 °C 10X1h	X	X
600 °C 1X10h	X	X
600 °C 10X1h	X	X

1X10= Continuous heating in one step, 10X1= Heating with cooling intervals

3.4.6.2 Strauss Test

This test is also used to detect susceptibility to intergranular corrosion associated with the precipitation of chromium rich carbides. Test procedure was according to ASTMG28E practice [137]. The specimens were embedded in a copper shot and exposed to the medium. The Strauss test was performed at a temperature of boiling copper-copper sulfate-16% sulfuric acid for a time of 15 hours. Strauss test solution was composed of 100 ml sulphuric acid (H_2SO_4), 100 g copper sulfate pentahydrate ($CuSO_4.5H_2O$) and 700 ml distilled water. The testing equipment consisted of 1-liter Erlenmeyer flask with an Allihn condenser. The samples were placed in the flask in a glass cradle, covered with splint of copper (electrolytic copper) whereupon the solution is added. The solution is heated to boiling temperature throughout the whole experiment. After exposure in the boiling solution, the specimens were bent through 180°. The bent specimens were examined under stereo and scanning electron microscope. The presence of fissures or cracks was considered as an indication to the presence of intergranular attack. A complete test plan is shown in table 3.12.

Table 3.12: Overview of a complete test plan for Strauss tests

Strauss Test	1.4509	1.4301
As Received	X	X
500°C 1X10h	X	X
500°C 10X1h	X	X
600°C 1X10h	X	X
600°C 10X1h	X	X

1X10= Continuous heating in one step, 10X1= Heating with cooling intervals

3.4.7 Polarization Measurements

Current density vs. potential measurements also known as polarization curves were used to screen the corrosion behaviour of both materials with different aging treatments. Materials and their details which were used during these measurements are provided in table 3.13. In all these tests, at least two runs per condition were performed to check reproducibility. These measurements were carried out in a three electrode cell using a potentiostat. Calomel (Hg_2Cl_2) electrode was used as a reference electrode which is equivalent to potential 240 mV$_{SHE}$ (Standard Hydrogen Electrode) and a platinum plate as a counter electrode. All measured potentials are stated relative to calomel electrode. The tests were carried out at room temperature with an artificial condensate having a pH value of 3.4. The same medium was used in dip and dry tests. The electrolyte content was: 19.2 g/l citric acid, 3.0 g/l sodium hydroxide and 8.2 g/l sodium chloride in distilled water. All measurements were done with aeration. Tests were applied on samples as in the received condition from the suppliers. Samples were cleaned with acetone in an ultrasonic bath before the

measurement. Open circuit potential (OCP) of all samples was measured 1 hour before polarization. Scan rate was 200 mV/h and reverse potential was reached at a current density of 1 mA/cm² for all the measurements. In figure 3.19 a schematic lay out of electrochemical cell is shown.

Table 3.13: Overview of potentiodynamic polarization measurements

Heat Treatment	1.4509	1.4301
As Received	X	X
300 °C 1X10h	X	X
300 °C 10X1h	X	X
400 °C 1X10h	X	X
400 °C 10X1h	X	X
500 °C 1X10h	X	X
500 °C 10X1h	X	X
600 °C 1X10h	X	X
600 °C 10X1h	X	X
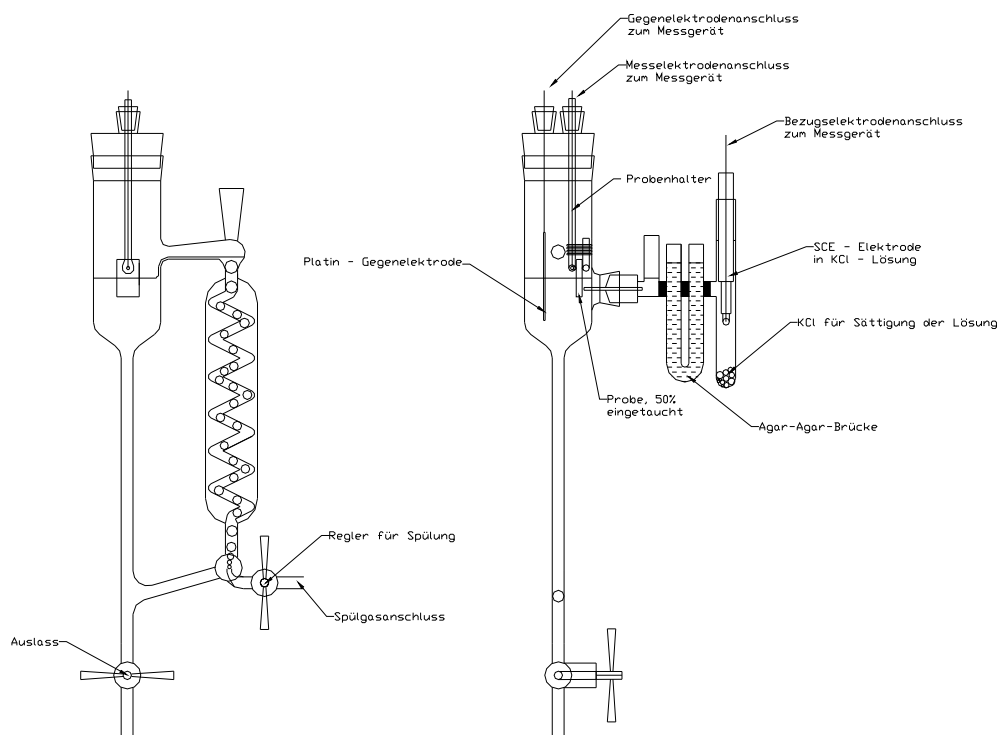
Figure 3.19: Testing setup used for all electrochemical measurements

3.5 Sample Evaluation

3.5.1 Microstructural Analysis

3.5.1.1 Optical Microscopy (OM)

Standard metallographic techniques were employed to prepare the cross section samples used in the optical microstructure characterization. The specimens were sectioned and mounted by standard metallographic technique, followed by grinding, polishing and etching to reveal their microstructures including the grain boundaries. Metallographic examination was performed in a conventional Olympus BX51M reflecting light microscope on all samples of investigated alloys.

3.5.1.2 Scanning Electron Microscopy (SEM)

The samples were investigated at high magnification in the as-polished condition using a Field Emission Gun Scanning Electron Microscope (FEG SEM), type Tescan VEGA SB, equipped with an Oxford INCA Energy EDS system. Reaction products and particles at the surface were examined by backscattered electrons (BSE) to reveal variations in chemical composition, and secondary electrons (SE) to reveal topographic details on the surface. EDS composition analysis and X-ray mapping in the cross section geometry were carried out in the surface-near regions and close to the corrosion pits to determine the element distribution within specific phases.

3.5.1.3 Transmission Electron Microscopy (TEM)

Thin foil preparation involves sectioning of the samples, mechanical thinning by a dimple grinder and electro-polishing. TEM investigations were performed with a Philips CM 200 microscope operating at 200kV. Both compositional analyses and X-ray mapping were carried out in the surface near region of the sample employing an EDAX system with DX-4 workstation computer.

3.5.2 Surface Analysis

3.5.2.1 2D Optical Microscopy

The use of conventional optical microscope to measure pit depths is one of the well known and oldest method which is still in practice [138]. It is a technique providing the characterization of specimen surfaces after corrosion tests in respect of quantity of pits and their location. With this method pit depth is the difference in height of a

specimen surface and bottom of a pit measured by focusing microscope's knob. This technique to measure pit depth implicates two disadvantages. On the one hand to locate and measure depths of pits on a complete specimen surface requires high personal efforts and on the other hand, the results precision is not very high, because of personal errors and less resolution [139]. In this work, optical microscopy was used for corrosion quantification of tested samples.

3.5.2.2 3D Optical Microscopy

The use of 3D optical microscope to quantify pitting corrosion is also common nowadays. Using these measuring tools enables quantification of corrosion damage with high resolution visualization. In this research an Infinite Focus Measurement (IFM) device 64 from Alicona was used to measure pit depths and to obtain 3D data of sample surface. Its operating principle is focus variation. This moves the focus plane of a known objective lens vertically over a surface which in conjunction with Smartflash illumination builds up a 3D full colour model of the surface to be examined. In this research entire surface of specimens were evaluated by an automated 3D optical microscope with statistical data analysis. Characterized parameters were the maximum pit depth and pit volume.

3.5.2.3 Radiography

Digital radiography is one of the oldest non destructive techniques (NDT), which has been in use for a long time as a monitoring method to detect major flaws and severe corrosion attacks in many industrial systems. In this method, X-rays are generated by means of specially designed high vacuum tubes (X-ray tubes). When electrically operated this tube emits penetrating radiation beams known as X-rays. The beam from equipment penetrates a piece of metal, and the amount the beam is attenuated depends on the thickness of the material. Hence, the intensity of the transmitted beam varies with position. Step wedges are used for calibration and standardization of X-ray machines. Also, when an object with various thicknesses is radiographed, a step wedge of the same material is used. The resulting radiograph shows the dimensional features of the part. In a photograph, the thinnest portion of a sample will cause dark image while the thickest portion where the intensity was low will cause a bright image. The principle of digital radiography is presented in figure 3.20.

X-ray tube   **X-ray radiations**   **Radiography film**
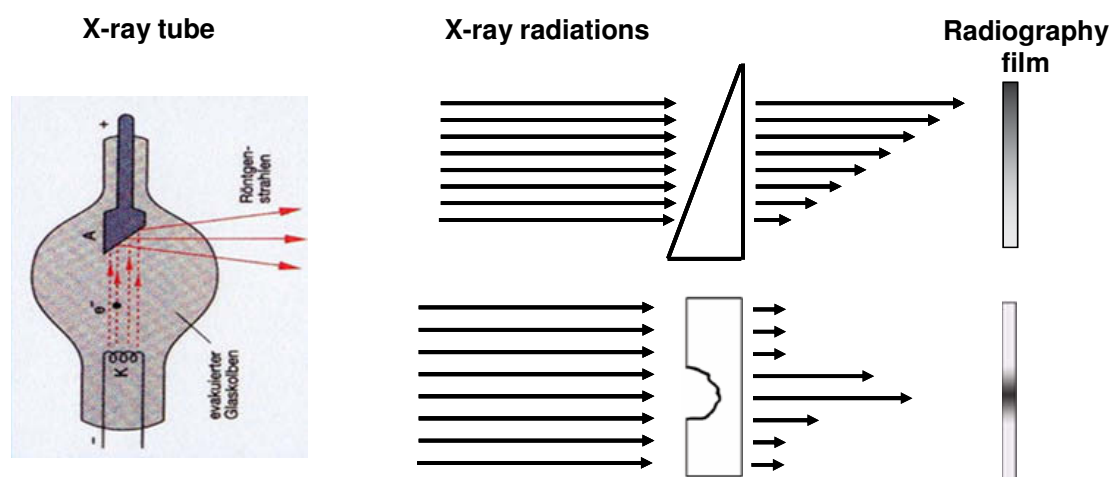
Figure 3.20: Radiographic schematic of calibration sample and corroded sample [140]

Comparison among 2D microscopy, 3D microscopy and radiography

To answer the upcoming question that why radiography was extensively used during this study, all three methods used, i.e. optical microscopy, 3D optical microscopy and X-ray radiography are systematically compared. There were 3 samples of different stainless steel grades used for the measurements. These samples were taken after performing the salt spray test. Table 3.14 shows the maximum pit depth measurements from the sample using all three pitting quantification methods. Example of visual comparison between 3D & 2D images from 3D microscope and image from radiography for one sample are shown in figure 3.20.

Table 3.14: Maximum pit depth for each sample

Sample	Side	Max 3D Microscopy (µm)	Max 2D microscopy (µm)	Max Radiography (µm)
101	A	131,83	162,00	146,00
	B	95,71	126,00	146,00
102	A	259,59	252,00	215,00
	B	175,94	180,00	215,00
103	A	131,12	216,00	148,00
	B	171,79	234,00	148,00
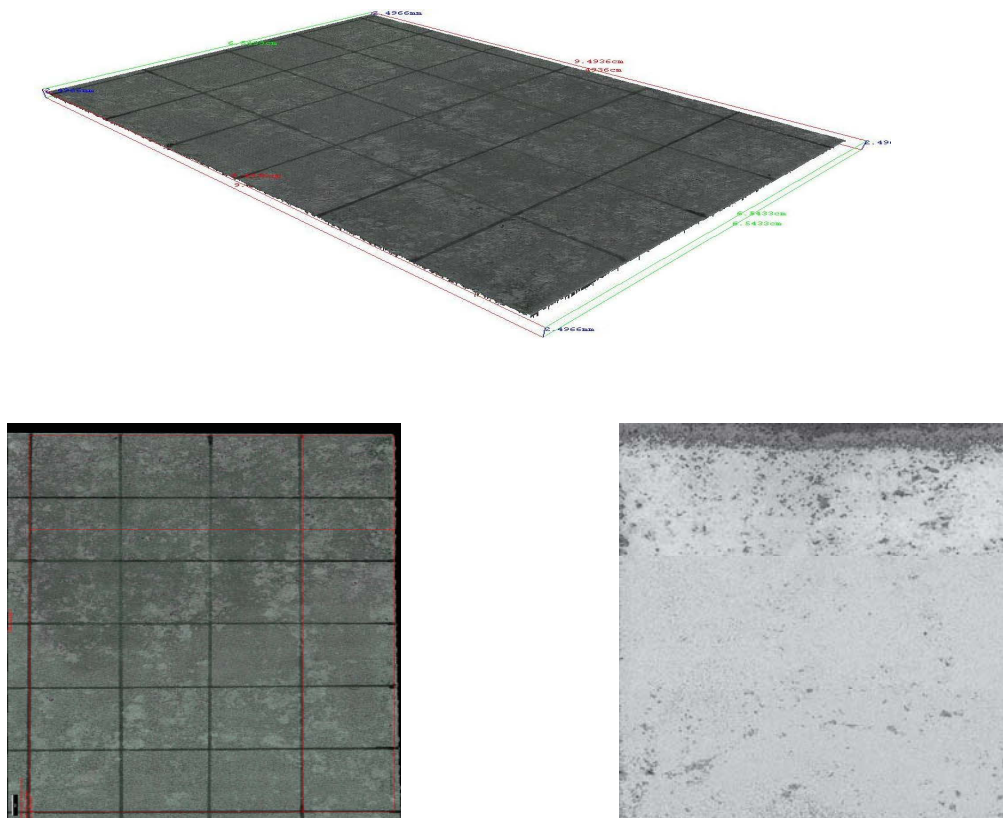
Figure 3.21: Example of visual comparison between 3D & 2D images from 3D microscope and image from radiography respectively from top for sample 103
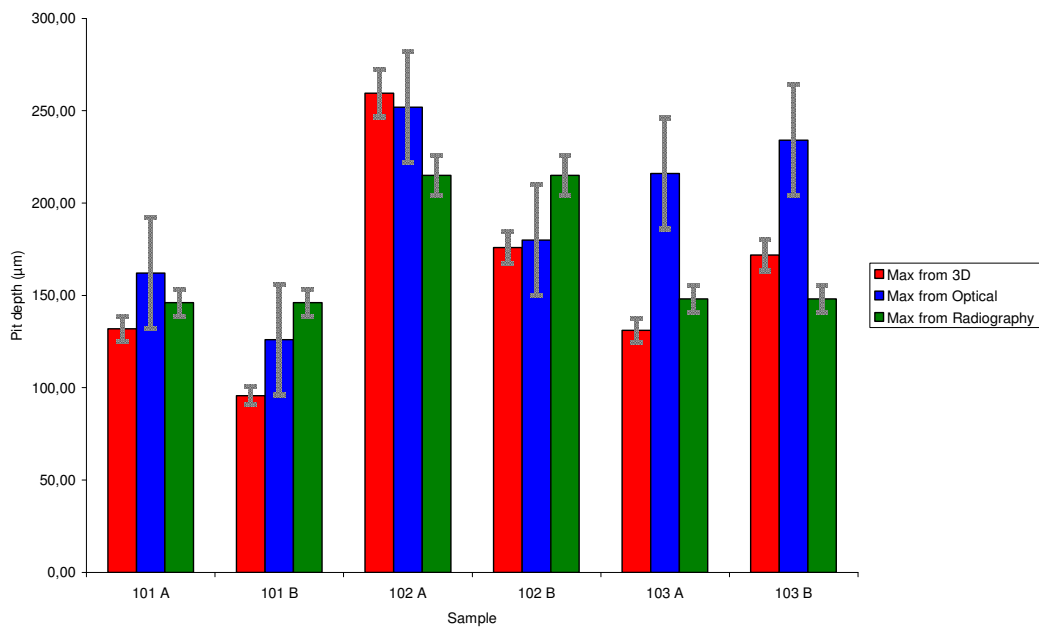
Figure 3.22: Pit depth graph from each sample with error range

As we can see from the graph, measurements from most of samples are well within the error range. The error range for optical microscope was taken to be 30 µm after comparison between pit depth measurements on same sample by different experimenter. Approximately 8% error range was taken for 3D microscope and the radiography after finding out the standard deviation from the maximum of each sample from each measurement. However, the maximum from each cell in 3D microscope measurement and radiography measurement are well within the each other's "error range" indicating the reliability in their measurement.

The main quantification problem with 2D optical microscope is human error. Since the whole operation mechanism depended on how the user handles the microscope and also on the varying eyesight of each user. Besides the problem with whole surface measurement in 3D microscope was uneven structure of the sample measured i.e. some samples were bent or had hollowed structure at some position thereby increasing the measurement depth from the topmost stable point causing increase in the measured pit depth as compared to the actual pit depth. 3D microscope with each cell measurement and radiography measurement had no such quantification problem and were considered suitable methods.

This comparison study has revealed that high resolution X-ray radiography is a powerful and easy method to quantify pitting corrosion both in terms of pit depths and percentage of affected area. This method overcomes common problems like high scatter of results, high personal and cost efforts with low reproducibility for other methods. The following conclusions can be drawn from this study that each of the explained methods has its own characteristics and advantages depending on the type and purpose of required information. The comparison has revealed the fact that none of the discussed method fulfils all the desired requirements. Every technique has its own merits and demerits but X-ray radiography appears amongst one of the suitable especially in terms of personal efforts and costs. The summary of all three methods in a form of comparison are explained in a table 3.15.

Table 3.15: Comparison of light microscopy, 3D microscopy and radiography

Size of specimen (700X700 mm)	2D Optical Microscopy	3D Microscopy	X-ray Radiography
Costs	Low	High	Medium
Required Time	Medium (1hr, dependent on corroded surface)	Medium (1hr, dependent on corroded surface)	Low (30 min, independent on corroded surface)
Possible Analysis	Pit depth measurement 2D photographs	Percentage affected area 2D & 3D photographs	Percentage affected area 2D photographs
Precision & Accuracy	Pit depths: Low (Till 30 µm exactness)	Pit depths: High (Till 1µm exactness)	Pit depths: Medium (Till 5 µm exactness)
Reproducibility	Low (Examiner dependent)	Very High	High

Low cost and time are obvious advantages of this technique, however, it has some limitations too. Sometimes, precise estimation of a pit is also difficult because of alignment of the pit relative to radiation beam. The most significant limitation of this technique is accessibility of both sides of the sample to X-ray radiations. The results of this work shows that radiography is a very promising way for quantification of pitting corrosion.

3.5.2.4 Scanning Electron Microscopy (SEM)

The surface analysis of the samples was done by using a scanning electron microscope (SEM). A direct image of the topographical nature of the surface was studied after different tests. It provides useful information concerning surface discontinuities and different corrosion mechanisms. The acceleration voltage was kept at 20 KV and the working distance was varied. The analysis was performed on samples before and after exposure testing.

3.5.2.5 X-Ray Diffraction (XRD)

When a beam of X-ray with a known wavelength contacts a solid material with a specific crystal structure, diffraction can occur under the conditions that the atomic spacing or the distance between two planes of atoms is similar to that of the beam wavelength and that the wave motion of the X-rays can be interfered [141]. Upon selecting a particular angle of incidence, known as Bragg's law, the X-rays will be scattered. If the scattered rays are in phase, they will reinforce each other to cause a constructive interference or a diffracted beam. Those angles that do not satisfy Bragg's law will scatter X-rays out of phase to cancel out each other and cause destructive interference in which no diffraction will be detected. A model 3003 TT (GE inspection technologies) was used during this study.

3.5.2.6 Time of Flight Secondary Ion Mass Spectroscopy (TOF-SIMS)

In SIMS, the sample is irradiated with a primary ion beam, the impact of which sputters away the surface atoms, some as neutrals and other as ions. Those atoms which become ionized are then detected in a mass spectrometer, where their masses are measured. It's most sensitive of all the commonly employed surface analytical techniques. TOF-SIMS analyses were performed using the instrument TOF-SIMS, ION TOF, Germany. Parameters: 25keV Bi liquid metal gun, bunched mode, charge compensation with a pulsed electron gun, 3keV Ar ion sputter gun, sputter angle 45°, sputter area 200 X 200 μm^2, analysis area in center of sputter crater about 60 X 60 μm^2, sputter/analysis process in interlaced mode. A summary of complete test plan and used characterization methods is given in table 3.16.

Table 3.16: Complete test plan with characterization methods

Testing Methods	Microstructural Analysis			Surface Analysis					
	OM	SEM	TEM	OM 2D	OM 3D	Radiography	SEM	XRD	SIMS
Sensitization of Materials	X	X	X				X		X
Modified VDA Salt Spray Tests	X	X		X	X	X	X	X	
Ferric Chloride Immersion Test				X		X			
Potential Measurements in Crevice				X					
Dip and Dry Test				X	X	X	X	X	
Component Testing	X	X		X			X	X	
To Determine Degree of Sensitization	X	X					X		
Potentiodynamic Polarization Measurements				X					

OM…Optical Microscopy, SEM…Scanning Electron Microscopy, XRD...X ray Diffraction, SIMS…Secondary Ion Mass Spectroscopy

4. Results

4.1 Sensitization of Materials

4.1.1 Continuous Oxidation Test

In this test, the oxidation behaviours of the ferritic stainless steel and austenitic steel were compared to understand the difference in oxidation rate of two materials. The results of the weight gain for both materials subjected to different oxidation temperatures for 10 and 100 hours is given in figure 4.1 and 4.2. From both figures it can be seen that the grade 1.4509 performs significantly better than the grade 1.4301. SEM micrographs of the top scale surface formed on 1.4509 and 1.4301 are shown in figures 4.3 and 4.4 respectively.
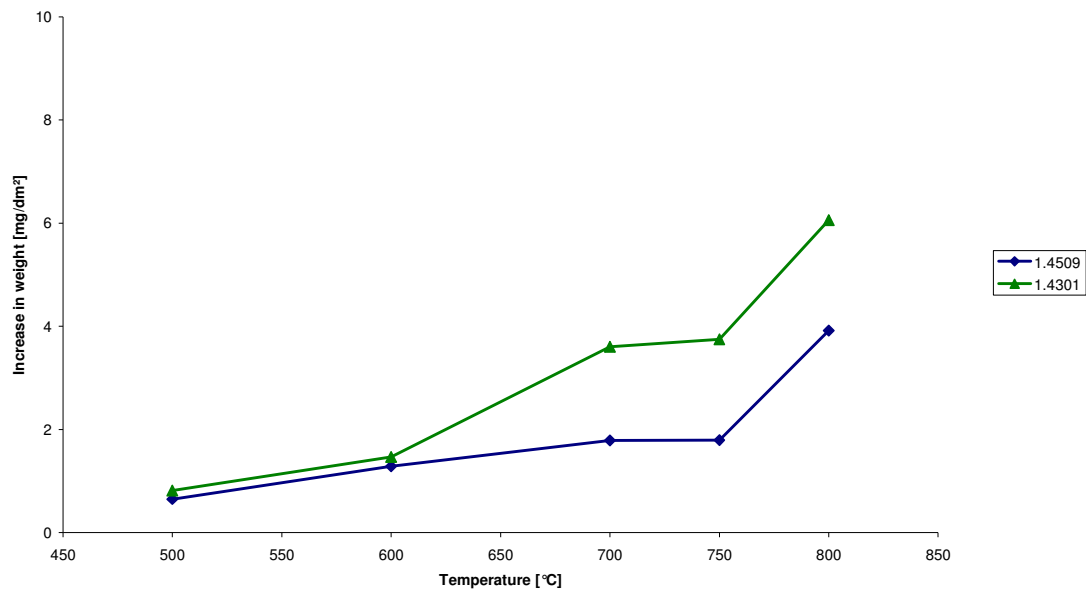
Figure 4.1: Weight gain of materials 1.4509 and 1.4301 as function of temperature, t=10h, air cooled, as rolled surface
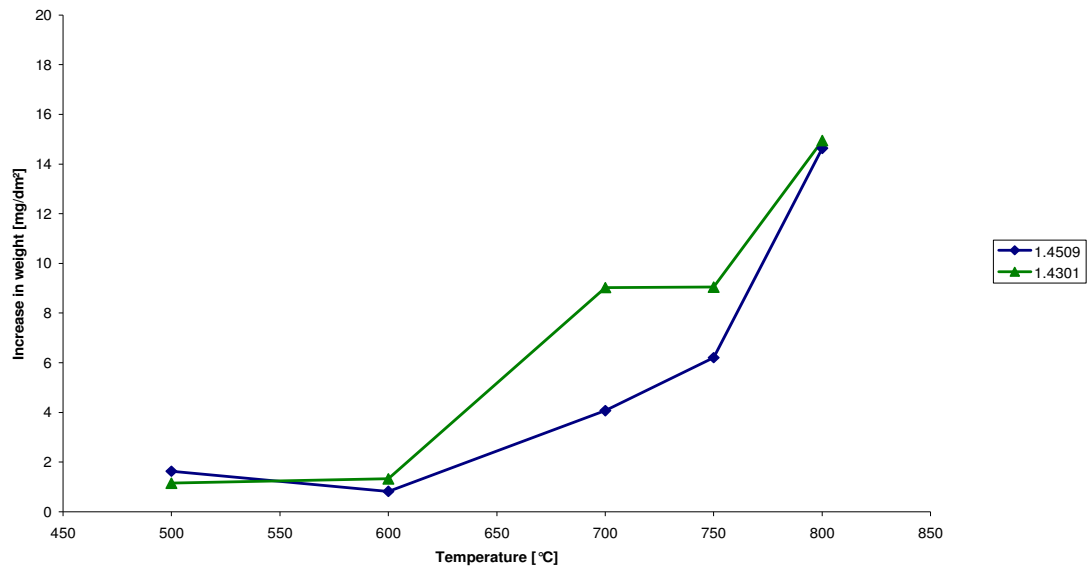
Figure 4.2: Weight gain of materials 1.4509 and 1.4301 as function of temperature, t=100h, air cooled, as rolled surface

1.4509	25X	250X
500°C 100 hrs		
800°C 100 hrs		

Figure 4.3: Surface oxides on 1.4509 after treatment of 500°C and 800°C after 100 hours showing continuous films

1.4301	25X	250X
500 °C 100 hrs		
800 °C 100 hrs		
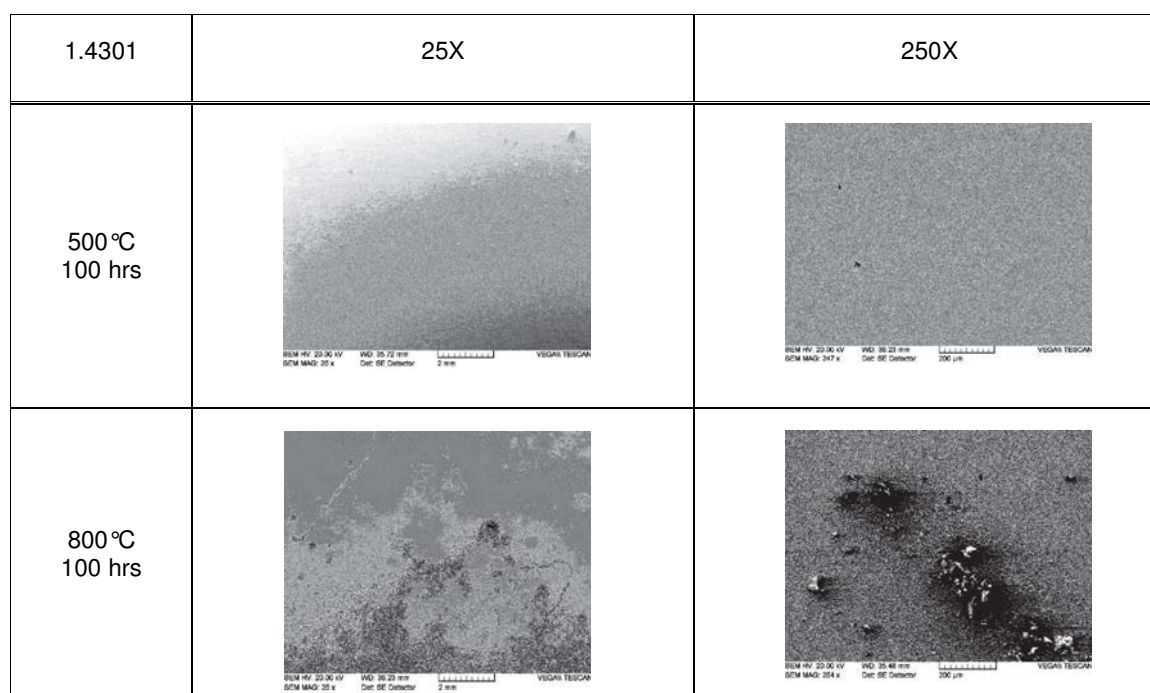
Figure 4.4: Surface oxides on 1.4301 after treatment of 500 °C and 800 °C after 100 hours showing ruptured films

From figures 4.3 and 4.4, it can be concluded that at 800 °C treatment, grade 1.4301 lost its surface layer while 1.4509 still have its surface layer. The 1.4301 sample clearly demonstrates islands of broken surface film and deep continuous attack. Discrete areas of blistering and oxide spallation occurred on the surface of 1.4301 sample. Ferritic stainless steels have a low coefficient of thermal expansion which supports reduced spalling or flake formation on surface. On the other hand, austenitic grades have high thermal expansion coefficient which makes them prone to high temperature corrosion. Also other researchers also found that ferritic stainless steels are superior to austenitic stainless steels under oxidation conditions [142-145]. The micro-structural examinations were done with the help of optical, scanning and transmission electron microscopy.

4.1.2 Effect of Temperature and Time on Microstructure

In this section, the influence of different holding temperatures for 100h on microstructure of steel grades is discussed. By optical microscopy, neither 1.4509 nor 1.4301 showed precipitations along grain boundaries below 500 °C after 100 hours. Micrographs of all treated samples at different temperatures for 100h are

shown in figure 4.5. It can be seen that grade 1.4301 showed precipitations along grain boundaries at 600°C whereas in 1.4509 no precipitation was found.

Temperature for 100h holding time	1.4509	1.4301
500°C		
600°C		
700°C		
800°C		
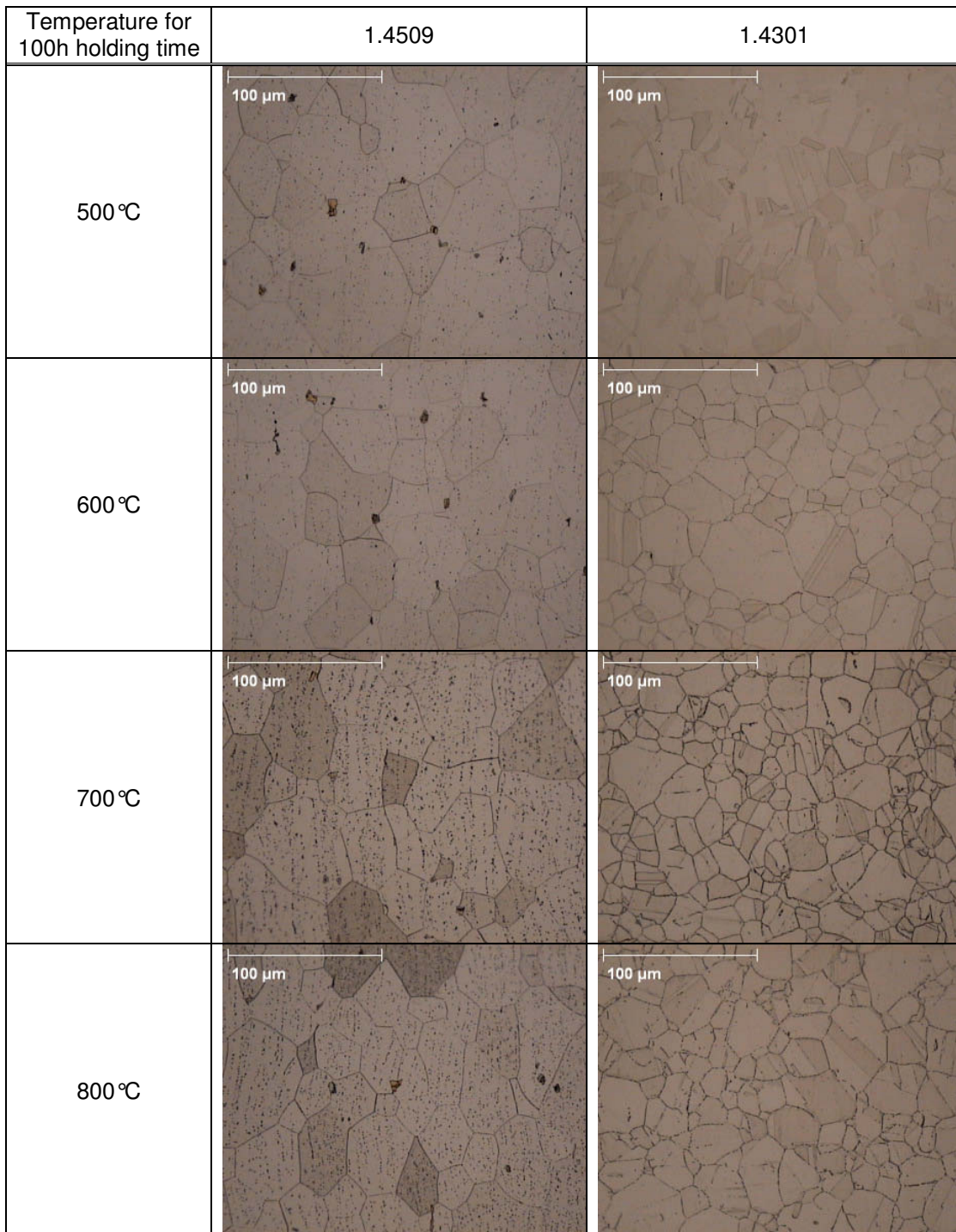
Figure 4.5: Microstructures of materials 1.4509 and 1.4301 as function of temperature, t=100h, air cooled, as rolled surface

Furthermore, a detailed investigation with the help of high resolution techniques like scanning electron microscopy and transmission electron microscopy was done for 500°C and 800°C treated samples. The temperature 500°C is the maximum possible temperature in the muffler and 800°C is the temperature in the hot end components.

4.1.2.1 Grade 1.4509 treated at 500°C and 800°C for 100 hours

SEM and TEM micrographs of grade 1.4509 treated at 500°C for 100 hours is shown in figures 4.6 and 4.7. No precipitations along grain boundaries were observed.
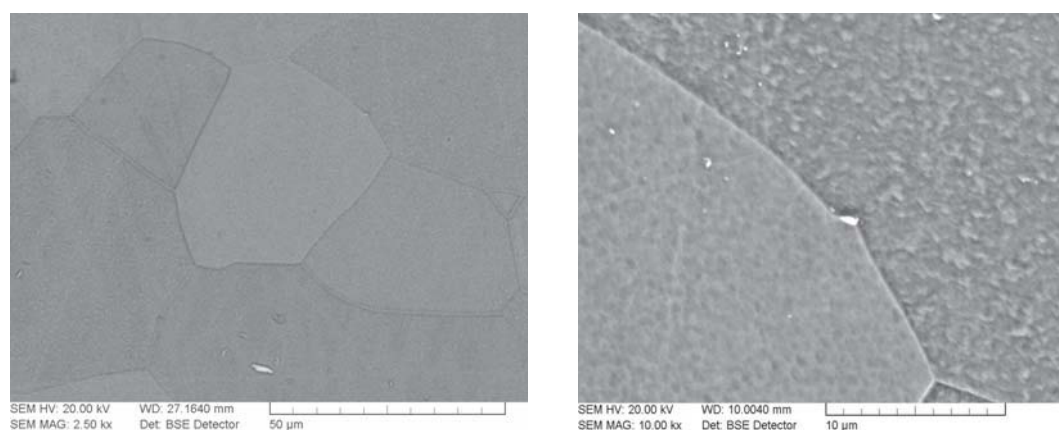
Figure 4.6: SEM micrograph 1.4509 treated 100h at 500°C
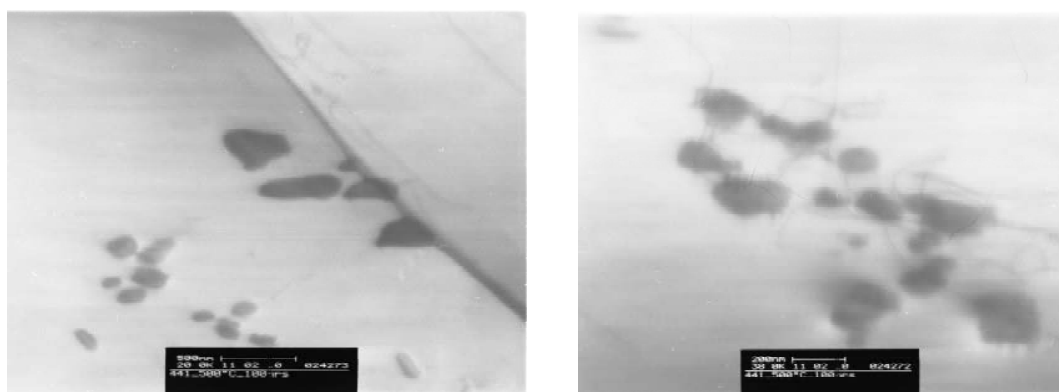
Figure 4.7: TEM micrograph 1.4509 treated 100h at 500°C

In TEM few fine precipitates were found which were scattered in the matrix. In this stabilized steel, the free standing (Ti, Nb)C were more homogeneously distributed around the sample and not only on the grain boundaries. This phenomenon is explained later in section 4.1.3 and 4.1.4 in further detail. SEM micrographs of grade

1.4509 treated at 800℃ for 100 hours are shown in figure 4.8. Some precipitations along grain boundaries were observed too.
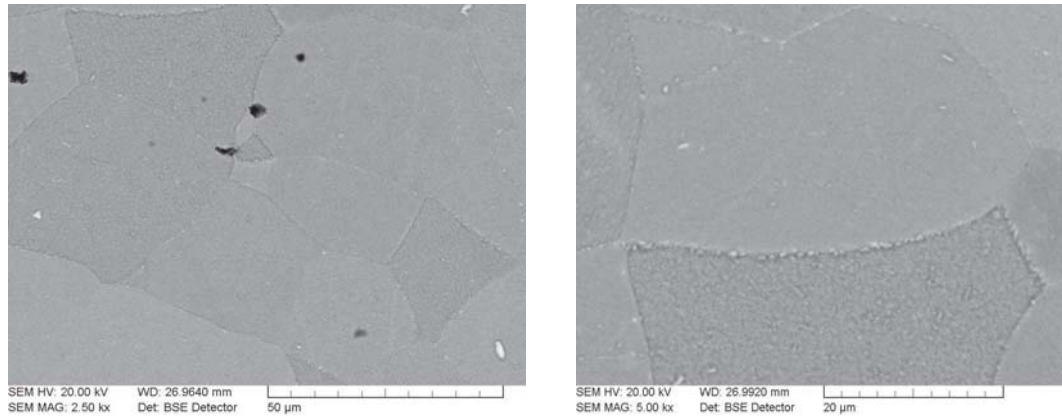
Figure 4.8: SEM micrograph 1.4509 treated 100h at 800℃, showing precipitations along grain boundaries

From figure 4.9 it can be seen that in spectrum 1 the whole area was selected and in spectrum 2 a point analysis was done directly on precipitates with the help of EDS.
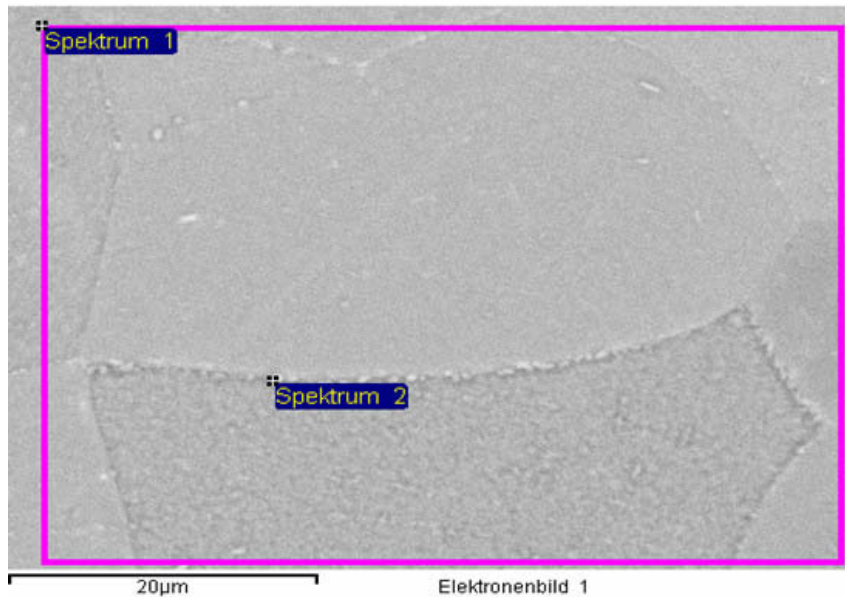
Figure 4.9: SEM micrograph 1.4509 treated 100h at 800℃

EDS analysis confirmed the difference in concentration of Ti and Nb between the centre of grains and near grain boundaries. It was partially altered by the formation of Ti and Nb carbides. In figure 4.10 it can be clearly seen that the peak of niobium is higher in spectrum 2 as compared to the spectrum 1 which indicates that in spectrum 2 we have an enrichment of niobium.
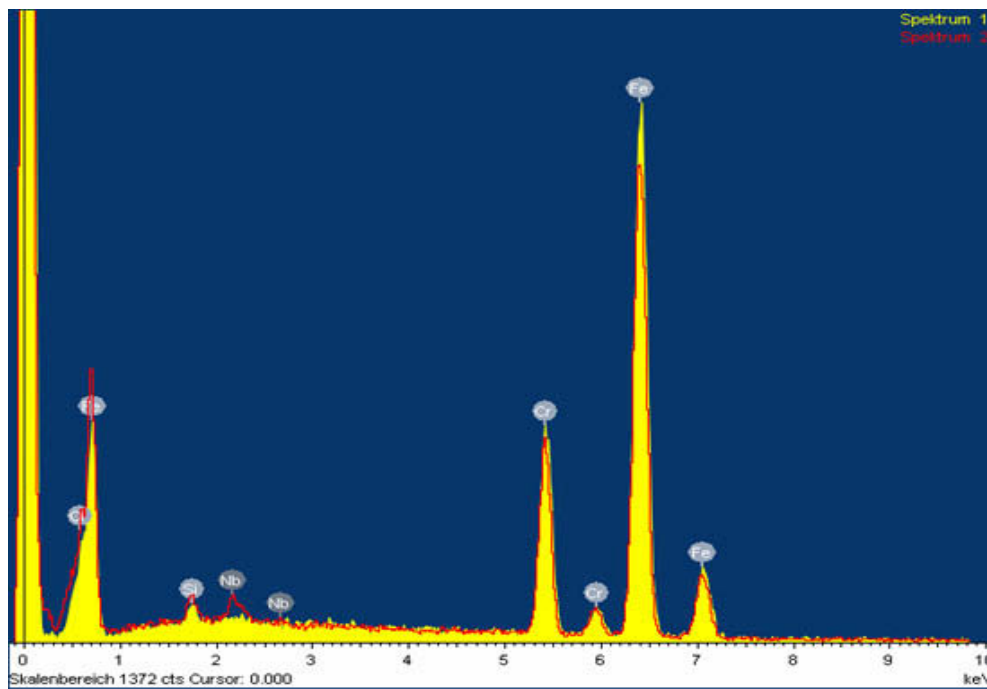
Figure 4.10: SEM/EDS analysis of 1.4509 treated at 800°C

Figure 4.11: TEM micrograph 1.4509 treated 100h at 800°C

Precipitation along grain boundaries was also found with the help of transmission electron microscopy. Furthermore, EDS analysis confirmed the presence of niobium and titanium enriched phases. Similarly, some precipitates of niobium were found directly in the grains. A point analysis from position 1 shows this effect where a niobium enriched phase was detected.
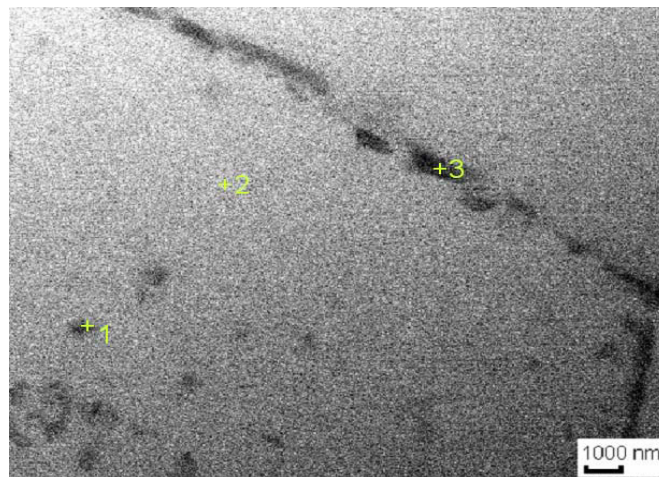
Figure 4.12: TEM micrograph 1.4509 treated 100h at 800 °C
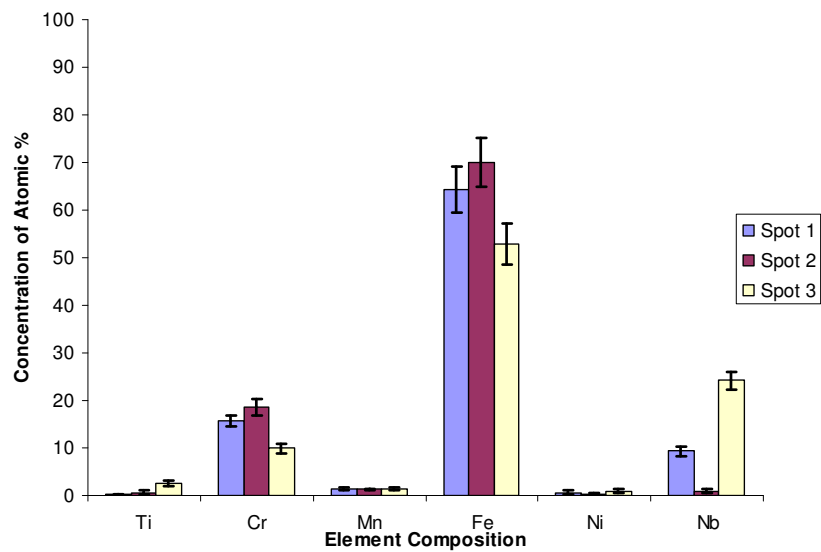
Figure 4.13: TEM/EDS analysis 1.4509 treated 100h at 800 °C

4.1.2.2 Grade 1.4301 treated at 500 °C and 800 °C for 100 hours

Also in grade 1.4301, there are no precipitations along grain boundaries below 500 °C. Both SEM and TEM results showed no grain boundary precipitation as shown

in figures 4.14 and 4.15. The microstructure of a specimen treated at 800 °C for 100 hours showed a strong attack along grain boundaries.
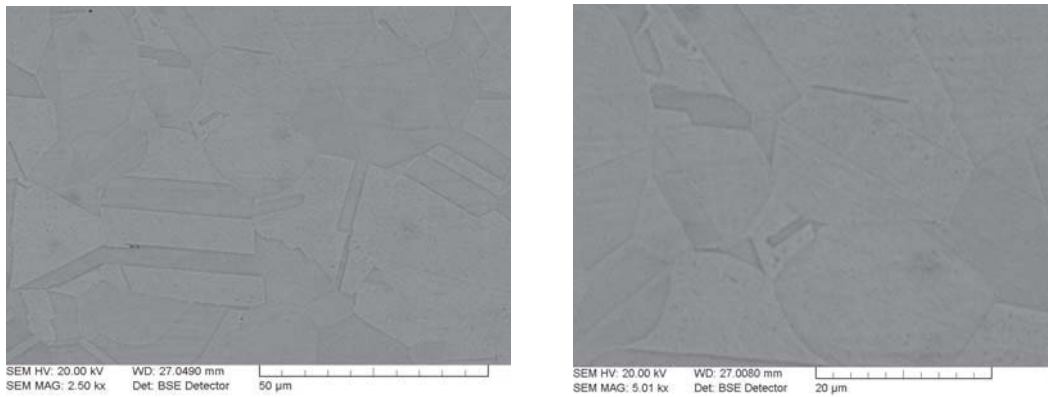
Figure 4.14: SEM micrograph 1.4301 treated 100h at 500 °C

A neat and clean microstructure without any discontinuities and imperfections are present at 500 °C both in micrographs of SEM and TEM.

Figure 4.15: TEM micrograph 1.4301 treated 100h at 500 °C

After heat treatment at 800 °C, the material shows a totally different behaviour. The microstructure investigations by SEM and TEM reveal the fact that the material is sensitized. Moreover, a high rate of precipitation along grain boundaries is found.
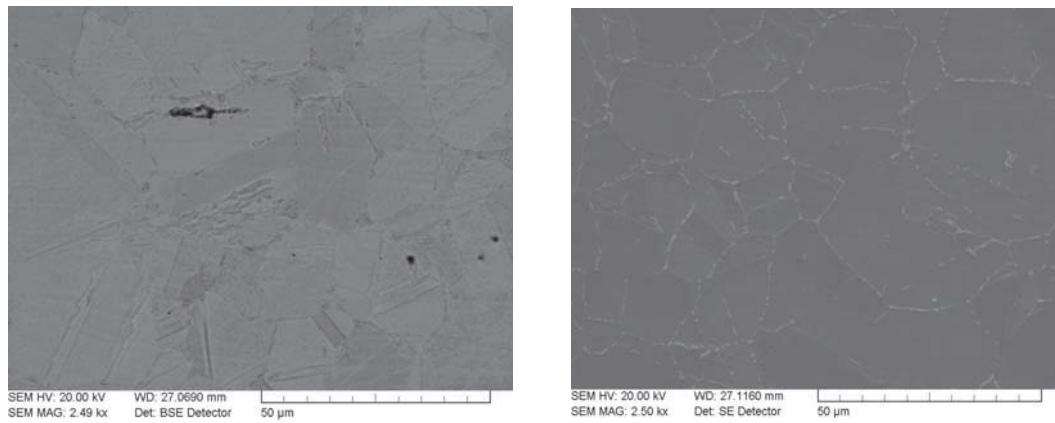
Figure 4.16: SEM micrograph 1.4301 treated 100h at 800 ℃
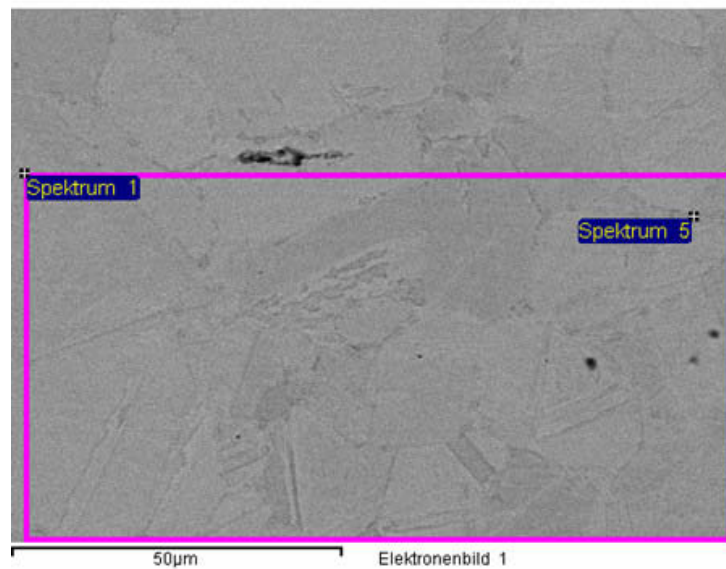
Figure 4.17: SEM micrograph 1.4301 treated 100h at 800 ℃

The EDS analysis with the help of SEM confirmed the chromium carbide precipitation along grain boundaries after this treatment. In spectrum 1 the whole area was selected and in spectrum 5 a point analysis was done directly on the precipitates with the help of EDS.
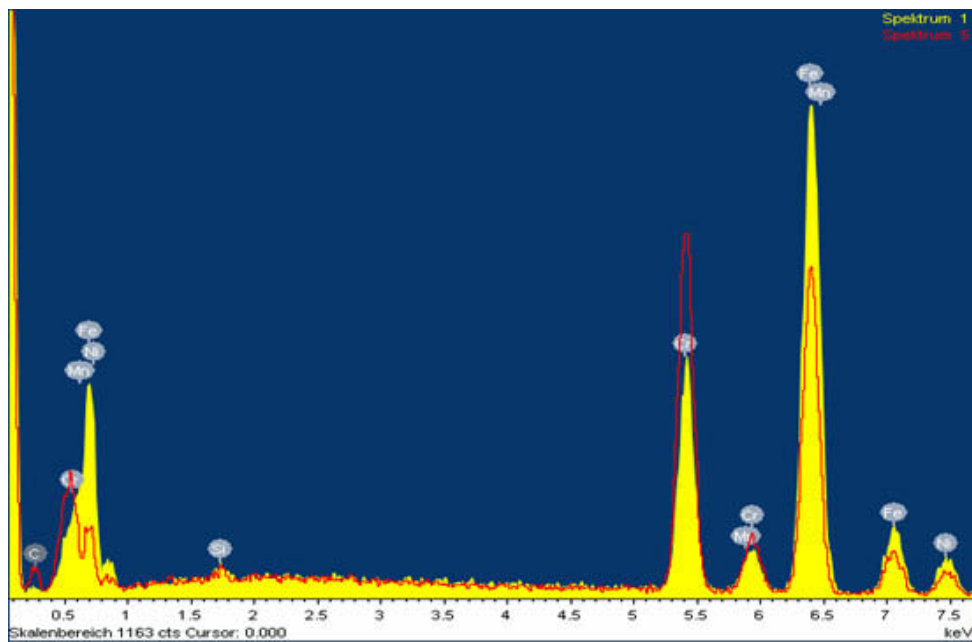
Figure 4.18: SEM/EDS analysis 1.4301 treated 100h at 800°C

The precipitation of chromium carbides can be noted at 800°C. The ditches at the grain boundaries were confirmed as chromium carbides with the help of EDS analysis shown in figures 4.18 and 4.21.
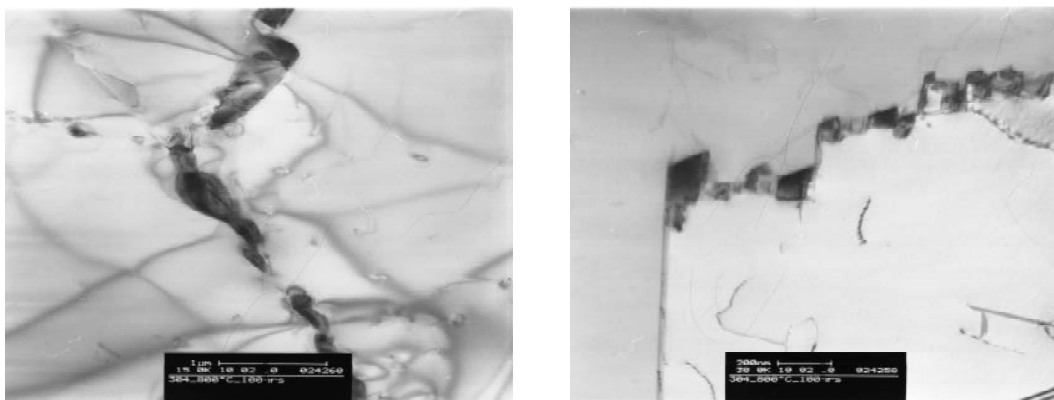
Figure 4.19: TEM micrograph 1.4301 treated 100h at 800°C, showing precipitations along grain boundaries
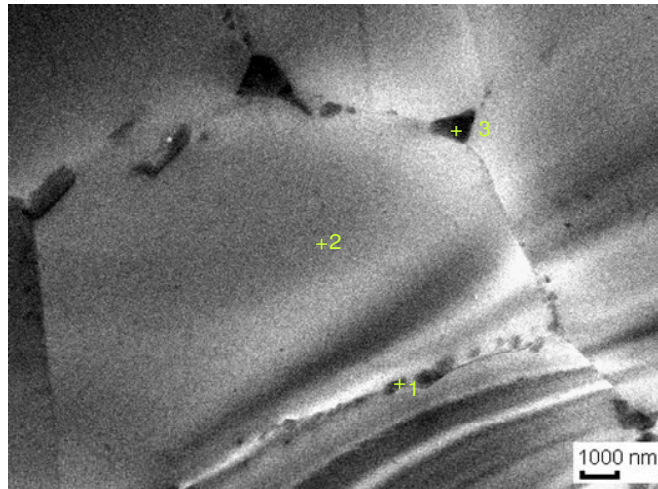
Figure 4.20: TEM micrograph 1.4301 treated 100h at 800°C

In point analysis, position 1 and 3 showed high percentage of chromium as compared to position 2, which was directly in the matrix.
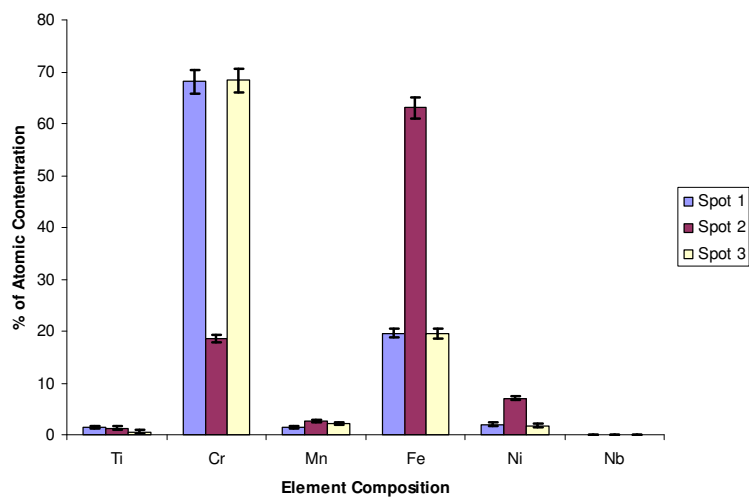
Figure 4.21: TEM/EDS analysis 1.4301 treated 100h at 800°C

4.1.3 Cyclic Oxidation Test

Heating with additional cooling cycles has a strong impact especially on ferritic grade. From figure 4.22, it can be seen that the microstructure of 1.4509 has some precipitates on the surface. These precipitates were confirmed as Ti and Nb enriched particles with the help of SEM-EDS analysis. One example is shown in figure 4.23. In a single continuous heating, they remained same and closed like in as received condition. Surprisingly, the behavior changed and these precipitations burst off and were totally opened during additional cooling cycles. In austenitic grade no surface change was observed due to these treatments.

Treatments	1.4509	1.4301
As received condition		
500 °C for 10 h		
500 °C for 10 h with cooling intervals		
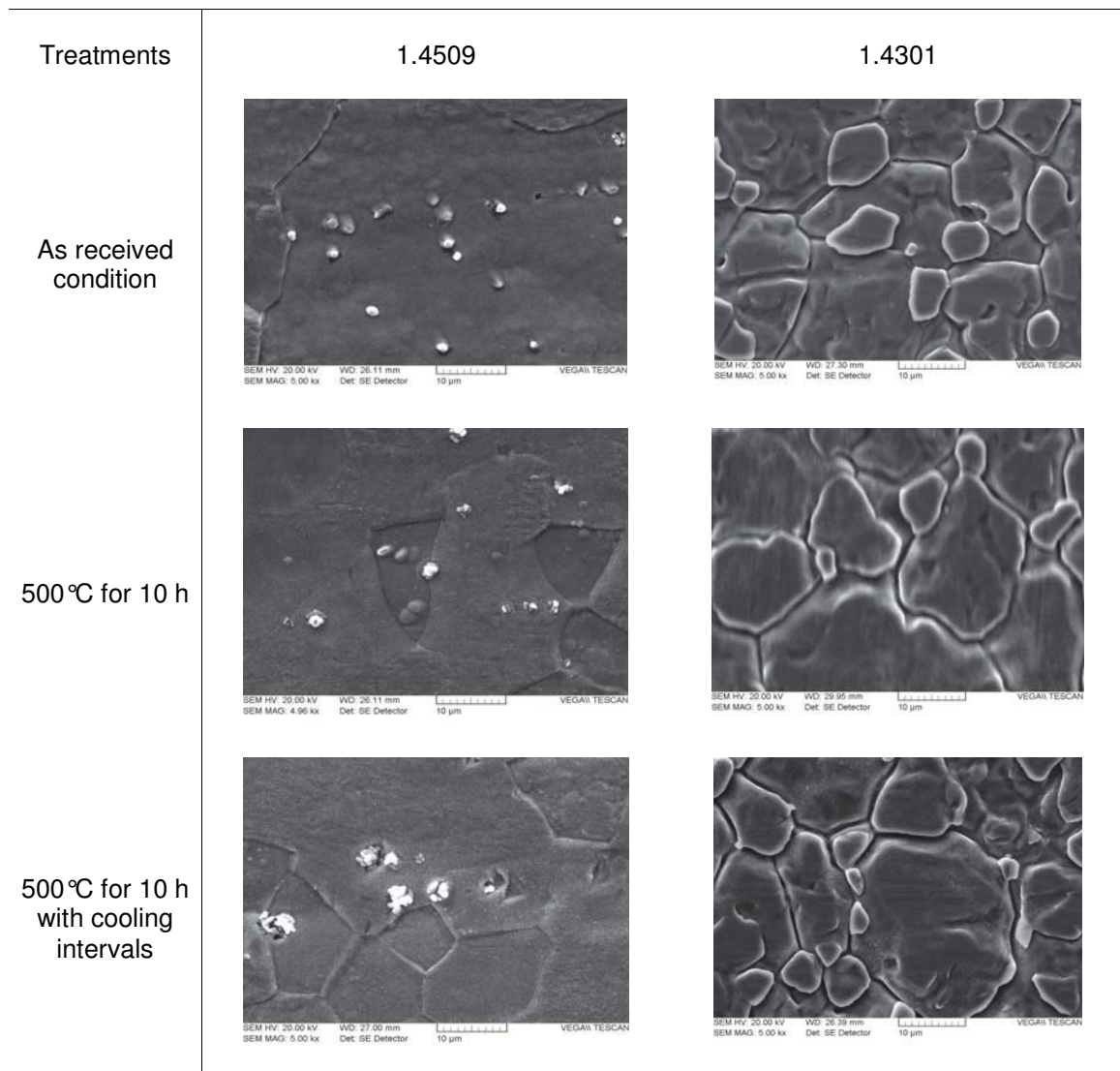
Figure 4.22: Surface topography of both grades after different aging heat treatments
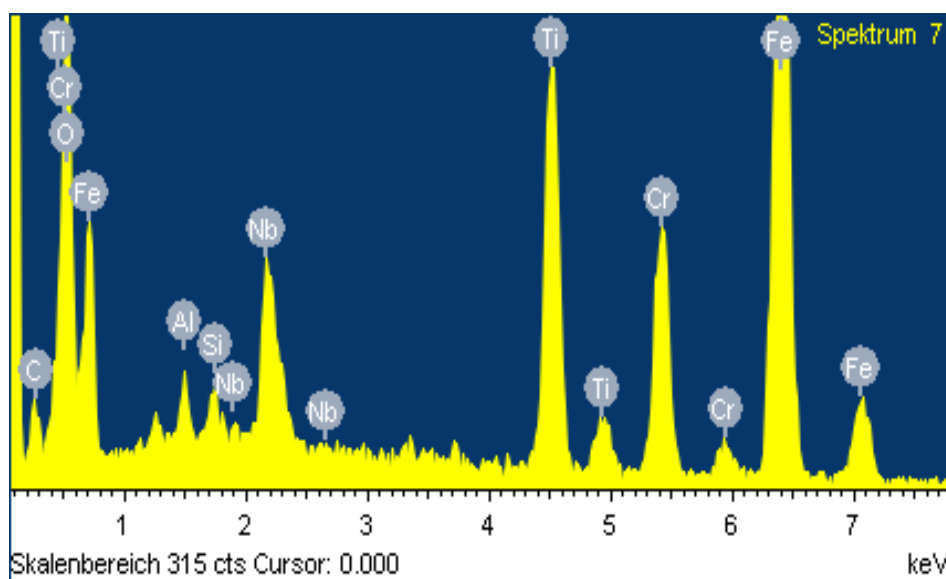
Figure 4.23: EDS analysis of precipitate confirming enrichment of Ti and Nb

4.1.4 Cyclic Oxidation Test in Combination with Ferroxyl Test

A well known ferroxyl test according to ASTM A-380 was performed to detect the presence of free iron or iron oxide after oxidation treatment. Samples after different heat treatments were studied. A few minutes were enough to detect the rough locations of the pores in the sample by the inspection of blue precipitates which occurred due to the reaction of solution with free iron. The reaction is given in equation 4.1. The formed blue precipitates grow rapidly in size, thus making it easy to examine [146]. Furthermore, scanning electron microscopic investigations were done to study the influence on surface characteristics before and after the test.

K^+ (aq) + Fe^{2+} (aq) + $[Fe(CN_6)]^{3-}$ (aq) → $KFe_{III}Fe_{II}$ $(CN)_6$ (s)   (Equation 4.1)
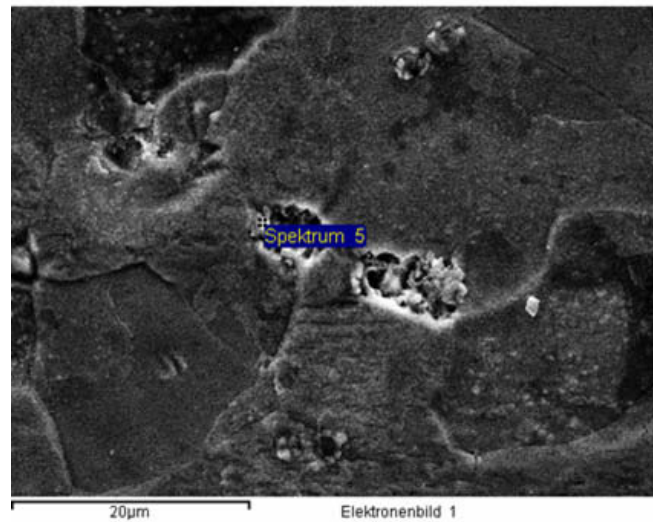
Figure 4.24: Microstructure of 1.4509 (500°C for 10 h with cooling cycles) after ferroxyl test

It was found that pitting initiates from the ruptured sites after periodic heating and cooling of the samples. Elemental analysis showed some Ti and Nb particles in EDS spectrum. Peaks of niobium and titanium are visible in figure 4.25.
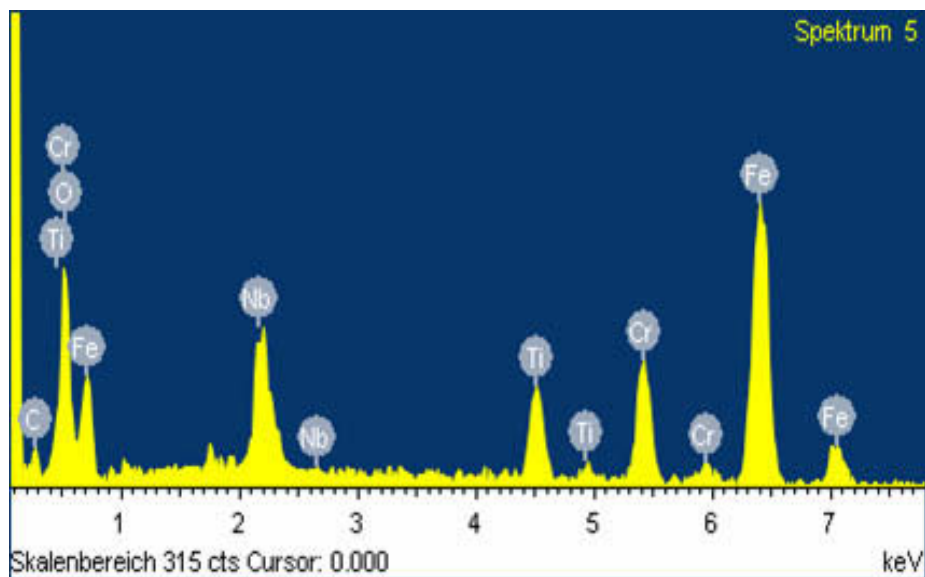
Figure 4.25: Elemental analysis from the opening in the surface

Pitting was found mostly in the positions in the matrix where Ti and Nb precipitates were present. The results showed that the grade 1.4509 was more prone to this type of localized corrosion because of discontinuities in its passive film.

4.1.5 TOF-SIMS Depth Profiles

The TOF-SIMS depth profile analysis on as received specimen and heat treated sample at 500°C were performed. The sputter profiles are presented in figures 4.26 and 4.27. The sputter depth can be calculated with the knowledge of the sputter performance. The sputter performance (nm/nA*s) depends basically on material and matrix (composition) as well as sputter parameters e.g. used projectile, angle, energy and current. The last parameters are known due to the sputter set up, but the effect of the special composition (matrix) is unknown. For pure materials in the used geometry is about Fe: 1/136.0 nA*s/nm and Cr 108.8 nA*s/nm. For the presented data to 20000 nA*s the sputter depth based on these calculated performances can be assumed in the magnitude of 147 nm (pure Fe) and 183 nm (pure Cr). Comparing the sputter profiles to each other there are visible differences in oxide layer thickness and also in the position of Cr-/Ti-/Nb signal maxima. The most intense signals in both profiles are Fe and Cr. The non-treated sample show a Cr and Fe maxima basely from the beginning falling down rapidly (below 1000 nA*s sputter count). Also the O-signal falls down in the same region of sputter counts to a marginal intensity. The 500°C heat treated sample show a local maximum in the Cr signal at about 1800nA*s and absolute maximum at about 39000nA*s. Also the O signal begins to fall down at this normalized sputter count value i.e. 3900 nA*s. This leads to the conclusion that the thickness due to the thermal treatment at 500°C is thicker (almost 16 times thicker) than those of the non-treated sample. Also it can be stated that there seems to be a Cr/Nb/ Ti rich layer in the interface of the bulk material and the oxide top layer.
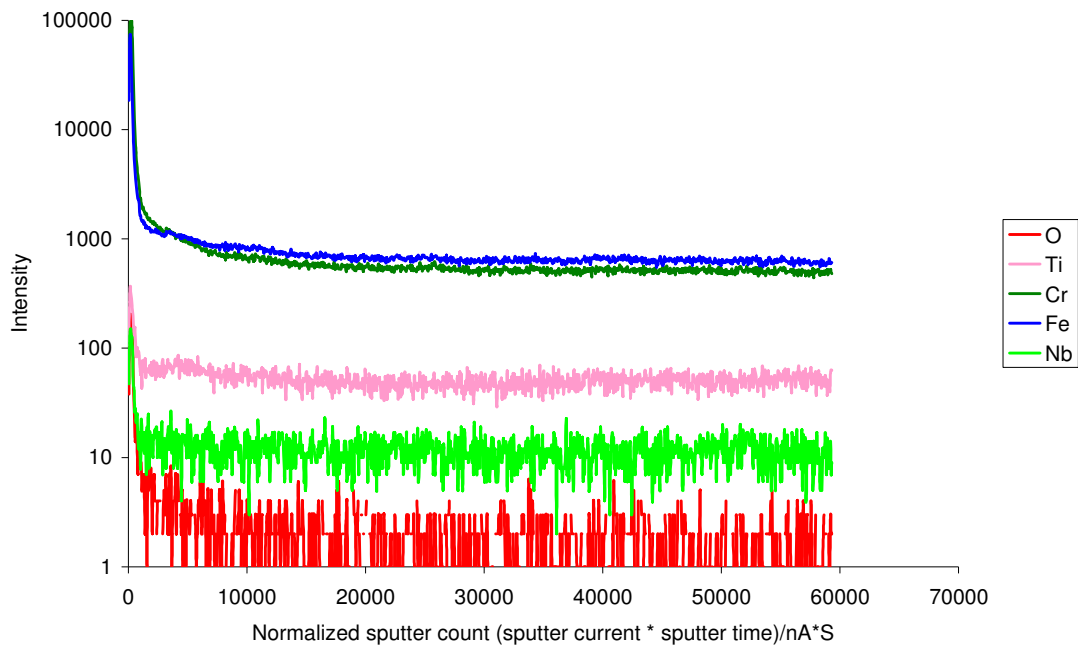
Figure 4.26: Depth profile analysis of 1.4509 as received condition
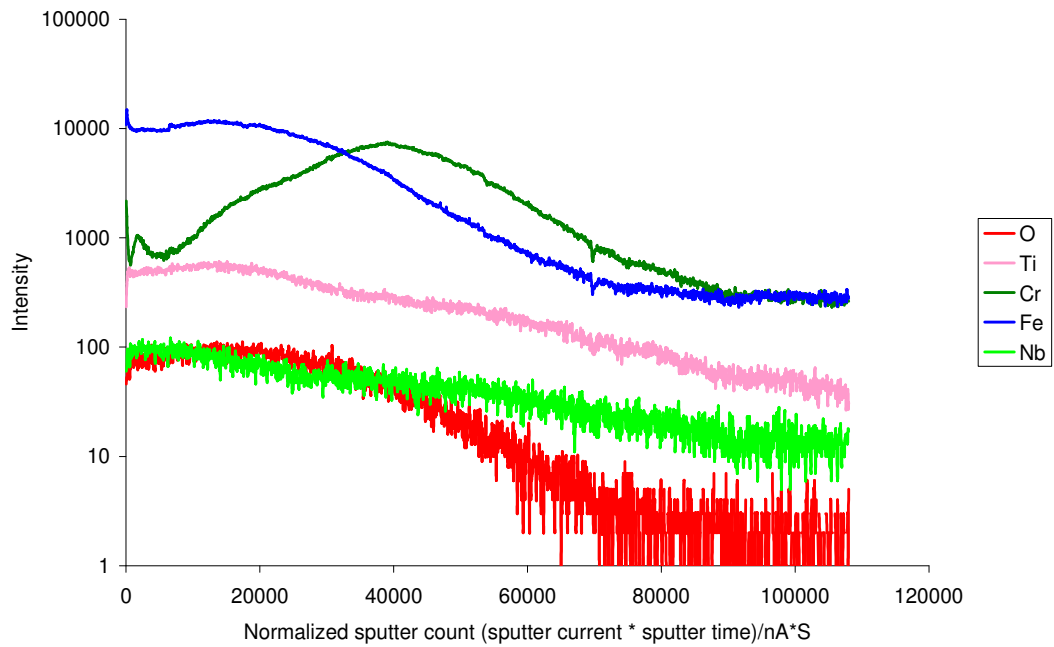
Figure 4.27: Depth profile analysis of 1.4509 heat treated samples at 500 °C for 10 hours

4.2 External Corrosion

4.2.1 Modified Salt Spray Tests

4.2.1.1 Influence of Heating cycle

Temperature is one of the critical factors that effects localised corrosion process [147]. It is well known that resistance against localised corrosion decreases as temperature increases [147-150]. In standard VDA 621-415 i.e. method A, no corrosion attack was found on both materials. Radiographic images from both samples are shown in figure 4.28. Sample with heating cycle showed high amount of pitting corrosion attack whereas, a very less pitting attack was found in un-treated sample. It can be clearly seen that additional heating cycles had strongly enhanced the corrosion.

Without Heating Cycle	With Heating Cycle
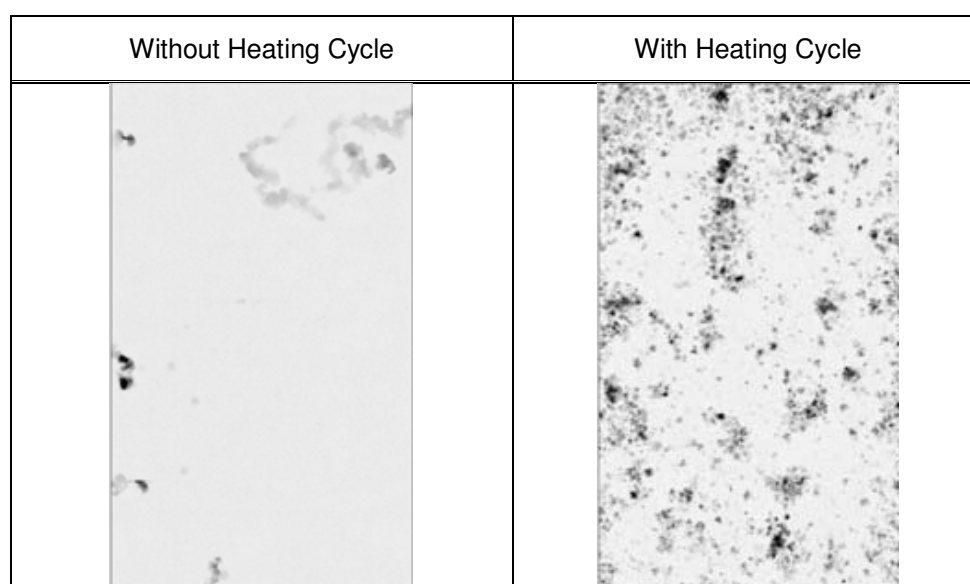
Figure 4.28: Radiographic images of crevice samples after 6 weeks
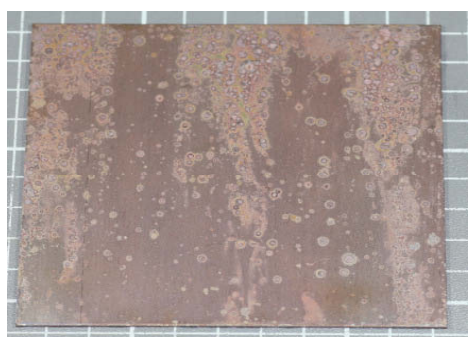
4.2.1.2 Influence of Different Test Methods

The simulation below consists of similar heating cycles and combinations. A comparative study was made among different salt spray testing methods. A brief summary of all test methods is given in table 4.1. Cyclic test D was found to be a good compromise between less aggressive method B and most aggressive method C. Photographs which were taken immediately after 1 week of exposure before the

corrosion products were washed off are presented in figure 4.29. In figure 4.30, results of radiography are given. Highest pitting corrosion attack was observed after method C.
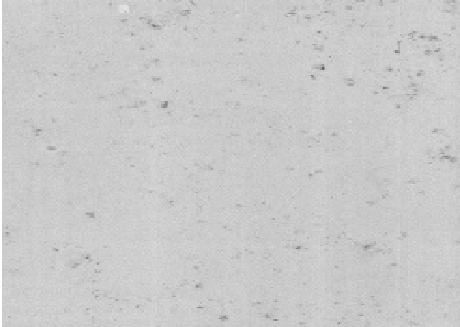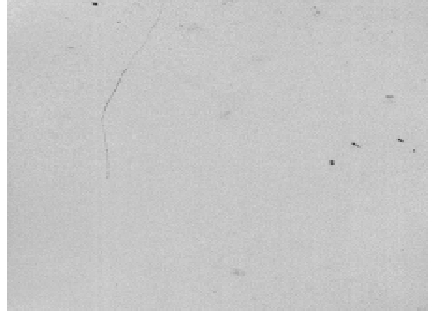
Table 4.1: Comparison of Modified VDA Salt Spray Tests

Methods After 1 week	Salt Spray Phase (h)	Condensed Water Climate (h)	Room Climate (h)	Heating Time (h)	Comments
A	24	96	48	0	No corrosion attack was found after 1 week
B	24	96	24	24	With weekly heating, a clear difference in amount of corrosion attack was observed
C	24.5	98	21	24.5	This cycle was used to compare with the method B. It was found to be the most aggressive method amongst all
D	24.5	24.5	87.5	24.5	It's a Faurecia's standard cycle with daily heating and during this study it was found that it's a good compromise between method B and method C. It's mild

Methods After 1 week of Testing	1.4509	1.4301
Method A		
Method B		
Method C		
Method D		

Figure 4.29: Overview of samples after different testing methods

Methods After 1 week of Testing	1.4509	1.4301
Method A		
Method B		
Method C		
Method D		

Figure 4.30: Radiographs for direct comparison after different testing methods, black spots presenting pitting corrosion attack

4.2.1.2 Influence of Crevice Gaps

The size of artificial crevices was 0.1, 0.5 and 1.0 mm. Quantification of corrosion attack on samples was done by measuring the pit depths by use of X-ray radiography. The radiographic images are shown in figure 4.31. The area above the red dotted line is the upper part of the samples where crevice opening (crevice mouth) was present.
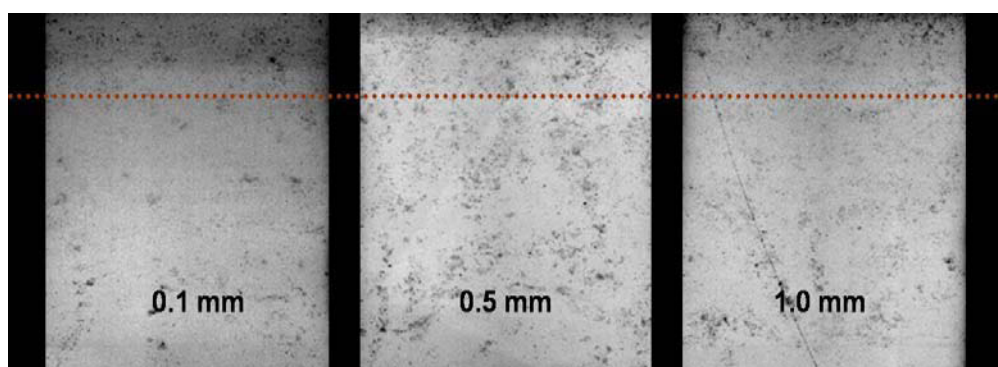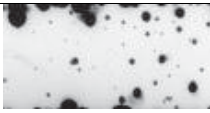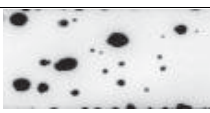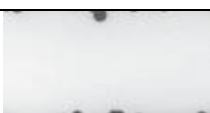
Figure 4.31: Radiographic images of crevice samples after 10 weeks Method D, area above dotted red line presenting crevice opening (crevice mouth)

It was found that all crevice coupons showed more severe corrosion in the opening i.e. near to crevice mouth as compared to bottom. The results showed that corrosion attack was higher in 0.5 mm gap but lower in 0.1 mm and 1.0 mm after ten cycles of testing. This test was repeated for several times to check the reproducibilty. It was found that on the basis of salt spray test it was very difficult to make a clear ranking among all the crevices because scattering rate was very high. Only some samples have shown a uniform behaviour like the above mentioned examples. The problem with this test method is that the electrolyte is applied in form of salt spray and only reaches to some portion inside the crevice samples. Electrolyte cannot penetrate easily into the crevice without capillary forces. Hence, the crevice has non uniform electrolyte distribution and most of the time remains dry or is only partially wet. This leads to different conditions inside the crevice and thus different conditions for each specimen resulting in no comprehensive behaviour. Therefore, from this study it can be concluded that the salt spray test is not suitable for studying the crevice corrosion phenomenon.
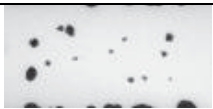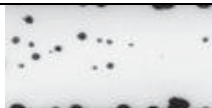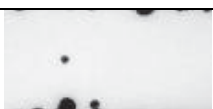
4.2.2 Ferric Chloride Immersion Test

After completion of the test, corrosion products were removed from the specimens and after cleaning, pitting quantification was done with the help of radiography. In figure 4.32 radiographs of specimens tested with different crevice widths are shown.

Setup type	Specimen number	Crevice width [mm]	Applied stainless steel sheet	Counter piece
1.4509 / Plexiglas	1	≈ 0		Plexiglas
	2	0.1		Plexiglas
	3	0.3		Plexiglas
	4	0.5		Plexiglas
	5	1.0		Plexiglas

Figure 4.32: Effect of crevice width on pitting in a crevice, 1.4509 with Plexiglas during ferric chloride immersion test (6% FeCl$_3$, 22°C, 1 week)

From figure 4.32, it can be concluded that a crevice width 0.5 and 1.0 mm crevice shows the lowest rate of corrosion. The specimen 1 i.e. ~0.0 mm which was without any crevice also showed very little attack. For the other crevice sizes 0.1 mm, 0.3 mm and 0.5 mm no clear ranking could be made. For tight crevice e.g. ≈ 0.0 mm, no penetration was possible. It can also be concluded that when the width of the crevice is large, the solution ions or oxygen transfer well through the outside and inside of the crevice, causing the concentration difference to decreases, with the result that crevice corrosion does not occur.

Setup type	Specimen number	Crevice width [mm]	Applied stainless steel sheet	Counter piece
1.4509/ 1.4509	7 / 8	≈ 0		
	9 / 10	0.1		
	11 / 12	0.3		
	13 / 14	0.5		
	15 / 16	1.0		

Figure 4.33: Effect of crevice width on pitting in a crevice, 1.4509 with 1.4509 during ferric chloride immersion test (6% FeCl$_3$, 22°C, 1 week)

From figure 4.33, one can say that the crevice with width 1.0 mm crevice showed the lowest rate of corrosion. The specimen 7/8, i.e. ~0.0 mm which was without any crevice also showed very little attack of edges. Therefore, it can also be concluded that for bigger crevice susceptibility to crevice corrosion decreases. For the other crevice sizes 0.1 mm, 0.3 mm and 0.5 mm no clear ranking could be made.

4.2.4 Potential Measurements in Crevice

4.2.4.1 Measurement in 6% FeCl$_3$ solution

After performing the electrochemical measurements, potential-time curves for each crevice size were plotted in a diagram. Results of 0.1 mm crevice size are presented in figure 4.34.

0.1 mm

The potential-time-curve, presented in figure 4.34, for 0.1 mm crevice width showed an average potential value of -650 mV during the test duration of 100 hours.
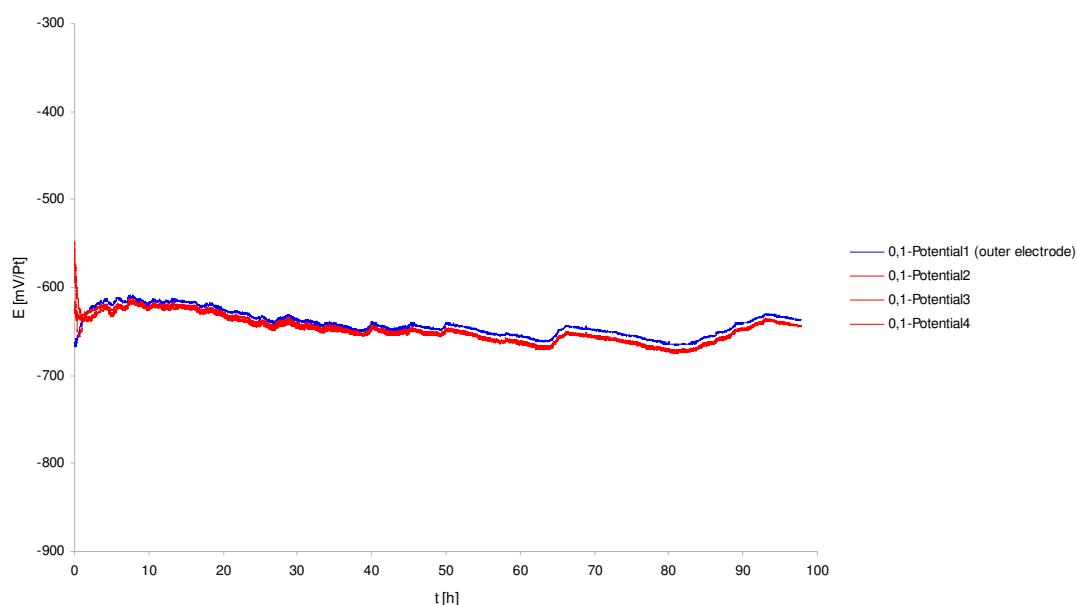
Figure 4.34: Potential time curve measured in 6% FeCl$_3$ – 0.1 mm crevice

In figure 4.35 the specimen surfaces, crevice and backside, are shown. Here, pits are marked in red circle as shown in both pictures. The other big pits on edge corners are due to crevice formers. This crevice corrosion happened where the ceramic shims were in contact with the sample. The pit in crevice grew throughout the whole thickness of the stainless steel sheet, leaving a big hole in the specimen.

Crevice side	Backside

Figure 4.35: 1.4509 specimen surfaces after measurement in 6% $FeCl_3$ – 0.1 mm crevice

0.5 mm

The potential-time-curve, presented in figure 4.36, for 0.5 mm crevice width stabilises at a potential of -650 mV for 100 hours.
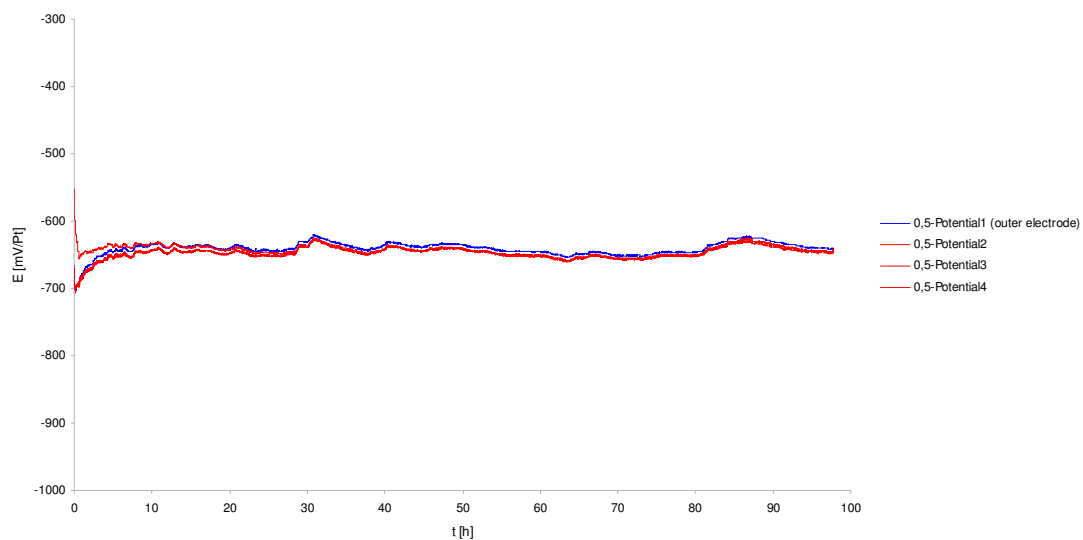
Figure 4.36: Potential time curve measured in 6% $FeCl_3$ – 0.5 mm crevice

In figure 4.37 the specimen surfaces, crevice and backside, are shown. Here, some big pits can be observed. On crevice side, crevice corrosion was seen where the ceramic shims were present. The pit, which is marked red in picture of crevice side and backside, grew throughout the whole thickness of the stainless steel sheet. After these measurements in the $FeCl_3$ medium no conclusions could be made to differentiate between two different crevice sizes. Due to the aggressiveness of the medium, it was not possible to detect the initiation point of crevice corrosion.

Obviously, only pitting has been obtained and minor crevice corrosion which would have been more uniform. FeCl₃ solution is too much aggressive resulting in immediate pit initiation in grade 1.4509. To overcome this issue in a next phase, a less aggressive medium was used.

Crevice side	Backside
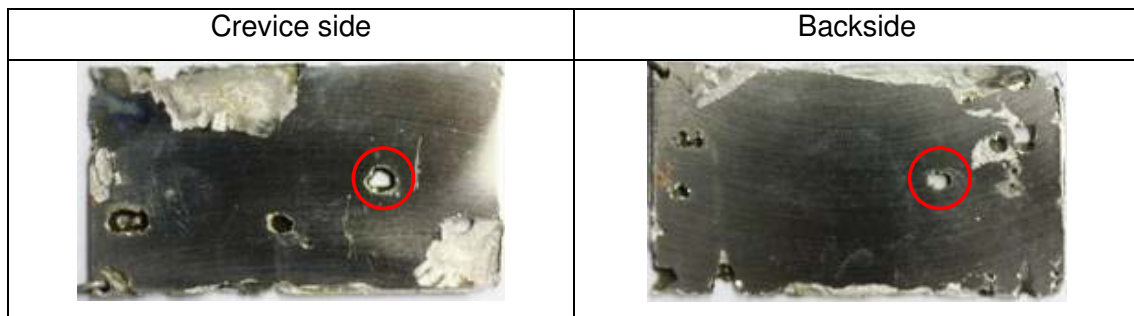
Figure 4.37: 1.4509 specimen surfaces after measurement in 6% FeCl₃ – 0.5 mm crevice

4.2.4.2 Measurement in 10 ppm Cl⁻ Solution

In figure 4.38, the results of 0.1mm crevice size in 10 ppm of Cl⁻ solution are given.
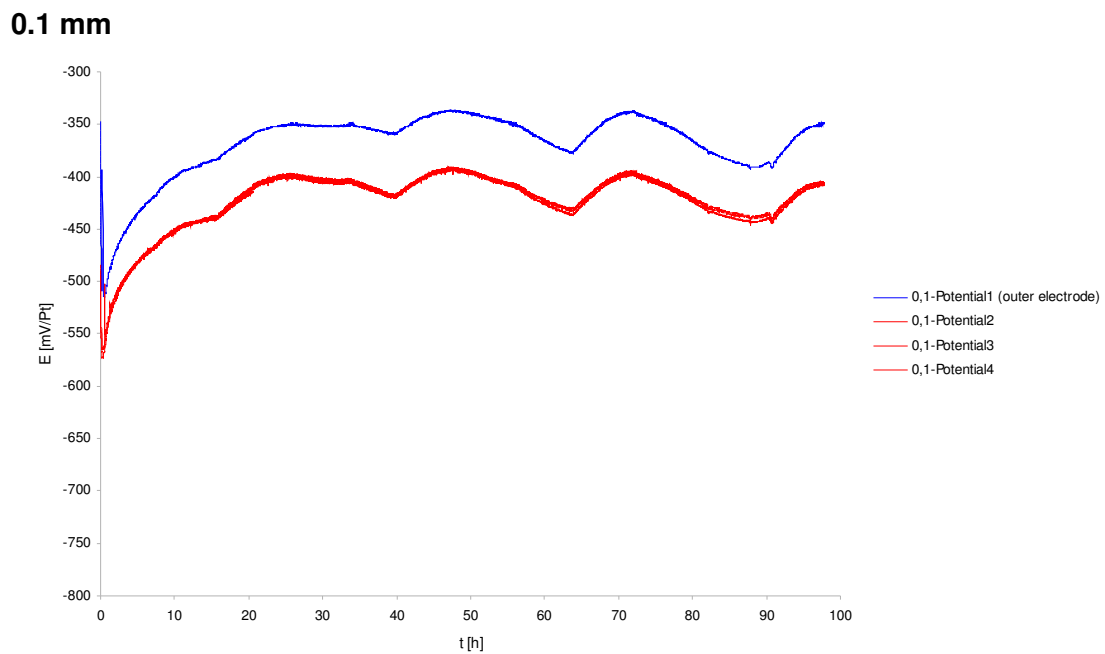
0.1 mm

Figure 4.38: Potential time curve measured in 10 ppm Cl⁻ – 0.1 mm crevice

The potential-time-curve for 0.1 mm crevice size measured for 100 hours shows an approximately stable behaviour, with some short breakdowns and repassivations. Average potential is about 425 mV. Furthermore, it was found that the potential for the outer electrode is 50 mV nobler than inside the crevice. No pitting corrosion attack was found inside the crevice because of low aggressiveness of the electrolyte.

0.5 mm
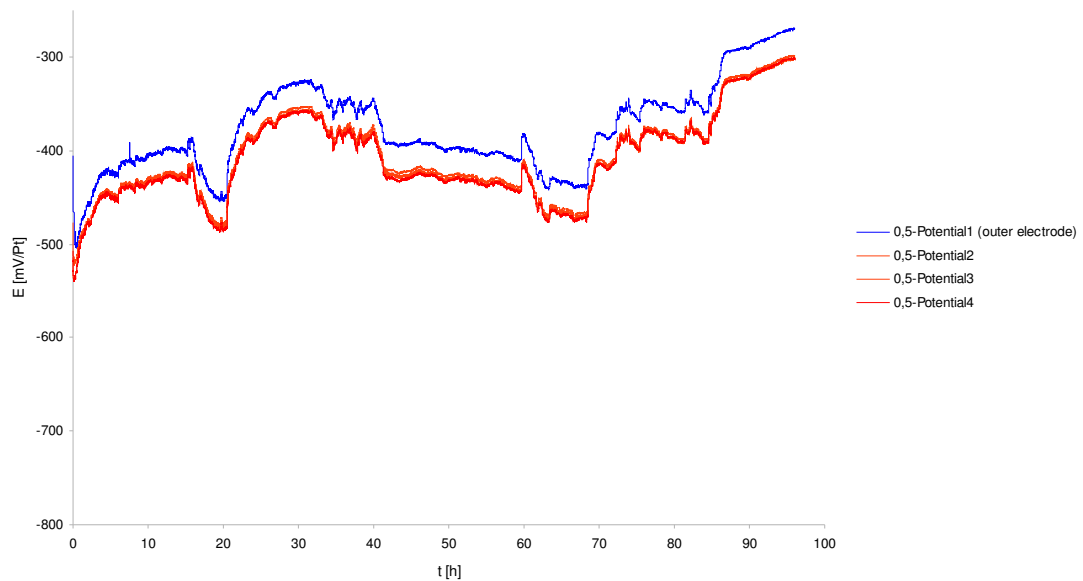
Figure 4.39: Potential time curve measured in 10 ppm Cl⁻ – 0.5 mm crevice

The potential-time-curve for 0.5 mm crevice size shows no stable behaviour during the whole measurement. Here, the average potential of about -40 mV is taken. The reason for this could be that 0.1 mm represents more severe crevice gap than 0.5 mm. Due to a very low aggressiveness of 10 ppm Cl⁻ solution, no crevice corrosion was noticed on specimen's surfaces after optical microscopy. Furthermore, different aeration cells were built during measurement. Likewise, it was found that the potential for the outer electrode is 25 mV nobler than inside the crevice. The difference was lower in a bigger crevice as compared to the tight crevice. No pitting corrosion attack was found inside the crevice because of less aggressiveness of the electrolyte.

4.2.5 Potentiodynamic Polarization Measurements

4.2.5.1 Influence of Temperature

The influence of temperature on corrosion was studied for both material grades. Results of electrochemical measurements of 1.4509 are shown in figure 4.40. For every treatment two measurements were done to check the reproducibility. Materials after every heat treatment were passive and showed a pronounced passive range in the current test solution of synthetic condensate at room temperature with aeration. The samples were heat treated at different temperatures for 10h hours. 1X10 presents continuous heating for 10 hours. After different heat treatments both stainless steels show a pronounced but shorter passive range than the as received condition. E_{pit} was not pronounced and deflection point was not visible in curves. A point 10^{-2} mA/cm^2 was defined as a reference point to measure the correspondent potential in every measurement. This method to give E_{pit} is commonly used by various steel suppliers. Grade 1.4509 exhibited a pitting potential of 110 mV and grade 1.4301 had a significant higher pitting potential of 105 mV as in received form.
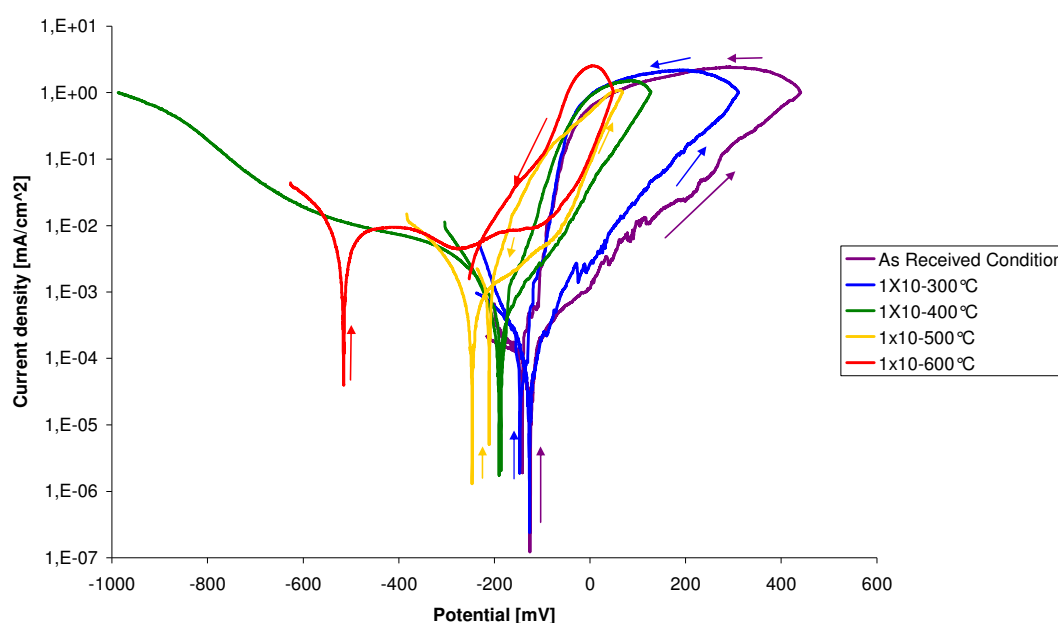
Figure 4.40: Potentiodynamic curves of differently sensitized 1.4509 in synthetic condensate with aeration at RT
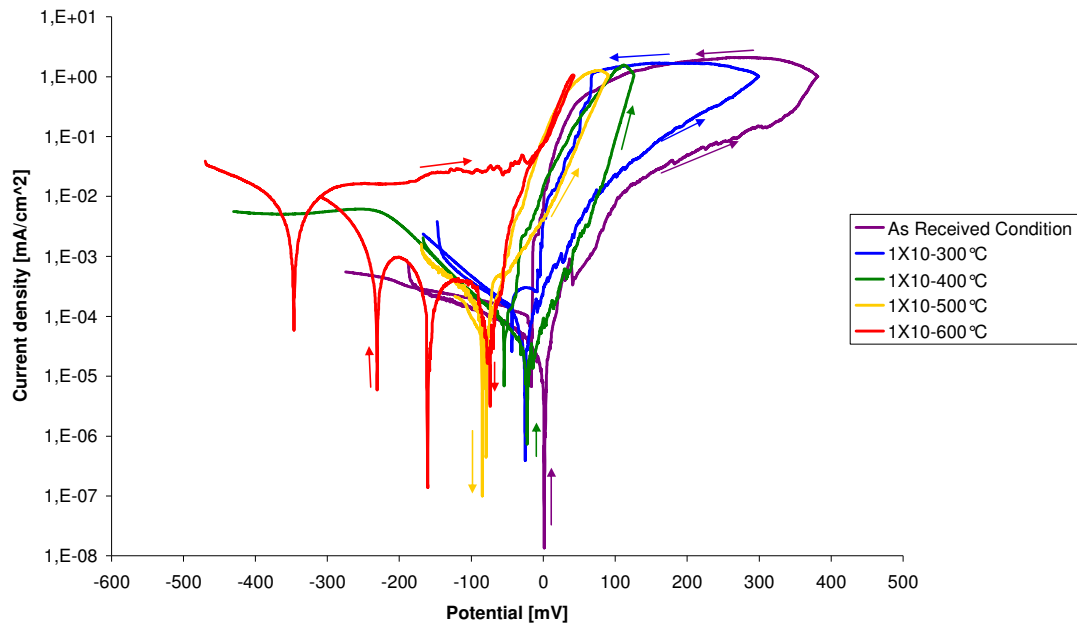
Figure 4.41: Potentiodynamic curves of differently sensitized 1.4301 in synthetic condensate with aeration at RT

In figures 4.40 and 4.41, it was found that in both grades, higher the sensitization temperature, less noble is OCP and lower is $E_{pit.}$ At sensitization temperature of 600°C, both grades showed no hysteresis in their current-potential curves. Thus, only uniform corrosion has happened and no pitting corrosion was found.

Table 4.2: Corrosion parameters obtained from the potentiodynamic curves of 1.4509

1.4509	As-Received	1X10-300°C	1X10-400°C	1X10-500°C	1X10-600°C
OCP [mV_{SCE}]	-99	-130	-203	-283	-526
E_{Pit} (at 0.01mA/cm^2) [mV_{SCE}]	110	71	-44	-57	-130
E_{Repass} [mV_{SCE}]	-105	-99	-150	-220	-170

Table 4.3: Corrosion parameters obtained from the potentiodynamic curves of 1.4301

1.4301	As-Received	1X10-300°C	1X10-400°C	1X10-500°C	1X10-600°C
OCP [mV$_{SCE}$]	-87	-46	-67	-90	-369
E$_{Pit}$ (at 0.01mA/cm^2) [mV$_{SCE}$]	105	78	73	24	-43
E$_{Repass}$ [mV$_{SCE}$]	-8	-10	-27	-58	-2

From table 4.2 and 4.3, it can be concluded that the pitting potential decreases with the heat treatment temperature in both tested grades. The temperature also narrows the passivity region.

Treatment	1.4509	1.4301
As Received		
300°C		
400°C		
500°C		
600°C		

Figure 4.42: Overview of samples after electrochemical test, 600°C samples showing uniform corrosion

4.2.5.2 Influence of Different Heating Procedures

The polarization measurements have confirmed that the corrosion properties of both grades drastically decreased at high temperatures. 10X1 means sensitization treatment for 10 hours but with additional cooling cycles. 1X10 is a continuous heat treatment for 10 hours without any cooling breaks. In tables 4.4 and 4.5, it can be seen that the grade 1.4301 is more susceptible to corrosion when treated with cyclic heating with additional cooling intervals. Results of electrochemical measurements are shown in figure 4.43-4.46.
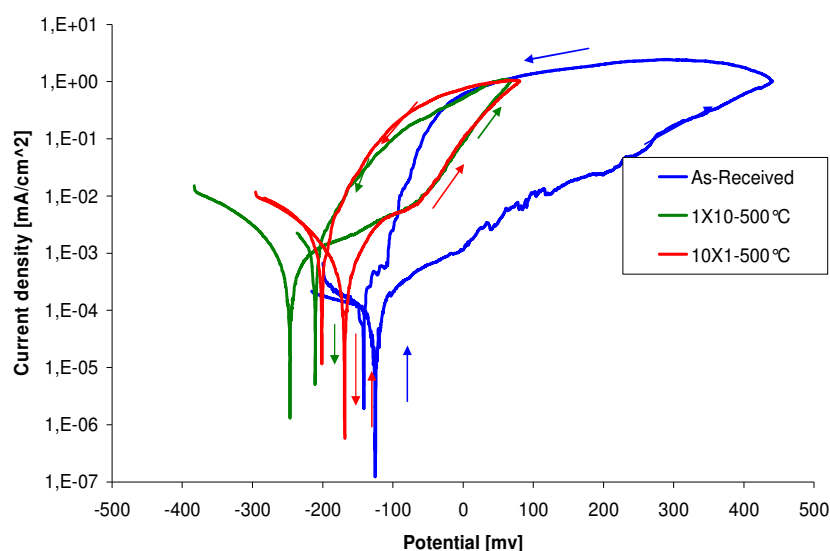
Figure 4.43: Potentiodynamic curves of continually heated (1X10) and periodically heated (10X1) 1.4509 at 500°C, testing in synthetic condensate with aeration at RT
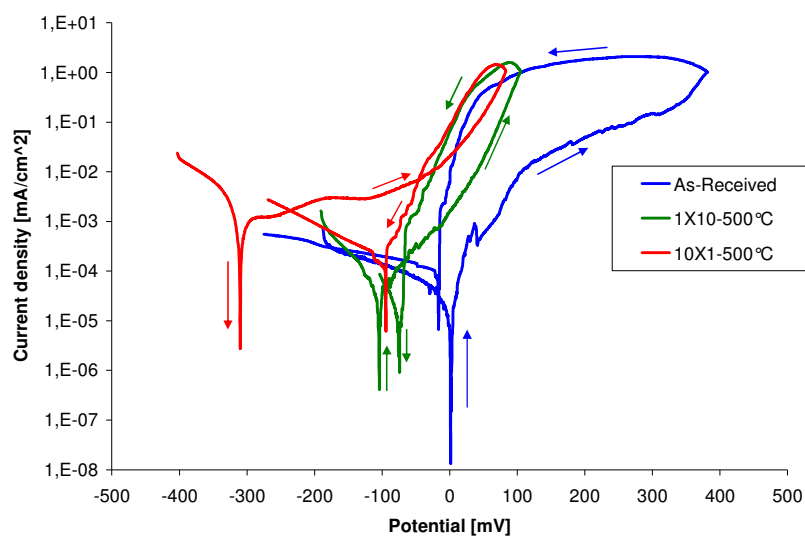
Figure 4.44: Potentiodynamic curves of continually heated (1X10) and periodically heated (10X1) 1.4301 at 500 °C, testing in synthetic condensate with aeration at RT
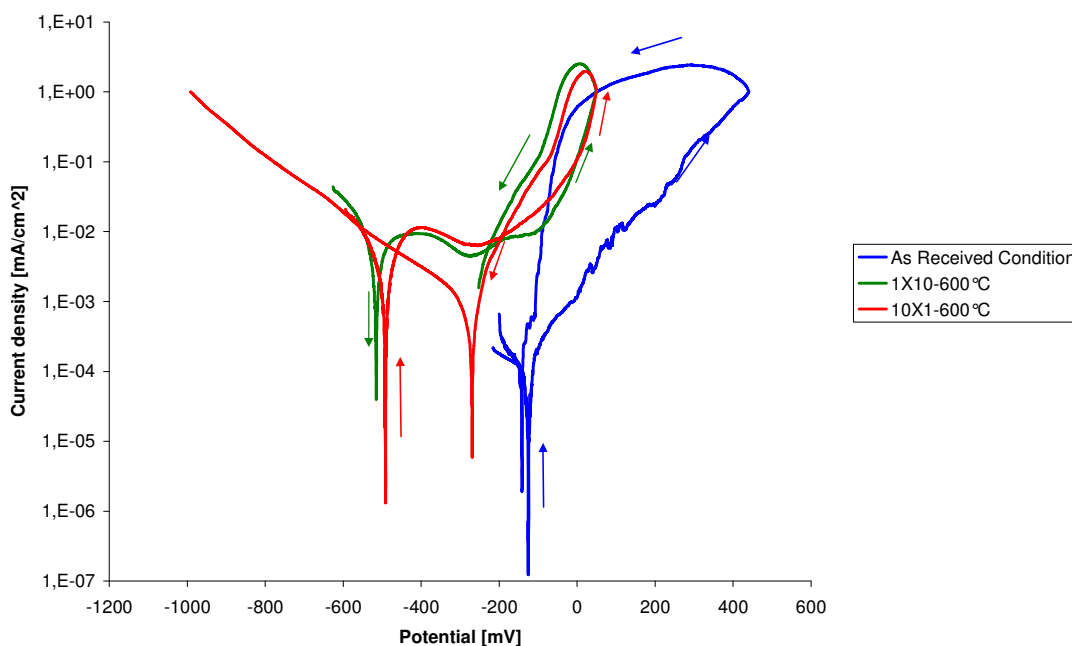
Figure 4.45: Potentiodynamic curves of continually heated (1X10) and periodically heated (10X1) 1.4509 at 600 °C, testing in synthetic condensate with aeration at RT
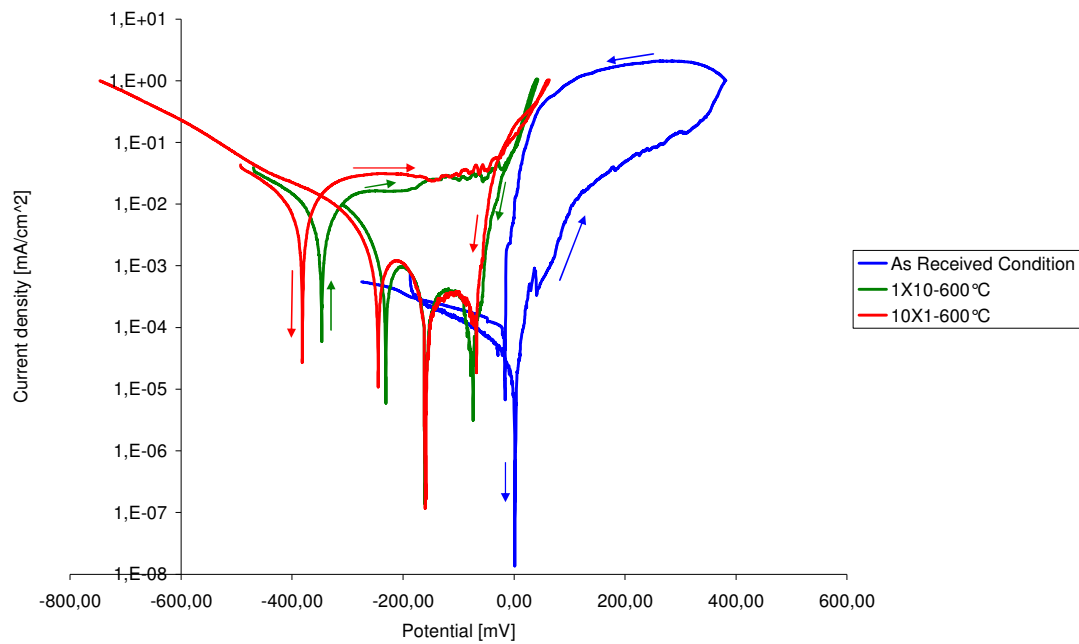
Figure 4.46: Potentiodynamic curves of continually heated (1X10) and periodically heated (10X1) 1.4301 at 600 °C, testing in synthetic condensate with aeration at RT

Table 4.4: Corrosion parameters obtained from the potentiodynamic curves of 1.4509

1.4509	As-Received	1X10-500 °C	10X1-500 °C	1X10-600 °C	10X1-600 °C
OCP [mV$_{SCE}$]	-99	-283	-195	-526	-494
E$_{Pit}$ (at 0.01mA/cm^2) [mV$_{SCE}$]	280	-60	-67	-60	10
E$_{Repass}$ [mV$_{SCE}$]	-105	-220	-180	-170	-107

Table 4.5: Corrosion parameters obtained from the potentiodynamic curves of 1.4301

1.4301	As-Received	1X10-500 °C	10X1-500 °C	1X10-600 °C	10X1-600 °C
OCP [mV$_{SCE}$]	-87	-90	-301	-369	-392
E$_{Pit}$ (at 0.01mA/cm^2) [mV$_{SCE}$]	320	3	-20	5	-30
E$_{Repass}$ [mV$_{SCE}$]	-8	-58	-50	-2	-30

4.3 Internal Corrosion

4.3.1 Dip and Dry Test

The whole test was applied until 5 cycles. After cycles 2, 3, 4 and 5 one sample from each grade and crevice size was taken out from the chamber. Corrosion products were removed and corrosion attack was quantified. Figure 4.47 shows visual appearance of 1.4509 steel with different crevice sizes. Crevices with sizes 0.1 mm, 0.3 mm and 0.5 mm tended to have more severe corrosion in the opening (crevice mouth) than at the bottom, whereas crevice with a size of 0.1 mm and 1.0 mm hardly developed any corrosion. This is probably an indication that the medium becomes more aggressive as water evaporates.
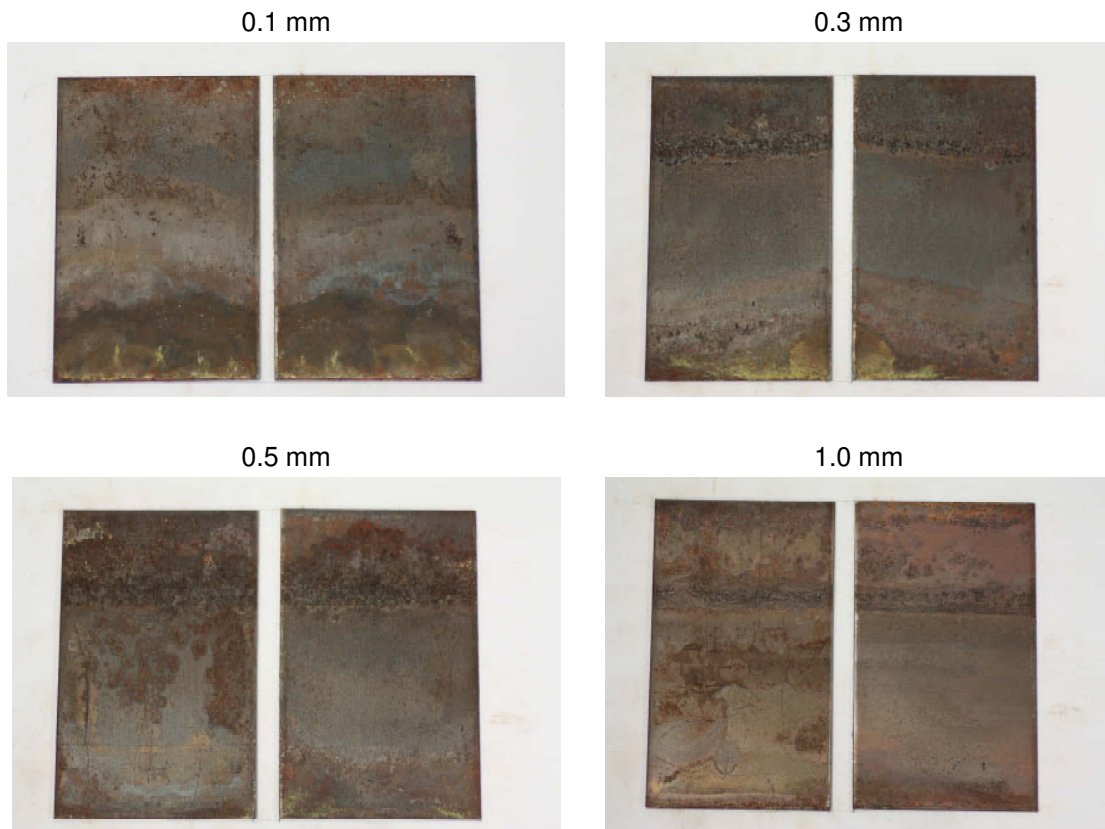
Figure 4.47: Overview of crevice samples grade 1.4509 after dip and dry test

Visual examination of the exposed samples after cleaning and drying revealed the evidence of corrosive attack. Some pits were observed in both materials and crevices. The quantification of corrosion attack on samples was done by measuring the pit depths with the help of X-ray radiography. From figure 4.48, it can be concluded, that 1.0 mm crevice results in the lowest rate of corrosion in both materials. The crevice width with 1.0 mm had the largest crevice size and it can be stated that larger the crevice better the protection against crevice corrosion. For the other crevice sizes i.e. 0.3 mm and 0.5 mm no real ranking could be made. It can be concluded that when the width of the crevice is large, the oxygen transfer will take place completely inside of the crevice, which results in no formation of concentration difference. The point, critical crevice solution does not reach and hence crevice corrosion does not occur.
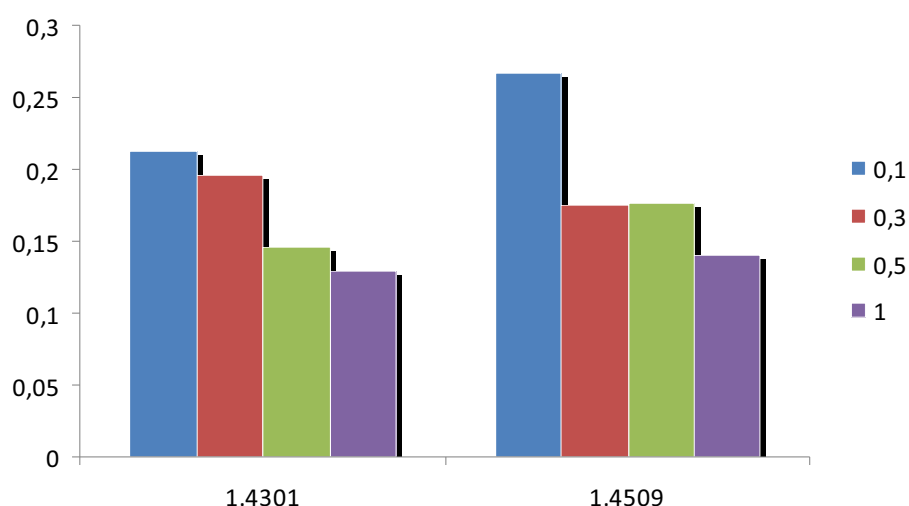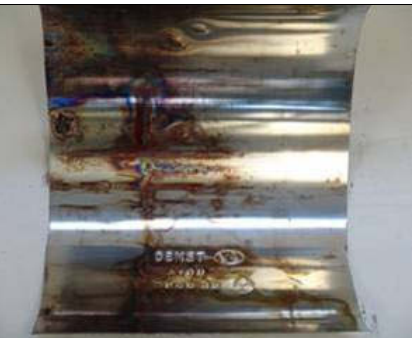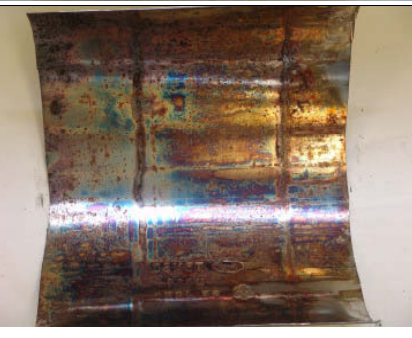
Figure 4.48: Average pit depth measurements µm in 0.1, 0.3, 0.5 and 1.0 mm after 3 cycles
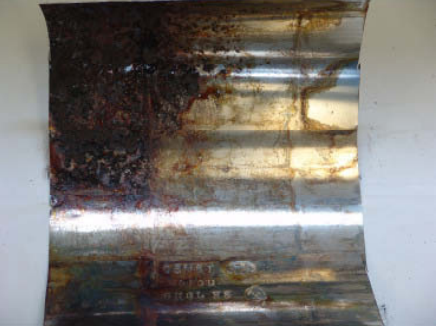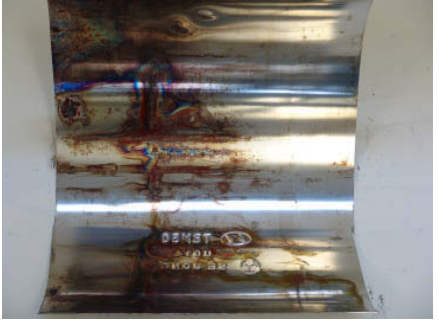
4.4 Component Testing

The objective of this study was to develop a type of testing procedure that could determine the combined effect of salt corrosion, condensate corrosion and high temperature corrosion. Corrosion resistance of different materials and designs were studied in this research. A comparative study was performed between field systems and test systems to establish a relation for the life time calculation.

After completion of the corrosion rig, the first task was to set parameters for a test which could simulate the real conditions in a normal routine. Initially, some trial tests were done to optimize the testing conditions. Parts from same vehicle having same material and design were chosen for these studies. A direct comparison was made between parts from the field and tested parts. The optical comparison was made at the first stage and afterwards pit depth measurements were done on samples from the same positions. The external appearance of both systems showed a good relation as shown in figure 4.49. The maximum corrosion attack was found on the same positions in the tested system like the field parts. In figure 4.49 the corrosion attack from inside can also observed. The corrosion initiation points were exactly the same as observed in the field.

System	Outer View	Inner View
CR Tested Part		
Field 1 54878 Km 6.3 Years 8665 Km/a		
Field 2 52825 Km 5.0 Years 10392 Km/a		

Field 3 28738 Km 4.8 Years 6050 Km/a		
Field 4 51135 Km 4.7 Years 10958 Km/a		
Field 5 50026 Km 4.4 Years 11327 Km/a		
Field 6 24081 Km 3.7 Years 6568 Km/a		

Figure 4.49: Comparison of different field and tested system

Some examples of pit depth measurements from same positions for all field mufflers and tested muffler are shown in figures 4.50-4.53. The upper error bar represents the deepest pit and the lower error bar represents the smallest pit depth. The rhombus represents the average values. Likewise, the field systems were separated into different

categories according their total life. The average kilometres per year were plotted against pit depth measurements. Field studies have revealed a bit scattered results for investigated systems. There was no clear relation found between corrosion progresses over a passage of time or a mileage. Even some other authors have proposed this effect which depends on various other influencing factors in real life like driving profile, region, cleaning and maintenance etc. [99]. The results are compared in terms of external corrosion and internal corrosion. The average pit depth results of tested systems and field system are plotted. For external corrosion, it was found that the depth of corrosion attack was relatively less in tested system, whereas it was more in field systems. Two examples for external corrosion i.e. outlet plate and outer sheet are given in figures 4.50 and 4.51.
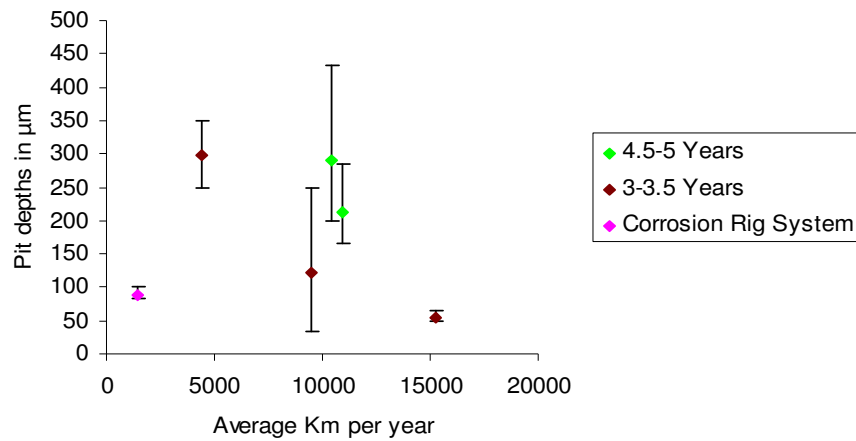
Figure 4.50: Pit depth results of end plate on inlet, representing external corrosion
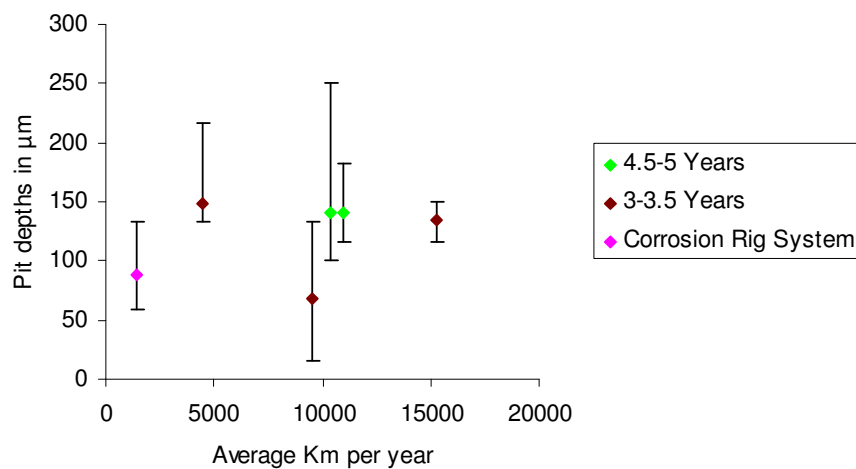
Figure 4.51: Pit depth results of end plate on outlet, representing external corrosion

The results of internal corrosion have revealed the fact that the pitting corrosion in tested and field systems is almost on the same level. The results from two inner baffles are shown in figures 4.52 and 4.53.
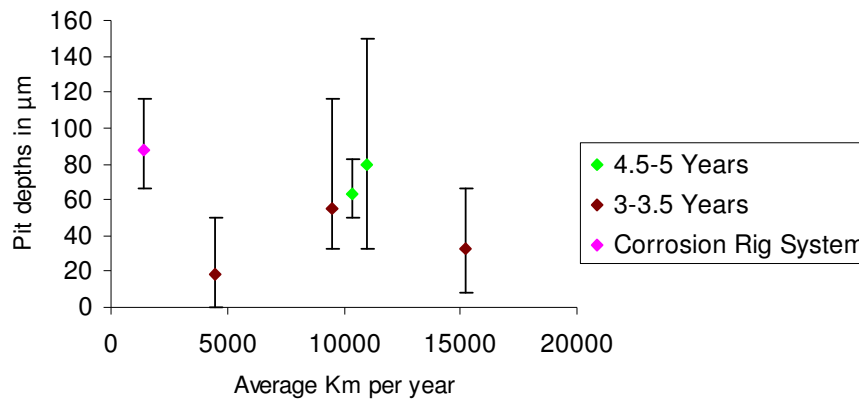
Figure 4.52: Pit depth results of inner baffler near to inlet, representing internal corrosion
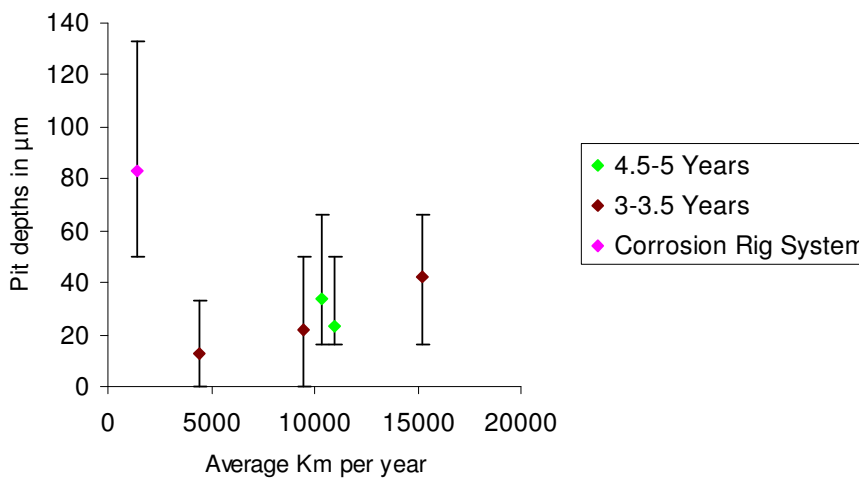
Figure 4.53: Pit depth results of inner baffler near to outlet, representing internal corrosion

In a nutshell, the optical appearance of the muffler after test was quite similar to the actual parts. The aggressive corrosion attack was found on the same positions in the test compared to the field parts. Some deformation on the inner sheet was also found in both cases. The results after corrosion quantification especially regarding internal corrosion also show a good relationship between both samples. Finally, it can be

concluded that with the help of this test both material and design can be validated for a component.

Furthermore, some corrosion products were collected from the tested mufflers from the corrosion rig. These reaction products were analyzed with the help of an X-ray powder diffraction method. Diffractograms are shown in figures 4.54 and 4.55. X-ray diffraction analysis showed that the corrosion products predominantly contained phases like magnetite (Fe_3O_4), hematite (Fe_2O_3) and lepidocrocite (α-FeOOH). Some corrosion products were also collected from different mufflers. X-ray diffraction analysis showed that the corrosion products predominantly contained phases like magnetite (Fe_3O_4), hematite (Fe_2O_3) and goethite (γ-FeOOH). It was confirmed during this study that in the field samples, presence of goethite instead of lepidocrocite was found. The phase lepidocrocite is usually formed in the early stages of atmospheric corrosion but as the exposure time increase it is transformed into goethite. [151, 152] Other phase which was found in field sample was magnetite.
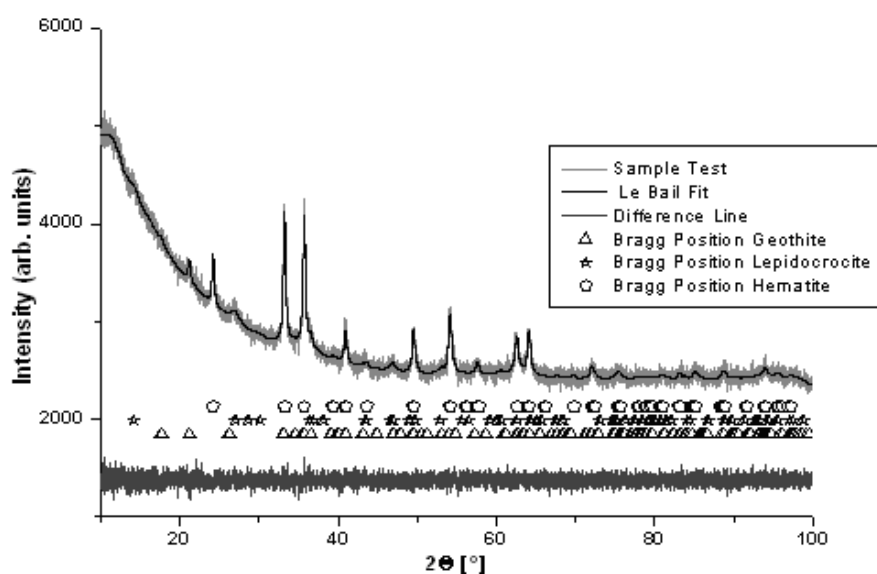
Figure 4.54: XRD spectra of a sample from test
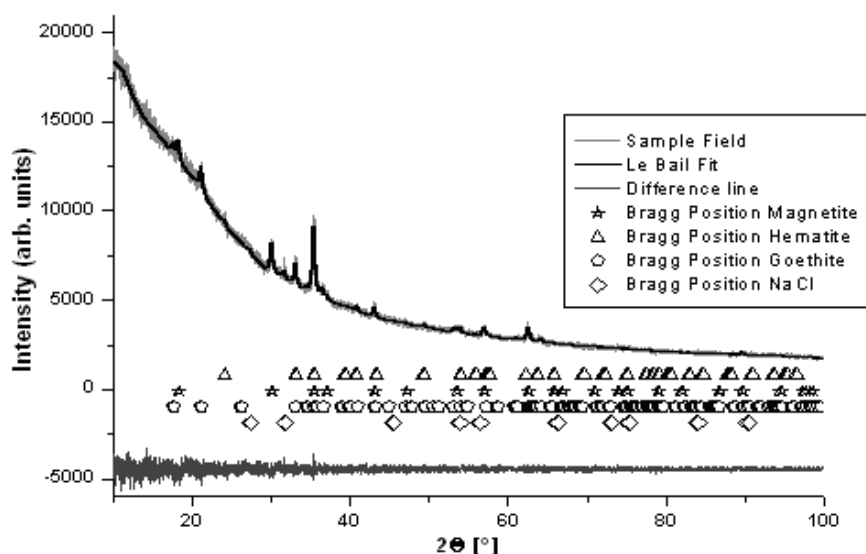
Figure 4.55: XRD spectra of a sample from field

4.5 Tests to Determine Degree of Sensitization

4.5.1 Streicher Test

Susceptibility to intergranular corrosion after various heat treatments of both grades was examined by using this testing method. Finally, the results were compared in terms of mass loss and micro-structural changes. During Streicher test amount of corrosive attack is determined by quantity of dissolved volume of chromium depleted zones as well as by the amount of dropped grains. The higher the sensitization of the specimen the higher the amount of dropped grains and therefore higher is the amount of dissolved volume. The results of mass loss of both grades as in received condition and sensitized by two different ways at 500°C for 10 hours are shown in figure 4.56. As determined by means of Streicher test and scanning electron microscopy, susceptibility to intergranular corrosion increased with higher sensitization temperatures. Furthermore, it can also be concluded that the corrosion rate of step annealed 1.4301 samples increased during the Streicher test whereas in 1.4509 a very small difference was observed.
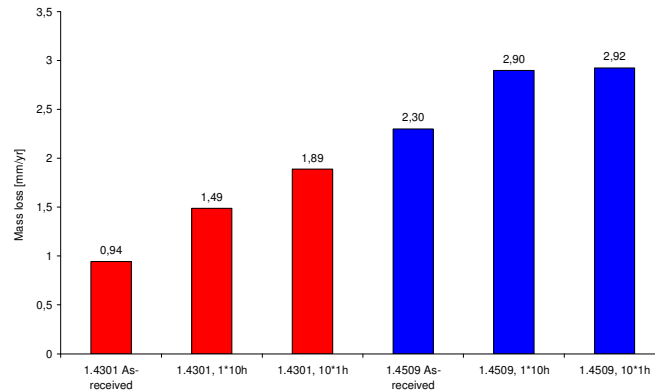
Figure 4.56: Mass loss after Streicher test, as received and 500°C treated samples

Figure 4.57 shows results of mass loss of samples treated at 600°C. The highest corrosion rate was measured after sensitization at 10X1-600°C for 1.4301. Samples were completely dissolved in a medium during all performed tests. The dissolved volume as well as the depth of the attack is clearly highest after sensitization at 600 °C. This is also in confirmation with figures 4.58 and 4.59.
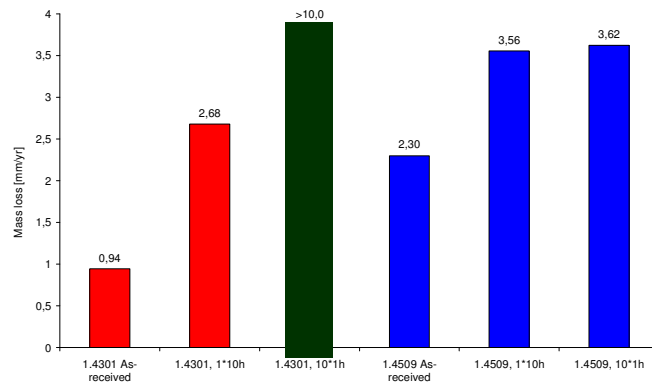
Figure 4.57: Mass loss after Streicher test, as received and 600°C treated samples, black bar representing complete mass loss

Grade 1.4509	1000 x	5000 x
As-Received		
500℃ 1X10		
500℃ 10X1		
600℃ 1X10		
600℃ 10X1		
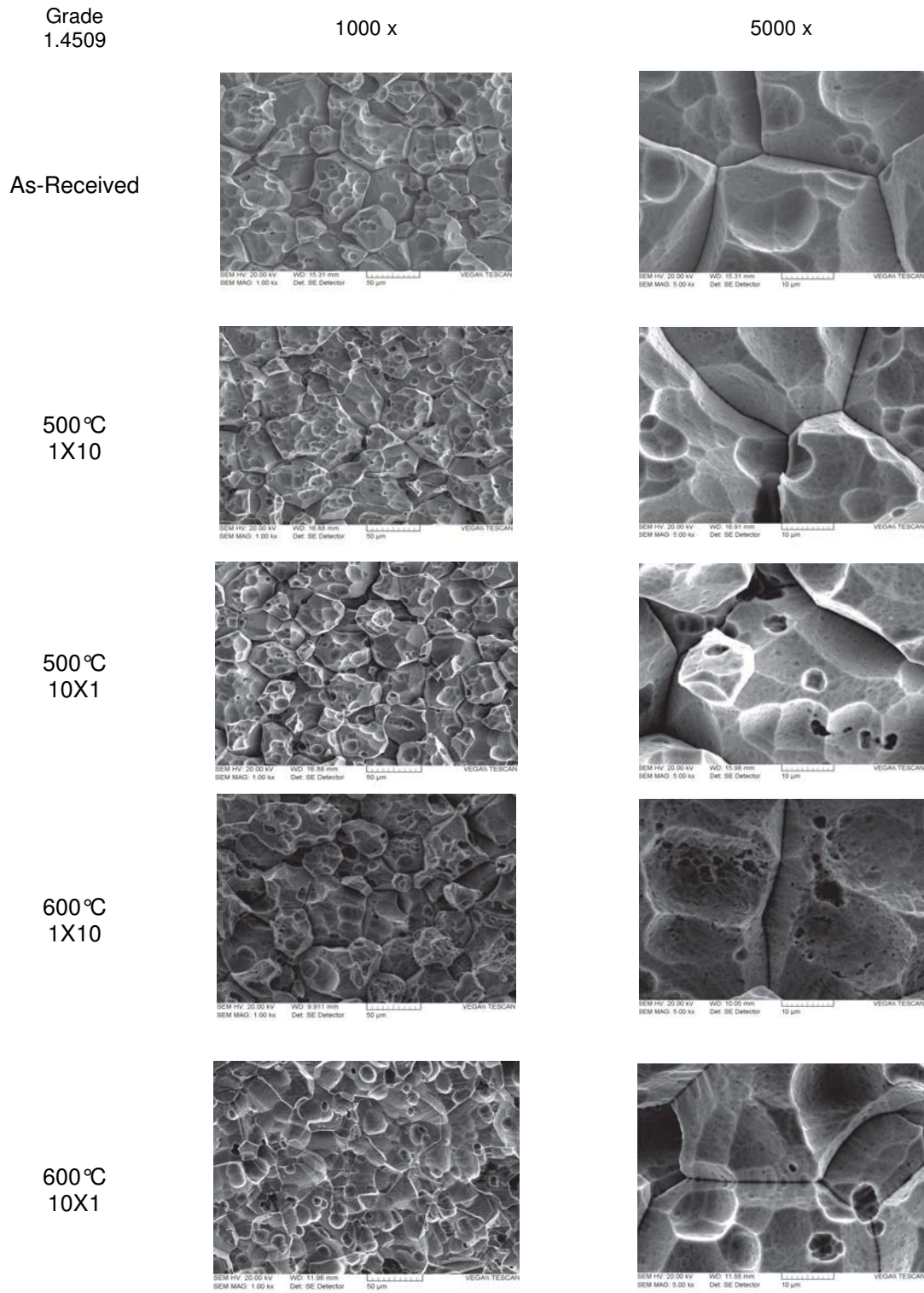
Figure 4.58: Microstructural characterization after Streicher test, grade 1.4509 after various heat treatments

Grade 1.4301	1000 x	5000 x
As-Received		
500 °C 1X10		
500 °C 10X1		
600 °C 1X10		
600 °C 10X1	Sample was completely dissolved during test duration	Sample was completely dissolved during test duration
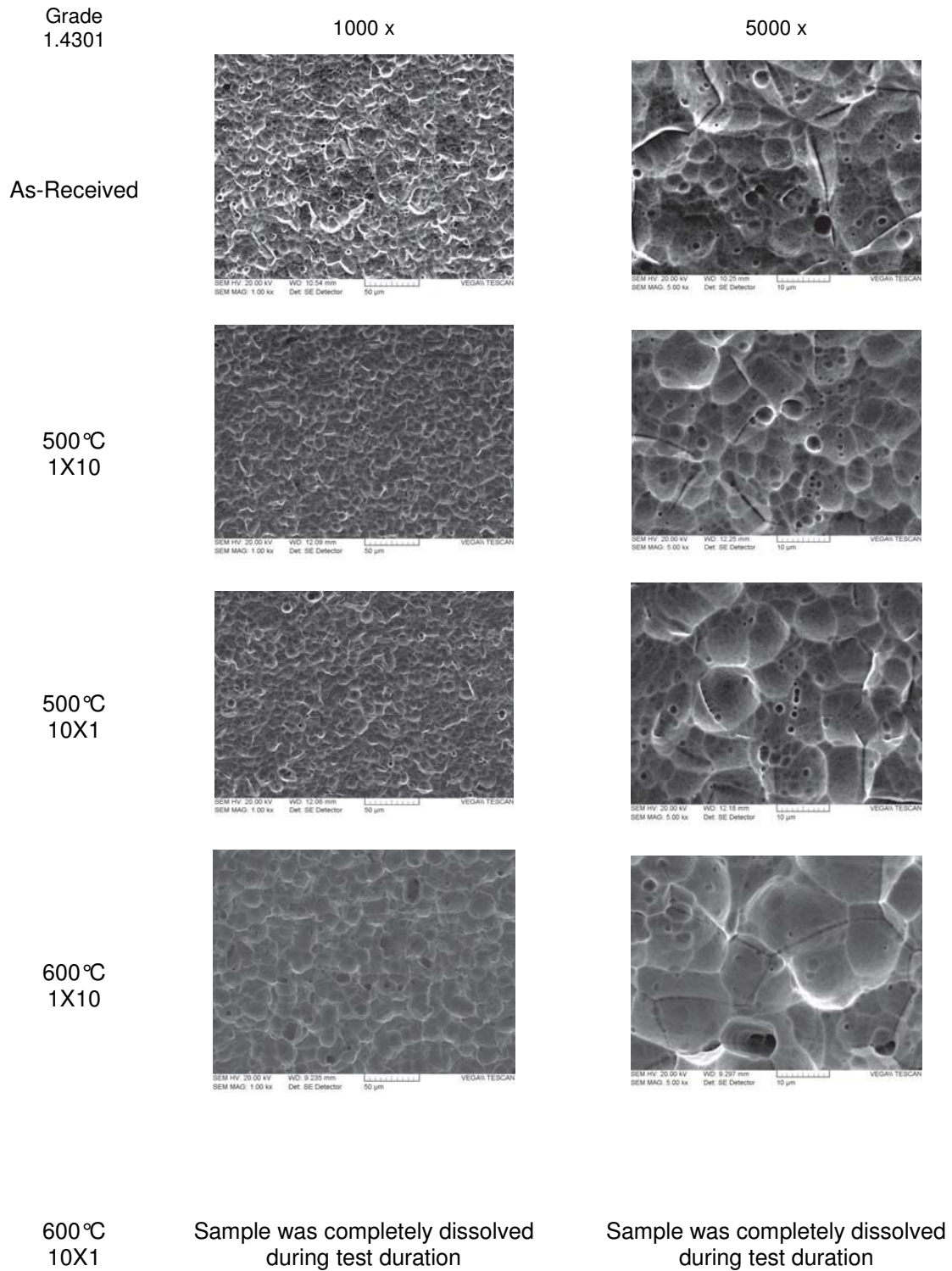
Figure 4.59: Microstructural characterization after Streicher test, grade 1.4301 after various heat treatments

4.5.2 Strauss Test

After exposure in a solution, the specimens were bent through 180°. These bent specimens were examined under scanning electron microscopy. Like Streicher test, no material sensitization was found in both materials until 500°C treatment. As it was found in previous results, 1.4509 showed some pitting corrosion attack in the positions where free standing Ti and Nb precipitates were present in the matrix. The results are given in figures 4.60 and 4.61.
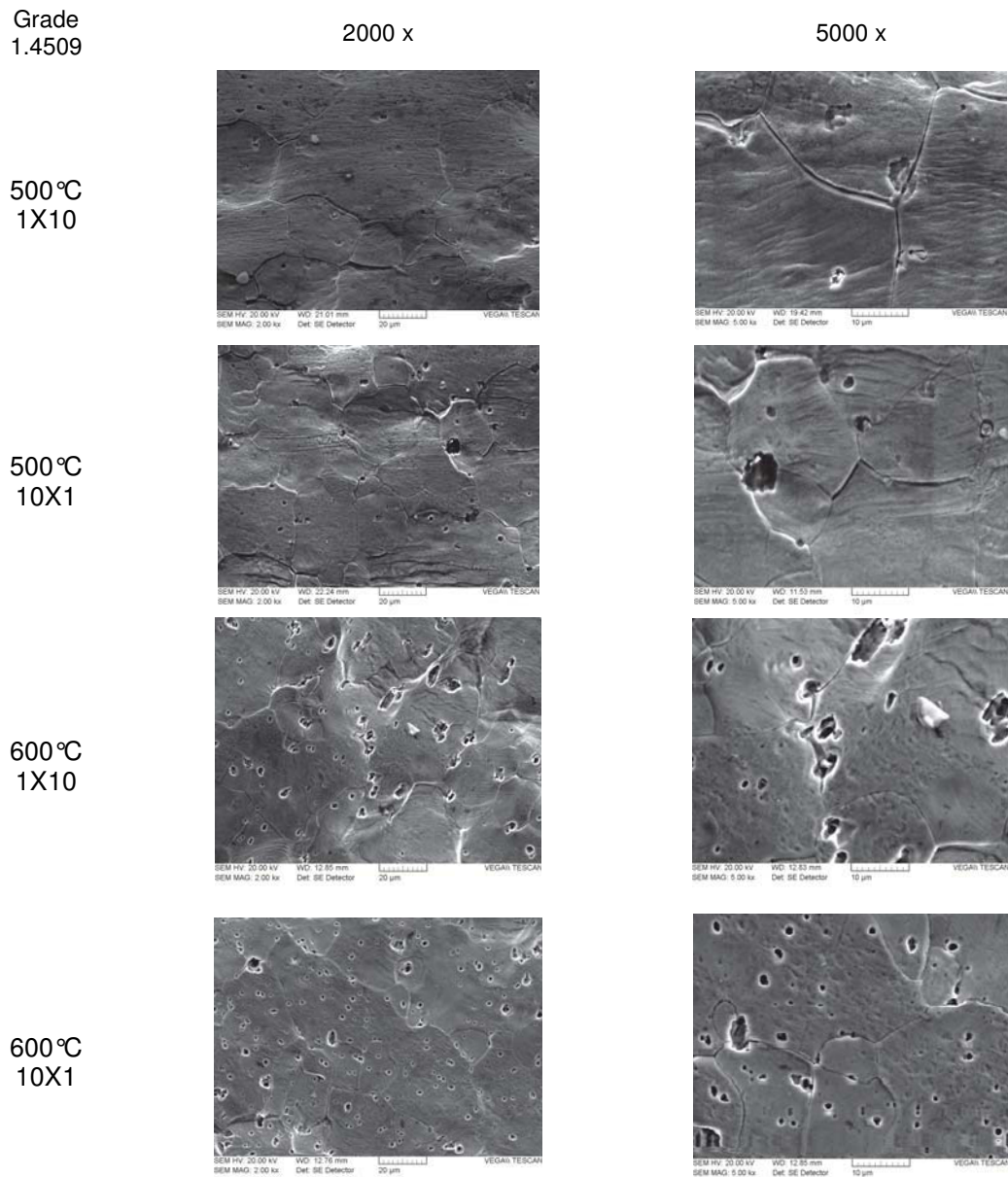
Figure 4.60: Microstructural characterization after Strauss test, grade 1.4509 after various heat treatments

Grade 1.4301	2000 x	5000 x
500°C 1X10		
500°C 10X1		
600°C 1X10		
600°C 10X1		
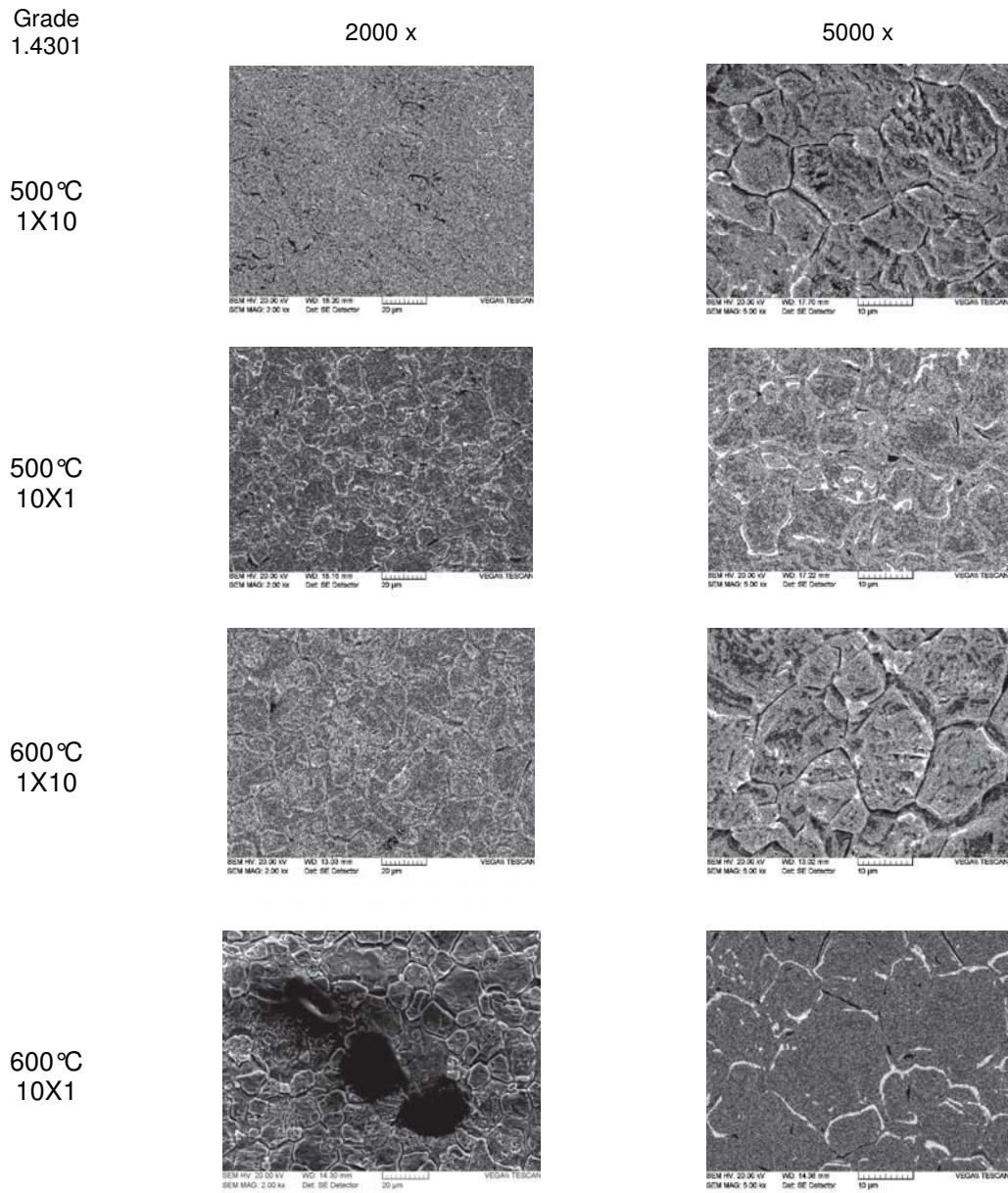
Figure 4.61: Microstructural characterization after Strauss test, grade 1.4301 after various heat treatments

5. Discussion

5.1 Summary of Results

The results obtained after all investigations are summarized as following:

1. Although having a same PREN, studied grades showed different corrosion behaviour in different testing methods.

2. The oxidation resistance and resistance to sensitization of 1.4509 was better than 1.4301 (1.4509 > 1.4301).

3. It was observed that during all oxidation treatments no material sensitization was found in both grades up to the temperature of 500°C.

4. At temperatures higher than 500°C chromium carbide precipitation along grain boundary was only found in 1.4301.

5. The grade 1.4509 showed ruptures and discontinuities on the surface during cyclic oxidation tests. These sites were found enriched in niobium and titanium.

6. It was found that all the modified VDA salt spray tests showed high rate of corrosion as compared to the standard VDA test. The wet corrosion resistance of 1.4301 was found better than 1.4509 (1.4301 > 1.4509).

7. Ferric chloride immersion tests and dip and dry tests revealed the fact that the biggest crevice showed the minimum amount of crevice corrosion.

8. With the help of potential measurements in different crevice assemblies, it was found that this method, crevice corrosion behaviour in different widths can be studied.

9. It was found that with the help of electrochemical measurements, potential difference in different crevice sizes can be measured. This potential difference is an indicator of oxygenated and deoxygenated areas. The results showed that in smaller crevice width i.e. 0.1 mm, the potential difference between outer and inner electrodes was more prominent.

10. In potentiodynamic polarization measurements, it was observed that 1.4301 grade showed no passive range after 600°C treatment. No pitting corrosion was found. Corrosion attack was uniform.

11. Based on different test results, following ranking can be made:

    ▪ Oxidation and Sensitization Tests: 1.4509 > 1.4301

    ▪ Aqueous Corrosion Tests: 1.4301 > 1.4509

12. The results of new component testing method showed a good agreement with the field analysis results. This test would be very helpful for validation of material and design combinations.

5.2 Role of PREN in Material Selection

As mentioned in earlier sections, in most of the cases material selection in automotive exhaust industry is done on the basis of PREN. The PREN value of 1.4509 is slightly higher than that of 1.4301. It is generally agreed that, alloys with higher PREN should exhibit greater resistance to pitting corrosion [8-13]. The higher the PREN value the better the pitting resistance. However, in PREN only the effect of chromium, molybdenum and nitrogen is considered.

Table 5.1: Studied materials with their PREN

Material	PREN
1.4509	17.9
1.4301	17.6

PREN = % Cr + 3.3 * % Mo + 16 * % N

In figure 5.1 some commonly used grades are given according to their PREN and alloy surcharge which is dependent on their alloying elements. The two different points for each grade represent the minimum and maximum possible value of PREN for each grade. It was found that the alloy surcharge is directly proportional to the material performance. Likewise, ferritic stainless steels have the lowest surcharge then come molybdenum stabilized ferritic stainless steels and the highest surcharge belongs to the austenitic stainless steels because of their nickel content. Surprisingly, if these alloys are ranked according to their PREN then some ferritic grades e.g. 1.4509 and 1.4510 lie in the same category with austenitic grades like 1.4301 and 1.4541. The cost of ferritic stainless steels is lower than austenitic ones because of the absence

of nickel alloying content. If the grades have almost same PREN values then definitely a normal user will choose the cost saving option i.e. ferritic stainless steel. During this study it was found that these two materials behave differently in different environments and conditions. Hence, selection on the basis of PREN is not ideal and suitable for this case. The outcome of this study has revealed the often ignored fact that the PREN concept is only a rough estimator and should not be used uncritically.
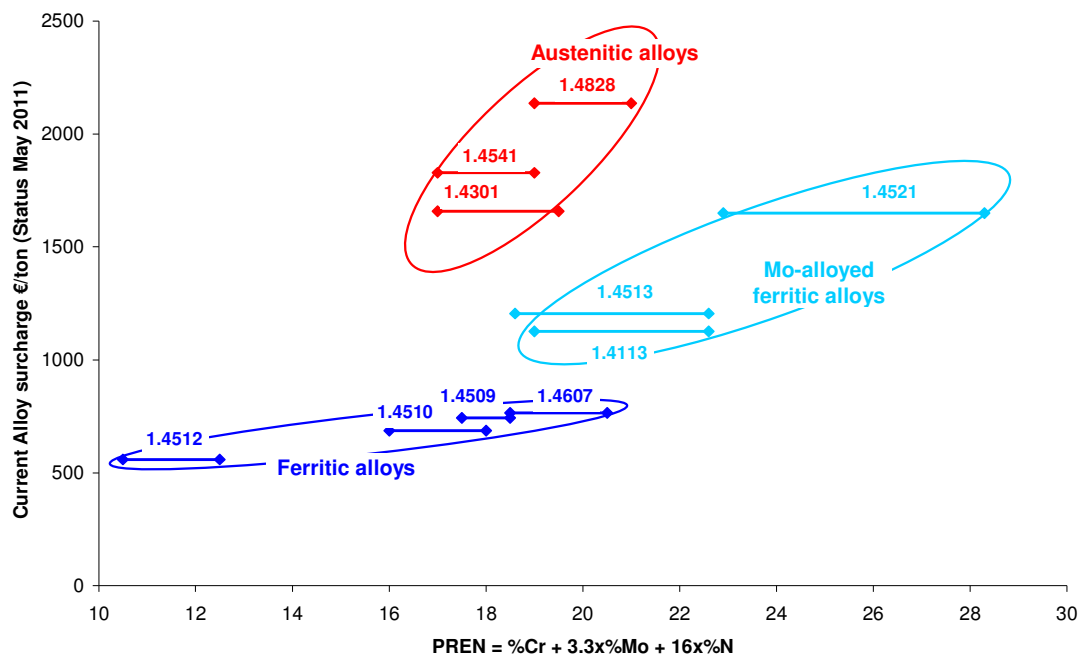
Figure 5.1: Alloy surcharge and PREN for some alloys used in automotive exhaust components

However, there is a considerable amount of uncertainty regarding the usage of PREN factor as a criterion in the selection of materials for wide range of temperatures and aggressive corrosion environments. Stainless steel grades are used in numerous applications above room temperature and different corrosive environments, so the criterion for selection of materials on the basis of PREN sounds inappropriate. In summary, this study shows that PREN is not a sufficient measure to rank stainless steels with regards to their corrosion resistant properties.

5.3 Role of Material Sensitization

Both effects, of sensitization time and temperature, could be explained by the relation between carbide precipitation and chromium diffusion from the bulk grain to the grain boundary. Several authors have found by examining concentration profiles with high resolution techniques that after annealing at high temperatures and/or after longer times the degree of sensitization could be smaller due to chromium and/or molybdenum depletion from the bulk material to the grain boundaries [153-155]. During this study, it was found that there is no issue of material sensitization till 500°C in both grades. All tests have confirmed these results. The grade 1.4509 also showed no chromium carbide precipitation at temperatures above than 500°C. After heating at temperature of 800°C for 100 hours, 1.4509 showed niobium and titanium carbides along grain boundaries but 1.4301 showed lot of chromium carbide precipitation along the grain boundaries. The results of Streicher test have also revealed the fact that grade 1.4301 is susceptible to intergranular corrosion at temperatures above than 500°C. During continuous oxidation tests, 1.4509 has performed better than the 1.4301. Some discrete areas of spalling and blistering occurred on the surface of the 1.4301 at temperatures higher than 500°C. 1.4509 has a low coefficient of thermal expansion which supports to reduce spalling or flake formation on surface. On the other hand, 1.4301 has high thermal expansion coefficient which makes them prone to high temperature corrosion. The other reason is that 1.4509 is a stabilized grade with niobium and titanium. Titanium and niobium have low free energies of formation when combined with carbon which prevents the formation of chromium carbides.

Table 5.2: Materials and their thermal expansion coefficients

Material	Mean Coefficient of Thermal Expansion $(10^{-6}K^{-1})$	
	20°C/200°C	20°C/400°C
1.4509	10.0	10.5
1.4301	16.5	17.5

The temperature range at which sensitization occurs and the kinetics of the process are significantly different from in both ferritic and austenitic stainless steels, as indicated schematically in figure 5.2. Sensitization occurs more rapidly in ferritics. It's because of differing properties of ferrite, as compared to austenite. Nitrogen has little effect in austenitic stainless steels because of high solubility. However, nitrogen and carbon has much lower solubility in ferrite and must be considered in the ferritic stainless steels. In austenitic stainless steels the diffusion coefficient for carbon and nitrogen are low as compared to ferritics. Because of the low solubility of interstitials in ferrite, the ferritic stainless steels sensitize much more rapidly and also at lower temperatures, as shown in figure 5.2.
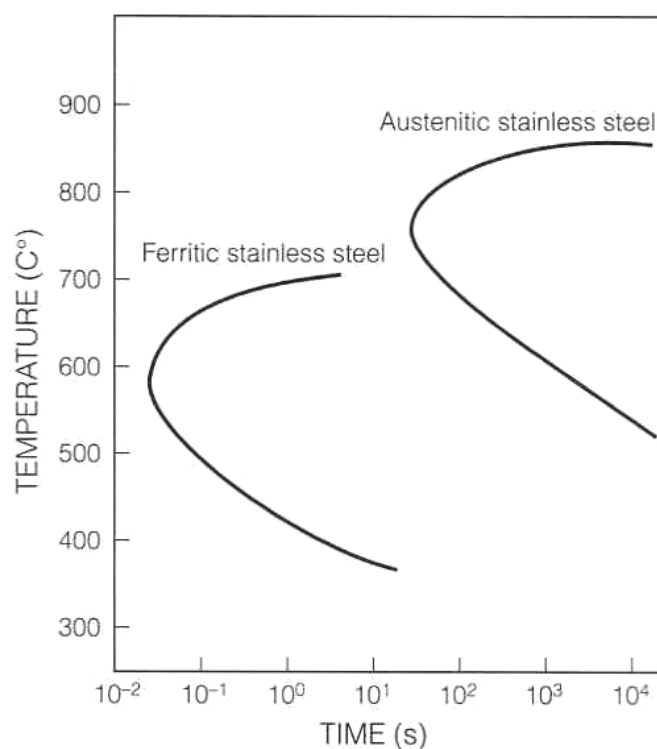
Figure 5.2: Differences in the location of time-temperature-sensitization curves of austenitic and ferritic steels of equivalent chromium content [156]

During this research it was found that the grade 1.4301 (austenitic) was more susceptible to intergranular corrosion as compared to grade 1.4509 (ferritic). Results of sensitization treatments (section 4.2) showed precipitation of chromium carbides along grain boundaries at 800°C for 100 hours annealed samples of 1.4301. In grade 1.4509 no chromium carbide precipitation was found along grain boundaries. Only

niobium and titanium carbides were observed in 1.4509. The results of Streicher and Strauss tests also showed high rate of grain dropping in 1.4301 treated at 600°C (section 4.2). The reason for the low rate of sensitization in 1.4509 is associated with the effect of additional stabilizing elements (niobium and titanium). These elements combine with carbon and nitrogen and do not allow carbon and nitrogen to precipitate as carbides and nitrides which lead to intergranular corrosion.

5.4 External Corrosion

It was found that all the modified VDA salt spray tests showed high rate of corrosion when compared to the standard VDA 621-415 test. In the VDA 621-415 test, both grades performed very well but as soon as the additional heating cycles were applied corrosion becomes more prominent. Pitting corrosion was observed in early stages of the tests. The appearance of the corrosion attack was quite similar to the appearance of parts in the field. Modified test cycles have brought this test closer to the actual problem. Type 1.4301 showed better corrosion resistance against pitting corrosion in wet external corrosion tests. In all modified VDA salt spray tests grade 1.4301 performed better than 1.4509. It was found that grade 1.4301 has better wet corrosion resistance as compared to dry corrosion. On the basis of this work, method D was selected as an appropriate method because it's more close to the actual issue and also more moderate when compared to heating with longer humid cycles. One can distinguish the change in material behaviour after different stages.

From this study, it can also be concluded that modified salt spray tests are not the appropriate testing methods to simulate the crevice corrosion behaviour between two sample sheets. The problem with this test method is that the electrolyte is applied only in a form of salt spray and does not reach to the crevices properly. Only little corrosion can be observed on crevice mouths. Therefore, due to improper access of medium inside the gap, larger area of the crevice remains almost dry from inside. This leads to different conditions inside the crevice. Thus, different conditions for every specimen lead to non uniform results.

5.5 Internal Corrosion

For simulation of internal corrosion i.e. condensate corrosion a unique testing setup called dip and dry test was built in the initial phase of the project. Experiments were performed with a synthetic condensate having a pH value of 3.4. The cycles and

medium of this test is different because these tests are related to the corrosion problem inside the muffler. During vehicle operation, condensate forms in the cold end and results in pitting corrosion due to its acidic nature. Like salt spray tests, the grade 1.4301 again showed better corrosion resistance against pitting corrosion in these tests. The 1.4301 is known to be superior grade in condensate conditions and the results of this investigation agreed with this. This trend was also found by other researchers [82-84]. This validates the credibility of the developed tests for internal corrosion of the cold end components. The tests done on different crevice samples also showed reliable results. Due to capillary action, penetration of electrolyte takes place in the crevice gap which is not possible in salt spray tests. It was found that the smaller crevice width i.e. 0.1 mm was the most critical whereas crevice with 1.0 mm showed least amount of corrosion.

5.6 Component Testing

For an accelerated corrosion test to be truly useful, a prime requirement is that the results should correlate with performance in the real world. This is something that has never been demonstrated with all the common routine tests. One aim of this work was also to develop and optimize a new corrosion testing method for exhaust silencers. The tests were carried out in different artificial conditions. A comparative study on the tested and real parts was performed. Obtained results indicate that the test conditions were very close to the real life conditons. A good agreement was found between tested and real parts. The initial results have confirmed that with the help of this testing method, a life time estimation of the component is possible.

Obtained results showed corrosion attack on same positions like in the field systems. A good agreement in terms of optical appearances was found between tested and real parts. After quantification of pit depths, it was noticed that external corrosion attack in tested part was relatively less as compared to the parts obtained from field. One has to keep in mind that there are some other influencing factors like air flow during normal driving cycle which completely dries the system from outside. In corrosion rig, complete dryness of part by applying air from outside is not possible. Due to this, a tested part will not dry completely in a chamber. Internal corrosion which was achieved during this test is in a range of field systems.

6. Conclusions

The basic conclusions that can be drawn from this investigation are the following:

1. The criterion of PREN should not be used any more for material selection. As the role of nickel is totally neglected in this formula thus making it completely inappropriate for comparison of ferritic and austenitic stainless steels.

2. The standard VDA 621-415 salt spray test should not be used to simulate the corrosion in exhaust components. This testing method is not suitable because the conditions in real environment have additional high temperature cycles.

3. Among all applied modified VDA tests, method D would be proposed as the method which is more relevant to the actual problem. The cyclic combinations are closest to the real world. It's mild and the results have shown a good agreement with field results.

4. After continuous oxidation test, it was found that both studied grades showed no material sensitization until 500°C. This temperature is the maximum possible temperature in exhaust mufflers.

5. The stabilized 1.4509 stainless steel showed lots of defects in form of some niobium and titanium precipitates on the surface. These irregular openings were found directly in the matrix. Later a corrosion indicator test confirmed these irregularities as the corrosion initiation sites.

6. It can be concluded that salt spray test method is not an appropriate method for crevice corrosion studies. The absence or insufficient intrusion of electrolyte in the crevice gap does not make possible to study the crevice corrosion mechanism.

7. Ferric chloride immersion tests and dip dry tests were proved reliable testing methods for crevice corrosion studies. Tighter crevices showed more corrosion while bigger crevices were only slightly affected. In both tests, the minimum corrosion attack was found in crevice gap of 1.0 mm.

8. Furthermore, electrochemical tests performed in different crevices showed that potential difference between outer and inner electrode in tighter crevice was high. In bigger crevices where convection can easily takes place, less potential difference was noticed.

9. From all crevice corrosion test results, it can be concluded that this phenomenon occurs rapidly and aggressively in tighter crevices. It can also be said that tighter

crevices induce higher potential gradients between external surfaces and crevice regions causing dissolution of passive films and rapid corrosion propagation rates.

10. The Streicher and Strauss tests have also confirmed the absence of material sensitization until 500°C treated samples from both studied stainless steels.

11. Potentiodynamic polarization measurements showed passive ranges for both grades till 500°C treatment. Likewise, 1.4301 reduces its corrosion resistance behaviour drastically at 600°C treatments.

12. The TOF-SIMS depth profile analysis of as received and heated specimens have also confirmed that the thickness of passive layer was predominantly more in heat treated specimen.

13. The initial corrosion rig tests and a comparison study between field parts have revealed the fact that this component testing technique would be of a great help to understand the influence of different materials and design combinations on corrosion.

7. Outlook

The work presented here is a good start to establish suitable testing methods for different scenarios in exhaust components, understanding the crevice corrosion phenomenon, and also behaviour of materials with different heating cycles in automotive exhaust applications. Based on the experimental challenges encountered in the course of this work, the following recommendations are made for future work:

1. The only electrochemical measurement method to simulate crevice corrosion used in this research was open-circuit potential measurement. For future study, some other techniques such as electrochemical impedance spectroscopy and electrochemical noise will aid in understanding this phenomenon to a deeper extent.

2. A method should be designed to measure the pH value inside the crevice which will help in understanding the mechanism.

3. The effect of increased temperature on the onset and extent of severity of the localized attack at the different locations in the crevice should be studied, for comparison with the results obtained at room temperature.

4. Time of exposure should be increased for wider crevice width to have an idea of the length of time required for wider gaps to undergo active corrosion.

5. Some other sophisticated microscopic techniques should be used to determine the properties of passive film at the different locations along the crevice, and electrochemical changes that occur on the surface of stainless steels during the induction and propagation phases of crevice corrosion.

6. Some potential measurements should be done on different sections of the muffler in the corrosion rig. The information about influence of different testing cycles on corrosion would be monitored online in this component test.

8. References

1.   **Ashok Sabata, T. W. Cordera and Mike Behling:** Localized Corrosion Resistance of Automotive Exhaust Alloys, NACE San Diego, 1998, paper no. 98549.

2.   **H.J.B. Alves, J. N. Carvalho, M. V. Aquino and M. J Mantel:** Development of Ferritic Stainless Steels for Automotive Exhaust Systems, 4th Stainless Steel Science and Market Congress, 10-13 June 2002, Paris, France.

3.   **R. Ashworth, D. Dulieu and K. J. King:** Materials Requirements for Modern Exhaust Systems, STFFI Times International, 1993, pp. 36-38.

4.   **J. A. Duthett:** Designing Stainless Exhaust Systems, Automotive Engineering, November 1995, pp. 45-49.

5.   **E. Sato and T. Tanoue:** Present and Future Trends of Materials for Automotive Exhaust Systems, Nippon Steel Technical Report No. 64 January 1995, pp. 13-19.

6.   **S. Chang**: Corrosion Resistance of Automotive Exhaust Materials, Journal of Materials Science 18, 1999, pp. 419-421.

7.   **Y. Inoue, M. Kikuchi:** Present and Future Trends of Stainless Steel for Automotive Exhaust System, Nippon Steel Technical Report no. 88, 2003.

8.   **C. Hoffmann, P. Gümpel:** Pitting Corrosion in the Wet Section of the Automotive Exhaust Systems, Journal of Achievements in Materials and Manufacturing Engineering. June 2009, pp. 115-121.

9.   **M. L. Doche, J. Y. Hihn:** A Novel Accelerated Corrosion Test for Exhaust Systems by Means of Power Ultrasound, Corrosion science 2006, pp. 4080-4093.

10.   **A. J. Sedriks:** Corrosion of Stainless Steels, 2nd edition. New York, NY: John Wiley & Sons Inc, 1996, pp. 111.

11.   **G. Herbsleb:** Werkstoffe und Korrosion 33, 1982, pp. 334.

12.   **P. Gumpel and E. Michel:** Thyssen Edelstahlwerke Technische Berichte 12, 1986, pp. 181.

13.   **J. E. Truman:** Proceedings of the U.K. Corrosion/87 (Houston, TX: NACE), 1987, pp. 111.

14.   **C. Voigt and G. Reidel:** Wirkung von Cr, Ni, Mn, S, Mo and Cu auf Passivierungs- und Lochkorrosionseigenschaften der Stahlsorte X6CrNiTi18-10 Werkstoffe und Korrosion 38,1987, pp. 725-737.

15.   **G. Hochörtler and K. Kriszt:** BHM 140, 1995, pp. 24.

16   **B. Wallen**: EFC Publications, No. 28, 1996, pp. 142.

17.   **J. Bernauer, G. Hochörtler and H. Lenger:** Development of High Nitrogen Steels at Böhler Edelstahl GmbH Kapfenberg, Materials Science Forum 318-320, 199, pp. 227.

18. **S. Ningshen, R. K. Dayal:** British Corrosion Journal 36, 2001, pp. 192.

19. **M. O. Speidel:** Proceedings of the Stainless Steels 87, York: The Institute of Metals, pp. 247.

20. **D. C Oliver and M. Sephen:** External Corrosion Resistance of Steel and Ferritic Stainless Steel Exhaust System, SAIM 2002.

21. **R. J. McKay:** Corrosion by Electrolyte Concentration Cells. Transactions of the Electrochemical Society 41, 1922, pp. 201-203.

22. **R. J. McKay:** The Common Occurrence of Corrosion by Electrolyte Concentration Industrial and Engineering 17, 1925, pp. 23-24.

23. **L. R. Wyche, L. R. Voigt, and F. L. Laque:** Corrosion in Crevice, Journal of the Electrochemical Society 106, 1959, pp. 468-470.

24. **M. G. Fontana and N. D. Greene:** Corrosion Forms in Corrosion Engineering, McGraw Hill, New York, 1967, pp. 41-44.

26. **J. W. Oldfield, and W. H. Sutton:** Crevice Corrosion of Stainless Steels I-A Mathematical Model. British Corrosion Journal 13, 1978, pp. 13-22.

27. **J. L Dawson and M. G. S Ferreira:** Crevice Corrosion on 316-Stainless Steel in 3-percent Sodium Chloride Solution, Corrosion Science, Vol. 26, 1986, pp. 1027.

28. **H. W. Pickering, K. Cho, and E. Nystrom:** Microscopic and Local Probe Method for Studying Crevice Corrosion and Its Application to Iron and Stainless Steel, Corr. Eng. Sc. Technol., 35, 1993, pp. 775-783.

29. **A. Alavi, and R. A. Cottis:** The Determination of pH, Potential and Chloride Concentration in Corroding Crevices on 304 Stainless Steel and 7475 Aluminum Alloy, Corrosion Science 27, No. 5, 1987, pp. 443-451.

30. **R. D. Klassen, P. R. Robergea and C. V. Hyattb:** A Novel Approach to Characterizing Localized Corrosion within a Crevice, Electrochimica Acta 46, No. 24-25, 2001, pp. 3705-3713.

31. **R. C. Wolfe, H. W. Pickering, and B. A. Shaw:** Microprobe Study of pH During the Induction Period Preceding Crevice Corrosion, J. Electrochem. Soc., 153, 2006, pp. B25-B32.

32. **Eun-Young Na, Jae-Yong-Ko, Shin-Young Baik:** Electrochemical Evaluation of Crevice Corrosion of 430 Ferritic Stainless Steel using the Microcapillary Tube Technique, Corrosion Science 2006, pp. 65-74.

33. **Eun-Young Na:** An Electrochemical Evaluation on the Crevice Corrosion of 430-Stainless Steel by Micro Capillary Tubing Method, J Mater Sci, 2006, pp. 3465-3471.

34. **F. Bocher, N. D. Budiansky, and J. R. Scully:** Investigation of Crevice Corrosion of AISI 316 Stainless Steel Compared to Ni-Cr-Mo Alloys Using Coupled Multielectrode-Arrays J. Electrochem. Soc., 155, 2008, pp. 279-295.

35.   **M. I. Abdulsalam and T. Shinohara:** Moire Based Method for Real-Time Crevice Corrosion Monitoring, Materials and Corrosion, 57 No. 10, 2006, pp. 783-788.

36.   **J. R. Scully:** Polarization Resistance Method for Determination of Instantaneous Corrosion Rates, Corr., 56, 2000, pp. 199–218.

37.   **Y.   Inoue and M. Kikuchi:** Present and Future Tends of Stainless Steel for Automotive Exhaust System, Nippon Steel Technical Report No. 88 July 2003, pp. 62-69.

38.   **A. Miyazaki, M. Gunzi and K. Yoshioka:** High formability R429X and Heat-Resistant R44EX Stainless Steels for Automotive Exhaust Manifold, Kawasaki Steel Technical Report No. 31, November 1994, pp. 21-28.

39.   **P. Monnartz:** Metallurgie 8, 1911, pp. 161.

40.   ASM International Handbook Committee 10th ed, Properties and Selection: Irons, Steels and High-Performance Alloys. 10th ed. Metals Handbook. Vol. 1. 1990, ASM International. 1063.

41.   Steel, A Handbok for Materials Research and Engineering. Vol. 2: Applications. 1992, Springer-Verlag: Dusseldorf. 839.

42.   **D. Peckner and I. M. Bernstein:** Handbook of Stainless Steels. 1977, Mc Graw-Hill.

43.   **P. Marshall:** Austenitic Stainless Steels - Microstructure and mechanical properties. 1984, Essex, England: Elsevier Applied Science Publishers Ltd. 431.

44.   **R. A. Lula:** Stainless Steel. 1986: ASME. 174.

45.   ASM Speciality Handbook, Stainless Steels, Edited by J.R. Davis, ASM International, 1996.

46.   **A. John Sedriks:** Corrosion of Stainless Steels, Second Edition, 1996.

47.   **David Talbot and James Talbot:** Corrosion Science and Technology, 1997.

48.   ASM Speciality Handbook, Stainless Steels, Edited by J.R. Davis, ASM International, 1996.

49.   **P. Lacombe, B. Baroux and G. Beranger:** Les Aciers Inoxydables, Les éditions de Physique, 1990.

50.   **Z. Szklarska-Smialowska:** Pitting and Crevice Corrosion, NACE International, 2005, pp. 210-216.

51.   **D. Webster, and J. H. Woodhead:** Effect of 0.3% Niobium on the Ferritic Grain Size of Mild Steel, J. Iron Steel Inst, 202, 1964, pp. 987-994.

52.   **A. Le Bon, J. Rofes-Vernis and C. Rossard:** Recrystallization and Precipitation During Hot Working of a Nb-Bearing HSLA Steel, Metal Science, 13, 1979, pp. 238-245.

53. **N. Fujita, K. Ohmura, M. Kikuchi, Z. Suzuki, S. Funaki, and I. Hiroshige:** Effect of Niobium on High-Temperature Properties for Ferritic Stainless Steel, Scripta Materialia, Vol. 35, No. 6, 1996, pp. 705-710.

54. **Luis J. Ruiz-Aparicio, C. I. Garcia, and A. J. DeArdo:** Development of {1 1 1} Texture in Intersticial Free Steels, Metall. Trans. A, 32A (2), 2001, pp. 417-423.

55. **C. P. Dillon:** Corrosion Resistance of Stainless Steesl, Marcel Dekker, Inc., New York, 1995.

56. **Y. Xu et.al:** Annealing Behaviour and Formability of Ferritic Stainless Steels, Low Carbon Steel for the Nineties, TMS-AIME, 1993, pp. 397-404.

57. **Eric J. Palmiere:** Suppression of Recrystallization during the Hot Deformation of Microalloyed Austenite, PhD thesis, University of Pittsburgh, 1991.

58. **A. J. DeArdo:** Fundamental Metallurgy of Niobium in Steel, Niobium 2001, AIME-TMS, 2001.

59. **V. Cihal:** Intergranular Corrosion of Steels and Alloys, New York, Elsevier Science Publishing Company, 1984, pp. 205.

60. **D. A. Jones:** Principles and Prevention of Corrosion, Simon and Schuster, New Jersey, 1996.

61. **J. R. Scully:** Electrochemical Methods of Corrosion Testing in Corrosion, Vol. 13, Laboratory Testing, ASM Inter., ASM Handbook, Ninth edition, 1987, pp. 213

62. **A. G. Revesz and J. Kruger:** Passivity of Metals, R.P. Frankenthal and J. Kruger, Ed., Electrochemical Society, 1978, pp. 137.

63. **R. P. Frankenthal and J. Kruger**: Passivity of Metals, Electrochemical Society, 1978, pp. 1-28.

64. Design Guidelines for the Selection and Use of Stainless Steel, Specialty Steel Industry of the United States. Washington, D.C., USA.

65. **Nestor Perez:** Electrochemistry and Corrosion Science, 2004, pp. 184.

66. **P. Lacombe, B. Baroux and G. Beranger:** Les Aciers Inoxydables, Les éditions de Physique, 1990.

67. **N. D. Tombashov and G. P. Chernova:** Passivity and Protection of Metals, 9, Plenum Press, New York, 1967.

68. **M. Farady:** Experimental Researches in Electrochemistry, 2, University of London, London, 1884.

69. **U. R. Evans**: The Corrosion and Oxidation of Metals, Second Supplementary Volume, Chapter 7, 1968.

70. **L. L. Schrier, R. A. Jarman and G. T. Burstein:** Corrosion, Volume 1, Metal/Environment Reactions, Third edition, 1994.

71. **R. Baboian:** Mechanisms of Automobile Corrosion and Prevention, Proceedings of the 11th International Corrosion Congress, Vol. 2, April 1990, Florence, Italy, 1990, pp. 489-498.

72. **C. W. Vigor, J. N. Johnson and J. E. Hunter:** Stainless Steel in Transportation Systems, Handbook of Stainless Steel, Published by Mcgraw-Hill Book Company, New York, 1977, pp. 39:1-39:15.

73. **D. C. Oliver and M. Sephton:** External Corrosion Resistance of Steel and Ferritic Steel Exhaust Systems, The Journal of the South African Institute of Mining and Metallurgy, Vol. 103, 2003, pp. 93-100.

74. **S. A. Bradford:** Corrosion Control, Second Edition, Casti Publishing Inc. 2002.

75. **D. A. Jones**: Principles and Prevention of Corrosion, Second Edition, 1996.

76. **N. Birks and G. H. Meier:** Introduction to High Temperature Oxidation of Metals, Edward Arnold Publication, 1983.

77. **K. H. Tostmann:** Korrosion- Ursachen und Vermeidung, Wiley- VCH Verlag, Weinheim, 2001

78. http://www.thyssenkrupp-nirosta.de/fileadmin/media/produkte/LZ2010.pdf (Last-access on 26.05.2011)

79. **J. H. Potgieter, M. Sephton, Z. W. Nikosi:** Corrosion of Hot End Automotive Components, Anti-Corrosion Methods and Materials, Vol. 54, 2007, pp. 180-187.

80. **Sekita Takashi:** Materials and Technologies for Automotive Use, JFE Technical report no.2, March 2004, pp. 12.

81. **Sermin Ornektekin:** Effect of Exhaust Gas on Corrosion of Metals, International Journal of Environmental Studies, Vol. 55, Issue 3, September 1998, pp. 199-210.

82. **G. E. Cayless:** Corrosion of the Exhaust Systems, Corrosion of Motor Vehicles, Mechanical Engineering Publications, 1974, pp. 66-105.

83. AK Steel Exhaust System Steels, The Catalyst, Issue No. 1, 2002.

84. **T. Chen, Cheng Jia Shang, J. Y. Wang and Dong Yang Li:** Corrosion Behavior of a New Developed Ferritic Stainless Steels Used in Automobile Exhaust System, Advanced Materials Research, Volumes 89-91, 2010, pp. 102-106.

85. **L. Bednar and R.A Edwards:** Corrosion Behavior of Aluminized Stainless Steels and Stainless Steels in Simulated Muffler Condensate-Corrosion Conditions, SAE Technical Paper No. 932345, 1993.

86. **J. Hirasawa, T. Ujiro, S. Satohg and O. Furukimi:** Development of High Corrosion Resistant Stainless Steels for Automotive Mufflers Based on Condensate Corrosion Test and Field Investigation, Presented at SAE 2001 World Congress, USA, March 2001.

87. **P. Weltens, P. Garcia and H. Walther:** Internal and External Corrosion of Exhaust Systems for Passenger Vehicles, Test Procedures, Laboratory and Field Results, 2001, pp. 1-22.

88. **P. Gümpel, D. Schiller, N. Arlt, D. Bouchholz:** Simulation of Corrosion Behaviour of Stainless Steels in Passenger Car Exhaust Systems Simulation of Corrosion Behaviour of Stainless Steels in Passenger Car Exhaust Systems" ATZ Worldwide e-Magazines Edition: 2004-04.

89. **L. Antoni, R. Bousquet, J. H. Davidson :** Simulation of Road Salt Corrosion in Austentic Alloys for Automotive Exhaust Systems. Mater. High Temp. 20, (4), 2003, pp. 561.

90. **R. Baoian:** Advances in Automotive Corrosion Resistance, Proceedings of the 13th International Corrosion Congress, November, 1996, Melbourne, Australia, Paper No. 076.

91. **G. E. Cayless:** Corrosion of the Exhaust Systems, The Institute of Mechanical Engineers, Corrosion of Motor Vehicles, Published by Mechanical Engineering Publications, London, November 1964, pp. 66-105.

92. **N. Chang, P. Pearson, and J. Chang:** Environmentally Sensitive Sanding and Deicing Practices, ESSD Research Group, University of Colorado, Denver, 1994.

93. Salt Institute, Deicing Salt and Our Environment, Alexandria, Virginia, 1990.

94. **Janis Keating:** Report on Deicing Salt, The journal for surface water quality professionals, 2000-2001.

95. **C. Kabi, K. P. Mukherjee & M. C. Rastogi:** Effect of Galvanic Coupling on Active-Passive Transition Behaviour of Austenitic Stainless Steel, J. Electrochem. Soc. India, 34, 1985, pp. 256-260.

96. **H. H. Uhlig and R. W. Revie:** Corrosion and Corrosion Control, 3rd ed., John Wiley and Sons, Inc., New York 1984

97. **Z. S Smialwska:** Pitting Corrosion of Metals, National Association of Corrosion Engineers, Houston, 1986, pp. 145.

98. **William D. Callister:** Materials Science and Engineering: An Introduction, Wiley International 6th edition, 2003, ISBN 0-471-22471-5.

99. **P. Gümpel, D. Schiller, N. Arlt, D. Bouchholz:** Simulation of Corrosion Behaviour of Stainless Steels in Passenger Car Exhaust Systems Simulation of Corrosion Behaviour of Stainless Steels in Passenger Car Exhaust Systems" ATZ Worldwide e-Magazines Edition: 2004-04.

100. **R. C. Newman:** Understanding the Corrosion of Stainless Steel, Corrosion, Vol. 57, No. 12, 2001, pp. 1031-1041.

101. **C. A. Olsson and S. E. Hornstrom:** An AES and XPS Study of the High Alloy Austenite Stainless Steel 254 SMO Tested in a Ferric Chloride Solution, Corrosion Science, Vol. 36, 1994, pp. 141-151.

102. ASM Metals Handbook, Corrosion, Volume 13. 1992. pp. 244.

103. **Z. Szklarska-Smialowska:** Pitting Corrosion of Metals, Houston, Tex., NACE, 1986.

104. **R. Winsten Revie and Herbert H. Uhlig:** Corrosion and Corrosion Control, Fourth Edition, 2008, pp. 178.

105. **K. E. Heusler and L. Fischer:** Kinetics of Pit Initiation at Passive Iron, Materials and Corrosion, Volume 27 1976, pp. 551-556.

106. **Pierre R. Roberge:** Handbook of Corrosion Engineering, 1999, pp. 336.

107. **E. Berdal:** Corrosion and Protection, 2003, pp. 123.

108. **K. Lorentz, G. Medawar:** Uber das Korrosionsverhalten austenitischer Chrom-Nickel Molybdän-Stähle mit und ohne Stickstoffzusats unter Besonderer Berücksichtigung ihrer Beanspruchbarkeit in Chloridhaltigen Lösungen. Thyssenforschung 1,3 1969, pp. 97-108.

109. **G. Mori:** Lecture notes, Corrosion, Montanuniversität Leoben, SS 2010, pp. 42.

110. **G. Herbsleb:** Der Einfluss von Schwefeldioxid, Schwefelwasserstoff und Kohlenmonoxid auf die Lochkorrosion von austenitischen Chrom-Nickel-Stählen mit bis zu 4 Massen-% Molybdän in 1 M Natriumchloridlösung, Werkstoffe und Korrosion 33, 1982, pp. 334-340.

111. **J. H Cleland:** Engineering Failure Analysis, 3, No 1, 1996, pp. 65-69.

112. **G. Mori:** User's View of Pitting Corrosion, NACE Corrosion, Louisiana, Paper No 04304, 2004. 247.

113. **S. Kadry:** Corrosion Analysis of Stainless Steel, European J. Sc. Research, 22, 2008 pp. 508-516.

114. **Mars G. Fontana:** Corrosion Engineering, Third Edition, Tata McGraw-Hill.

115. **Zaki Ahmad:** Principles of Corrosion Engineering and Corrosion Control, First Edition 2006.

116. **N. J. Laycock, J. Stewart and R. C. Newman:** The Initiation of Crevice Corrosion in Stainless Steels, Corr. Sc., 39, 1997, pp. 1791-1809.

117. **A. J. Betts and L. H. Boulton:** Crevice Corrosion: Mechanism, Modelling and Mitigation, B. Corr. Journal, 28, 1993, pp. C256-C268.

118. **J. H. Payer:** Material Performance, May-Nov. 1980.

119. **E. L. Hall and C. L. Briant:** Metall. Trans. A, 15A, 1984, pp. 793-811.

120. **S. Lamb and J. E. Bringas:** eds, Practical Handbook of Stainless Steels and Nickel Alloys ASM International, 1 edition, 1999.

121. **L. E. Murr, A. Advani, S. Shakar, D. G. Atteridge:** Effects of Deformation and Heat Treatment on Grain Boundary Sensitisation and Precipitation in Austenitic Stainless Steels. Material Characterization, 24, 1990, pp. 135-158.

122. **N. Parvathavartini, R. K. Dayal:** Influence of Chemical Composition, Prior Deformation and Prolonged Thermal Aging on Sensitization Characteristics of Austenitic Stainless Steels, Journal of Nuclear Materials, 305, 2002, pp. 209-219.

123. **E. A. Trillo and L. E. Murr:** Effects of Carbon Content, Deformation, and Interfacial Energetics on Carbide Precipitation and Corrosion Sensitization in 304 Stainless Steel, Acta Mater., Vol. 47, 1999, pp. 235-245.

124. **J. R Davis:** ed., Stainless Steels in ASM Speciality Handbook, 1st ed, Materials park, OH, ASM International, 1994, pp. 18, 770.

125. **A.S.M. Paroni, N. Alonso-Falleiros, and R. Magnabosco:** Sensitization and Pitting Corrosion Resistance of Ferritic Stainless Steel Aged at 800°C, Corrosion, Vol. 62, No. 11, 2006, pp. 1039-1046.

126. **P. Lacombe, B. Baroux and G. Beranger:** Stainless Steels. Les Editions de Physiques, Les Ulis, 1993.

127. ASM Metals Handbook, Corrosion, Volume 13. 1992. pp. 264.

128. Report of Australian Wright Metals, Sensitization of Stainless Steels, 2002.

129. **J. Charles, J. D Mithieux:** The ferritic Stainless Steel Family: The Appropriate Answer to Nickel Volatility, Proceedings of the 6th European Stainless Steel Science and Market Conference, Helsinki, Finland, 2008.

130. Preliminary Data Bulletin: Stainless Steel AL 466, Allegheny Ludlum Steel Corporation, Pittsburgh, PA, 1988.

131. **J. Rege:** Annealing Behavior and Formability of Ferritic Stainless Steels, M.S. Thesis, Materials Science and Engineering, University of Pittsburgh, 1993.

132. **Y. Xu et al:** Annealing Behaviour and Formability of Ferritic Stainless Steels, Pro. Int. Symp. On Low Carbon Steels for the 90's, eds. R. Asfahani and G. Tither, TMS, Warrendale, PA, 1993, pp. 397-404.

133. **W. Siklay, R. Soto, X. Bano, C. Issartel, G. Rigaut and A. Charai:** Advanced Microscopy Techniques Resolving Complex Precipitates in Steels, The European Journal of Physics, AP 6, 1999, pp. 243-250.

134. ASTM B117-07: Standard Practice for Operating Salt Spray Apparatus, Vol. 03.02, 2007.

135. **N. LeBozec, N. Blandin, and D. Thierry:** Accelerated Corrosion Tests in the Automotive Industry, A Comparison of the Performance Towards Cosmetic Corrosion, Materials and Corrosion, Vol. 59, No. 11, 2008, pp. 889-894.

136. **Kasem K. Kasem and Stephanie Jones:** Platinum as Reference Electrode in Electrochemical Measurements, Platinum Metals Rev., 2008, 52 (2), pp. 100-106.

137. ASTM International: Standard Practices for Detecting Susceptibility to Intergranular-Attack in Austenitic Stainless Steels, Designation A 262-02a.

138. ASTM International: Standard Guide for Examination and Evaluation of Pitting Corrosion, G46-94, 2006.

139. **J. Gelz, M. Yasir, G. Mori, B. Meyer, H. Wieser:** Problems in Quantification of Pitting Corrosion, Proceedings of the 13th Middle East Corrosion Conference, Bahrain, 2009.

140. **J. Gelz:** Qualification of a New Stainless Steel for Automotive Exhaust Applications, Diploma Thesis, Hochschule Aalen, submitted in August 2008.

141. **B. D. Cullity:** Elements of X-Ray Diffraction, Second Edition, Addison Wesley-Publishing Company Inc, 1978.

142. AK Steel data bulletin 2003.

143. Allegheny Lundulum Technical Data Blue Sheet, 2003.

144. **Chassagne, F. Antoni, L. Cleizergues, O. Lovato:** Development of a Nb Stabilised 15%Cr Ferritic Stainless Steel for Hot Part of Automotive Exhaust Systems, 4th Stainless Steel Science and Market Congress, Paris, France, June 2002.

145. **A. Miyazaki, M. Gunji and Y. Baba:** Feriitic Stainless Steels and Pipes for Automotive Exhaust Systems to Meet Weight Reduction and Stricter Emission Requirements, Kawasaki Steel Technical Report No.46, June 2002, pp. 19-24.

146. **Erhard Klar, K. Samal Prasan:** Processing, Microstructures and Properties, Powder Metallurgy Stainless Steels, ASM International, 2007.

147. **G. Cragnolino:** Proc Int. Conf on Localised Corrosion, Orlando, Florida, USA, 1, pp. 413-431, 1987.

148. **N. J. Laycock and R. C. Newman:** Corrosion Science, 40, No 6, 1998, pp. 887-902.

149. **G. T. Burstein, P. C. Pictorius and S. P. Mattin**: Corrosion Science, 35, No 1- 4, 1993, pp. 57-62.

150. **J. R. Saithala:** Pitting Corrosion of Stainless Steels in Chloride Solutions at Elevated Temperatures, Sheffield Hallam University, 2008.

151. **T. Misawa:** Protective Rust Layer Formed on Weathering Steel by Atmospheric Corrosion for a Quarter of a Century, Journal of the Iron and Steel Institute of Japan, v.79, n.1, 1993, pp. 69-75.

152. **Renato Altobelli Antunes:** Characterization of Corrosion Products Formed on Steels in the First Months of Atmospheric Corrosion, Materials Research v.6, n.3, 2003, pp. 403-408.

153.   **Y. M. Pan, D. S. Dunn, G. A. Cragnolino, N. Sridhar:** Grain-Boundary Chemistry and Intergranular Corrosion in Alloy 825, Metallurgical and Materials Transactions A 31A, 4, 2000, pp.1163-1173.

154.   **H. Sahlaoui, H. Sidhom, J. Philibert:** Prediction of Chromium Depleted-Zone Evolution during Aging of Ni-Cr-Fe Alloys, Acta Materialia 50, 2002, pp. 1383-1392.

155.   **H. Sahlaoui, K. Makhlouf, H. Sidhoma, J. Philibert:** Effects of Ageing Conditions on the Precipitates Evolution, Chromium Depletion and Intergranular Corrosion Susceptibility of AISI 316L: Experimental and Modeling Results, Materials Science and Engineering A 372, 2004, pp. 98-108.

156.   **R. L. Cowan and C. S. Tedmon:** Advances in Corrosion Science and Technology, Vol. 3, Plenum Press, New York, 1973, pp. 293.

9. List of Figures

10. List of Tables

11. List of Abbreviation and Symbols

CC	=	Crevice corrosion
IGC	=	Intergranular corrosion
DOS	=	Degree of Sensitization
IGA	=	Intergranular attack
SEM	=	Scanning electron microscopy
TEM	=	Transmission Electron Microscopy
EDX	=	Energy dispersive X-ray analysis
XRD	=	X Ray Diffraction
TOF-SIMS	=	Time of Flight Mass Spectroscopy
SS	=	Stainless steel
ASTM	=	American Standard for Testing of Materials
AISI	=	American Iron and Steel Institute
DIN	=	Deutsches Institut für Normung
VDA	=	Verband der Automobilindustrie
NDT	=	Non Destructive Testing
°C	=	Degree Celsius
M^+	=	Metal ion
NA	=	Not applicable
Km	=	Kilometre
Mm	=	Millimetre
h	=	Hour
T	=	Temperature
mV	=	Milli-volt
RE	=	Reference electrode
CE	=	Counter electrode
WE	=	Working electrode
PTFE	=	Polytetrafluoroethylene
Pt	=	Platinum
SCE	=	Saturated Calomel Electrode
OCP	=	Open circuit potential
FCC	=	Face centred cubic
BCC	=	Body centred cubic
PREN	=	Pitting Resistance Equivalent Number